Synthesis and reactivity of low-coordinate diamagnetic Rh and Ir complexes and paramagnetic Rh(II) complexes

By

Nan Zhang

A Thesis submitted to the Faculty of Graduate Studies of

The University of Manitoba

In partial fulfillment of the requirements of the degree of

MASTER OF SCIENCE

Department of Chemistry

University of Manitoba

Winnipeg

Abstract

Low-coordinate complexes generally show high reactivity and the lower the coordination number is, the higher the reactivity would be. Oxidative addition of C-H and X-H bonds is one of the most important and basic steps in organometallic catalysis. In this work, oxidative addition of Si-H, Sn-H and B-H bonds (E-H) at low-coordinate Rh and Ir β-diiminate (BDI) complexes to form dihydride and trihydride complexes are described. In addition, ligand functionalization via a cleavage of an Sn-C bond was obtained by the treatment of (^{Me}BDI)Rh(COE)(N_2) (^{Me}BDI = (2,6-$Me_2C_6H_3N$=CMe)$_2$CH) with $SnMe_4$ and H_2. Steric effects are significant controlling the reactions with EH substrates. To explore the limits of steric hindrance, reaction of (^{Me}BDI)Rh(COE)(N_2) with bulky PPh_3 was tested, leading to a complex containing a tautomerized BDI ligand.

Paramagnetic complexes of platinum group metals often show high and radical-like reactivity. They have one or more single electrons which typically show wide and broad peaks on NMR and they are usually characterized by EPR. Starting from [(^{Me}BDI)Rh]$_2$(μ-Br)$_2$, low-coordinate monomeric Rh(II) complex (^{Me}BDI)Rh(2,6-$^{i}Pr_2C_6H_3NH$) was successfully isolated through reaction with lithium 2,6-diisopropylanilide. Reactions with less hindered anilides resulted in eventual formation of diamagnetic final products.

Reactions of $[(^{Me}BDI)Rh]_2(\mu\text{-}Br)_2$ with lithium 2,6-dimethylanilide involves benzylic C-H activation while C-N coupling is observed with unsubstituted lithium anilide.

Acknowledgements

Firstly, I would like to thank my supervisor, Prof. Peter H.M. Budzelaar, who gave me the opportunity coming to Canada and join the group. I still remember the first day I came to the lab, at which time I only had little experience of organometallic chemistry. Prof. Budzelaar taught me the theoretical part of the project patiently on that small white board in his office and I have gradually learned about how to use Schlenk line and glovebox from him day by day. Under Prof. Budzelaar's supervision, my improvement is significant, especially in handling air-sensitive complexes. He is a responsible and kind professor not only in the lab, but also in my life. That was the first time I went abroad. Prof. Budzelaar picked me up in the airport and sent me to my university residence. Sometimes he looks pushy, but it is obvious that he is trying to help me and explore my potential. When something really happens, he is always telling me 'Please do not worry too much, we can handle it. It is my honor and luck meeting him and working together with him for two years.

Secondly, I would like to thank Prof. Van Wijngaarden and Prof. Herbert. Prof. Wijngaarden is a kind professor, without whom I would not get the opportunity coming to Canada. Prof. Herbert is a pushy and strict professor. The first class of me was given by Prof. Herbert and my English skill,

especially in chemistry, was not good at that time. He was strict to me and asked me a lot of questions. After the first class, I felt very nervous every time I went to his class. But this has pushed me to learn very fast and I could clearly see my improvement day by day. I would like to say that it is very important to have Prof. Herbert in my graduate student life.

Dr. Gurmeet Singh Bindra has helped me a lot since the first day I came to the lab in both living and experimental work. I was showed how to use glovebox and Schlenk line properly, how to carry out air-sensitive reactions and how to grow crystals by him. Thanks.

Thank you to my committee members: Prof. Peter H. M. Budzelaar, Prof. David Herbert and Prof. Georg Hausner. And Eric Cuthbert and Nasser Rahimi are greatly appreciated for their help in the lab.

Finally, I would like to thank my father and my grandmother who have always been supporting me no matter what happened.

Table of Contents

List of Figures

List of Equations

List of Schemes

List of Tables

Formula Index

2.1 (^{Et}BDI)Rh(HSiEt$_3$)$_2$

2.2 (^{Me}BDI)Rh(HBPin)$_2$

2.3 (^{MeO}BDI)Rh(HSn^{n}Bu$_3$)$_2$

2.4 (^{Me}BDI)Rh(HSn^{n}Bu$_3$)(HSiEt$_3$)

2.5 (^{Et}BDI)Ir(HSiEt$_3$)$_2$

2.6 (^{Me}BDI)Ir(HSiEt$_3$)$_2$

2.7 ($^{i Pr}$BDI)Ir(H)$_3$(SiEt$_3$)

2.8 ($^{i Pr}$BDI)Ir(H)$_3$(GeEt$_3$)

2.9 ($^{i Pr}$BDI)Ir(H)$_3$(BPin)

2.10 ($^{i Pr}$BDI)Ir(H)$_2$(BPin)$_2$

2.11 ($^{i Pr}$BDI)Ir(H)(BPin)(COE)

2.12 (*iso*-^{Me}BDI)Rh(PPh$_3$)$_2$

2.13 (^{Me}BDI)Rh(HSnMe$_3$)$_2$

2.14 (^{Me}BDI^SnMe$_3$)Rh(HSnMe$_3$)

3.1 (^{Me}BDI)RhNH(2,6-^{i}Pr$_2$C$_6$H$_3$)

3.2 [(^{Me}BDI)Rh]{μ-[η^4-NH(2-CH_2-6-CH_3-C_6H_3)-η^4]}[Rh(^{Me}BDI)]

3.3 (^{Me}BDI)Rh{NH(*o*-Me)C_6H_3(*o*-CH_2)}{μ-NH(2,6-$Me_2C_6H_3$)}Li{NH_2(2,6-$Me_2C_6H_3$)}$_2$

3.4 (^{Me}BDI)Rh{2-(PhN)-η^4-C_6H_3NH}Rh(^{Me}BDI)

3.5 (^{Me}BDI)Rh(2,2'-bipy)

3.6 (^{Et}BDI)Rh(2,2'-bipy)

3.7 (^{Me}BDI)Rh(2,2'-bipy)$(Br)_2$

3.8 (^{Me}BDI)Rh(2,2'-bipy)$(I)_2$

Abbreviations and Symbols

Acetate	OAc
Acetylacetone	acac
Alkyl and aryl substituents	R
Angle	θ
Angstrom	Å
Aryl group	Ar
Benzyl group	Bn
Beta	β
Bipyridine	bipy
β-diiminate	BDI
tert-butyl	^{t}Bu
Celsius	°C
Chemical shift	δ
Coupling constant	*J*
Diethyl ether	Et_2O
Doublet	d
Electron pulse Resonance	EPR
For example	e.g.
Halogen	X

4,4,5,5-tetramethyl-1,3,2-dioxaborolane	HBPin
Hertz	Hz
Hours	h
In the reaction	in situ
Ligand	L
Methyl	Me
Milligram	mg
Milliliter	mL
Millimole	mmol
Minutes	min
Mole	mol
Nuclear magnetic resonance	NMR
Parts per million	ppm
Percent	%
Phenyl	Ph
Iso-propyl	^{i}Pr
Sigma	σ
Singlet	s
Tetrahydrofuran	THF

That is	i.e.
Under vacuum	*in vacuo*
X-ray diffraction	XRD

Chapter 1

Introduction

1.1 Organometallic chemistry for catalysis

The study of organometallic chemistry mainly focuses on understanding the interactions of organic molecules or groups with metals. These metals can be divided into main group metals and transition metals. Main group metals are located in the *s* and *p* blocks of the periodic table. Organometallic complexes of the electropositive main-group metals, such as n-BuLi, show high reactivity and are of great value in organic synthesis. Different from main group metals, the interactions of organic groups with transition metals also involve *d* and sometimes *f* orbitals.[1] The six platinum-group metals are noble metals and the corresponding organometallic complexes often show high reactivity and selectivity when they act as catalysts.

Industrial processes, especially the production of organic compounds and polymers, rely heavily on transition metal organometallic catalysts.[2] The goal of industrial chemistry is making higher added value (HAV) products from cheaper precursors. Organic molecules usually have a hydrocarbon skeleton, and the goal here is to make complicated organic compounds from simpler

skeletons. Thus, precise control over how to modify the skeleton is a key factor. Organometallic catalysis is one versatile way to achieve that. Reactive metal complexes can activate C-H bonds and functionalize hydrocarbon skeletons.[3] Key issues are reactivity and selectivity and every metal has its own typical range of reactions it supports. In the present thesis, we are particularly interested in the C-H[4], C-Si and Si-H[5] activation possibilities offered by Rh and Ir complexes in combination with the β-diiminate ligand (Figure 1-1). Other reaction type catalyzed by Rh and Ir complexes include hydrogenation[6, 7] and hydroformylation.[8, 9]

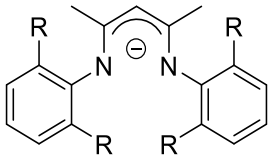

Figure 1- 1. The β-diiminate (^{R}BDI) ligand.

Hydrocarbon functionalization,[10, 11] which involves the activation of C-H bond,[12] is one of the "holy grails" of organometallic catalysis. C-H bonds are traditionally considered unreactive but can be activated by coordination. Previously, many C-H bond activations could only be achieved under harsh reaction conditions. In recent years, organometallic catalysts have become another important and efficient approach to activate inert C-H bonds.[13] In addition to C-H activation, the cleavages of other bonds such as Si-H, Sn-H and B-H bonds[14] can be part of processes converting abundant alkanes into

functionalized complex organic molecules.

Oxidative addition is involved in many transition-metal-catalyzed reactions. Starting with highly unsaturated low-valent metal compounds such as (^{Me}BDI)Ir(COE)[15] and (^{Me}BDI)Rh(COE)[16] (Scheme 1-1) is one strategy to achieve the cleavage of the inert chemical bonds. Since the reverse reaction (reductive elimination) is typically needed to complete a catalytic cycle, the preference for a higher oxidation state also should not be too strong. Otherwise, the complex would get "stuck" after the oxidative addition.

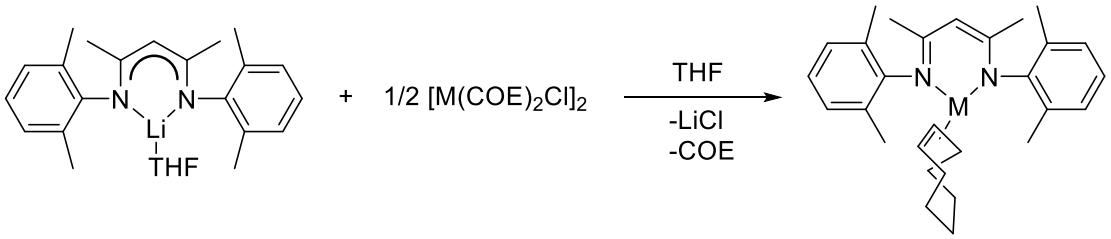

M=Rh, Ir.

Scheme 1- 1. Synthesis of (^{Me}BDI)Rh(COE) and (^{Me}BDI)Ir(COE).

However, achieving a full catalytic cycle is not easy. To move to useful and effective catalysis, side reactions that produce unwanted products or kill the catalyst must be avoided. In addition, the "active species" must be regenerated at the end of the catalytic cycle, which implies the product needs to be released or displaced. Normally, intramolecular chemistry is useful as a model for intermolecular catalysis.[17] Intramolecular reactions are favored by entropy

and hence usually easier to achieve than intermolecular variations, but the intramolecular variation is usually not useful by itself.

In recent years, as the concerns of climate change and green chemistry,[18] organometallic catalysts have shown their value in energy storage. For instance, splitting water into H_2 and O_2 can convert electrical energy into chemical energy which has attracted organometallic chemists.[19] In addition, the storage of energy and the release step also require catalysis.[20-23]

1.2 β-diiminate ligand

The β-diiminate ligands (BDI) were first introduced in 1968 (Figure 1-1).[24] They are the analogues of acetylacetonate (acac) ligands, where the oxygen atoms have been replaced by NAr groups (hence, they are also called "nacnac" ligands). The replacement of O by NAr not only changes the electronic properties of the ligand, but also introduces groups at N that can be used for steric and possibly electronic tuning. In contrast, the acac ligand itself can in practice only be tuned by replacing the backbone methyl groups, and these are so remote from the metal centre that steric effects of such changes are minimal.

There are three common routes for the synthesis of β-diiminate ligands.[25] The most convenient route (A) is the reaction of an aromatic amine with acetylacetone. For less reactive diketones, a reagent might be added to

chemically bind the released water (e.g. $TiCl_4$). Route B is especially useful for the synthesis of β-diiminate ligands with bulky groups (Scheme 1-2) and asymmetric ligand (R1 ≠ R2).

Route C (Scheme 1-3) has been used for the synthesis of β-diiminate ligands with CF_3 substituents (where standard condensation does not work), but is not effective for bulky Ar groups.

Route A.

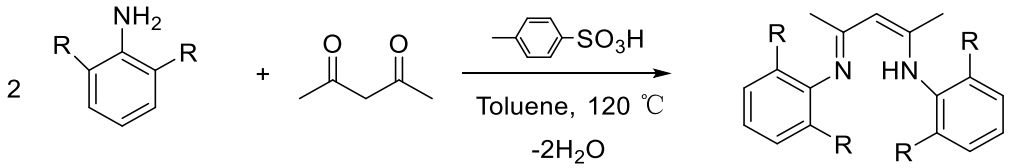

Route B.

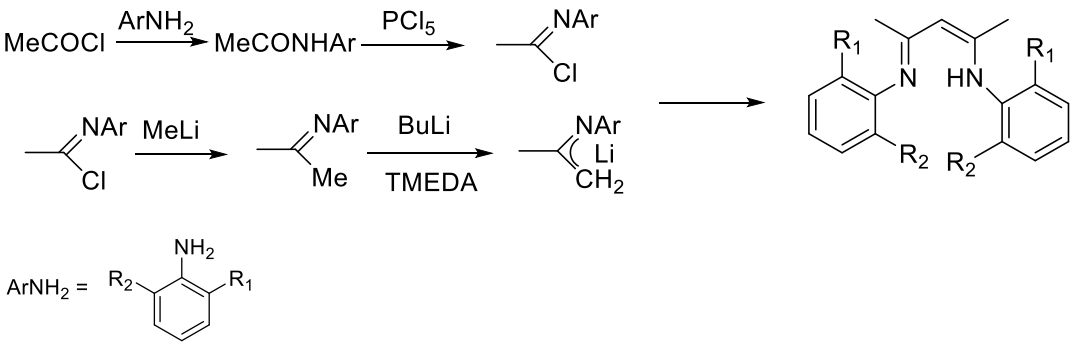

Scheme 1- 2. The synthesis of β-diiminate ligand.

Route C.

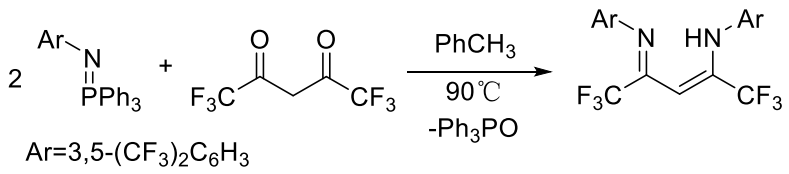

Scheme 1- 3. Synthesis of BDI with CF_3 substituent.

These ligands are special in some aspects.[26] One advantage of this ligand is the flexibility of the synthesis due to the wide variety of substituted anilines that are commercially available (Figure 1-2). For example, bulky R groups can be used to narrow the space and direct the way to the metal centre and the selectivity of the reaction could improve through this way. The replacement of CH_3 groups by CF_3 will lead to an electron-poor ligand.[27, 28]

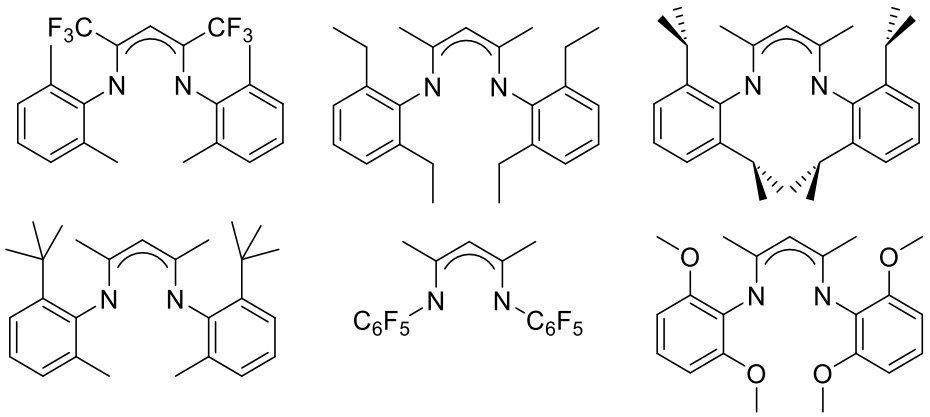

Figure 1- 2. Ligand variation of β-diiminate ligand.[29-31]

The BDI ligand is usually introduced as its Li salt, used in a straightforward salt metathesis reaction (Equation 1-1).[32]

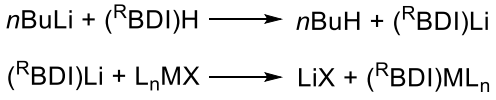

Equation 1- 1.

If the Li salt is prepared in THF, there are usually one or two equivalents of THF coordinating to the lithium atom, depending on the bulkiness of the substituents (Scheme 1-4).

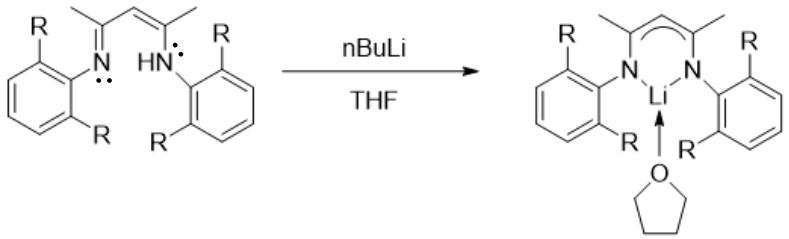

Scheme 1- 4. Synthesis of (^{R}BDI)Li(THF).

The β-diiminate ligand has 4 σ and 6 π electrons available for metal-ligand bonding, although not all can be used simultaneously. The coordination of β-diiminate ligands with late transition metals such as iridium or rhodium has become more popular in recent years because of the high and special reactivity of those complexes.[15, 26] The oxidation states of rhodium could be 0 to 5 and the preferred oxidative states are Rh(I) and Rh(III).

1.3 Low-coordinate complexes and geometries

The reactivity of a complex not only depends on the oxidation state of the metal, but also on the coordination number and electron count of the metal center. In general, the lower the coordination number is, the higher the

reactivity would be. To break a bond, forming new and strong bonds is an essential step. Low coordination number means additional strong bonds could be more easily formed and low-coordinate complexes provide open coordination sites for the association step which plays an important role preceding bond-activation. However, unwanted side reactions would also be more likely to happen and intramolecular reactions tend to be easier than intermolecular ones. Thus, the protection of the metal center against unwanted side reactions by proper ligands is necessary.

In general, complexes with low electron counts (14 or less for the platinum metals) are called low-coordinate complexes and bulky ligands are usually required to stabilize such species.[33] Each coordination number has one or more corresponding geometries if small distortions are ignored. For example, T-shape and Y-shape geometries are typically found in d^8 with coordination number 3, coordination number of square planar and tetrahedral geometries is 4 and coordination number of octahedral geometry is 6. In this thesis, the reactivity of three-coordinate Rh and Ir complexes will be illustrated, once the additional bonds are formed in these complexes, the coordination number of the metal center go up to 4, 5 and 6 with square planar, trigonal bipyramidal and octahedral geometries if distortions are

ignored (Figure 1-3).

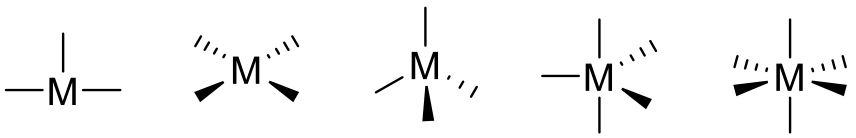

Figure 1- 3. The T-shape, square planar, tetrahedral, trigonal bipyramidal and octahedral geometry.

For example, a three-coordinate copper complex with significant radical character was reported by the group of Warren.[34] The reactivity of this complex is identified by the unpaired electron at the amido N atom through the reaction with NO which is another radical species (Scheme 1-5). The product indicates the formation of a Ph_2N-NO bond.

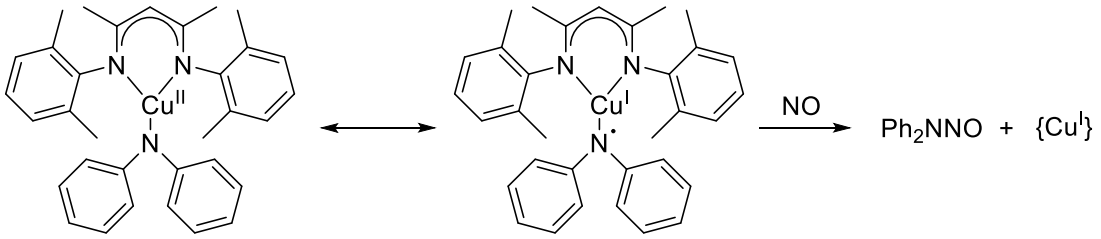

Scheme 1- 5. Reactivity of copper aminyl complexes.

Dugan et al. have reported the activation of C-F bond by a two-coordinate cobalt(I) complex with a bulky β-diiminate ligand.[35, 36] The reactivity of this complex was tested by the reaction with fluorobenzene. The addition of fluorobenzene results in a binuclear oxidative addition with the cleavage of strong C-F bonds (Scheme 1-6). The cobalt dimer was characterized by X-ray while the Co-Ph complex was only identified by NMR. Both examples have

shown interesting reactivity that low-coordinate complexes have.

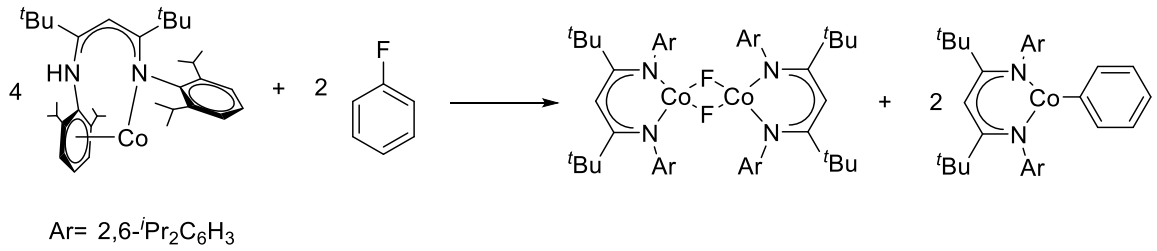

Scheme 1- 6. Activation of C-F bond by two-coordinate Co complex.

In crystal-field theory, each geometry has an associate d-orbital splitting pattern.[1] In an octahedral arrangement (Figure 1-4, a), electrons in d_{z^2} and $d_{x^2-y^2}$ are concentrated close to the ligand, while the electrons in d_{xy}, d_{yz} and d_{xz} orbitals are concentrated between the ligands. Therefore, the latter three orbitals are repelled less strongly by the negative charge on the ligands than the former two orbitals and lie at a lower energy. Furthermore, group theory indicates that three t_{2g} orbitals have the same energy and so do two e_g orbitals. The d-orbital spitting of a square-planar arrangement is also shown below (Figure 1-4, c). In this arrangement, $d_{x^2-y^2}$ rises above all the other orbitals, thus the crystal field is strong enough and the low-spin configuration is favored.

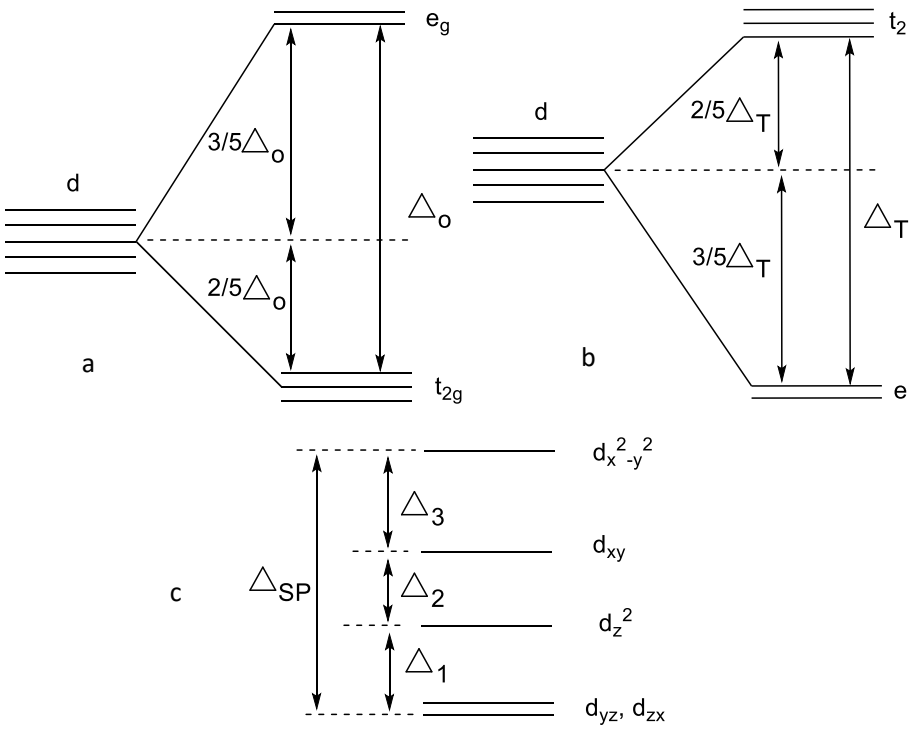

Figure 1- 4. The orbital spitting patterns for octahedral, tetrahedral and square planar complexes.

A large part of this thesis focuse s on synthesis and characterization of (^{R}BDI)M(HE)$_2$ complexes, where M is rhodium or iridium and H-E is a silane, germane, stannane or borane. A key issue of these complexes is the nature of the M-HE interaction, which could in principle vary between the extremes of a pure σ-complex (side-on interaction of E-H bond with metal) and full oxidative addition (full M-H and M-E bonds, complete loss of the H-E bond). This can be studied by a variety of techniques such as NMR, Xray, IR, XPS and Neutron diffraction.

1.4 General Experimental Techniques

1.4.1 Characterization

The most important and relevant characterization techniques used for (^{R}BDI)Rh/Ir complexes are (multinuclear) solution-phase NMR spectroscopy and single-crystal X-ray diffraction.

NMR spectra show the averaged picture of solution phase and most of the complexes in this thesis are dynamic in solution. On the NMR timescale (~10^{-2}s), the substrates could exchange positions fast and become equivalent. Although it is not as quantitative as X-ray, major changes in structure are usually obvious among related complexes. In our case, the chemical shift of the BDI central proton is around 5 ppm which is typical and used for identifying the ligand. The peak of the N-H proton in free ligand is found around 12 ppm and is typically somewhat broadened. Observation of this signal in crude reaction mixtures can be regarded as an indication of instability of the desired product. Furthermore, a high-field hydride resonance in ^{1}H NMR is the most characteristic feature of the complexes (^{R}BDI)Rh(HE)$_2$ studied in this work. For rhodium, the hydride chemical shift is around -15 ppm. Because the nuclear spin of rhodium is ½ and it couples to the hydride, the splitting pattern of the hydride is usually a doublet. For iridium complexes studied, the hydride peak is found at slightly higher field (around -16.5 ppm)

and there is no observable coupling to iridium (Figure 1-5). Hydrides are at <0 or <<0 ppm, because they are inside the electron cloud of a partially filled metal d-orbital shell. This produces an effect similar to ″ring current″ (as in benzene) but much stronger. Such high-field shifts with d^0 or d^{10} complexes cannot be observed.

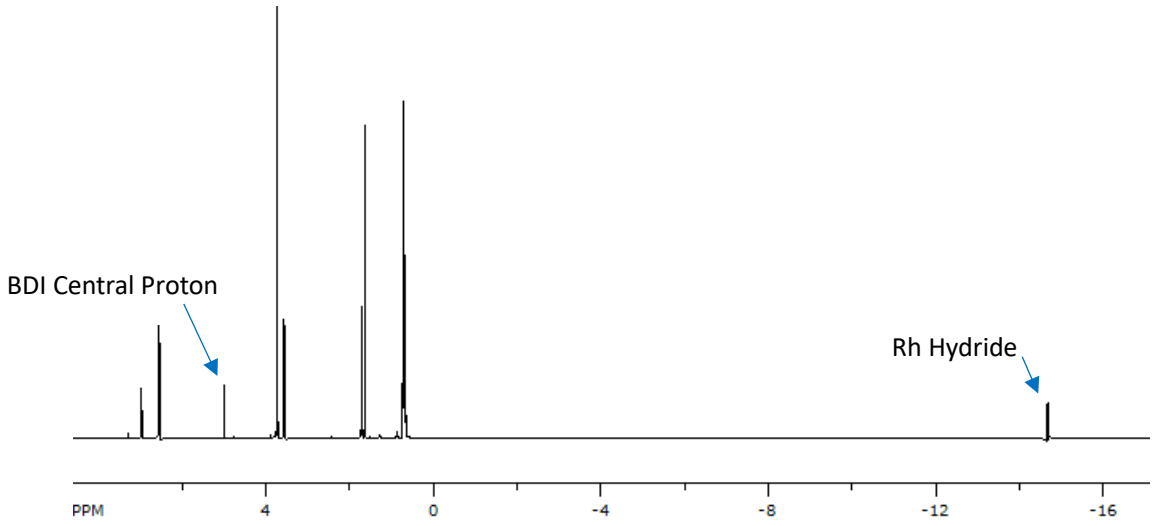

Figure 1- 5. ^{1}H NMR spectrum of (^{OMe}BDI)Rh(HSiEt$_3$)$_2$.

The hydride peaks of BH adducts are broad in our complexes. The dominant isotope of B (^{11}B) has spin $^3/_2$ so the spin-spin coupling between it and the hydride should result in a 1:1:1:1 splitting pattern in ^{1}H NMR. However, due to fast relaxation, broadness is typically observed of the otherwise expected line or coupling pattern. In addition, dissociation (exchange) of HE ligands may cause additional broadening.

Single-crystal X-ray diffraction yields a picture of a solid-state and usually

frozen-out structure, so solid state and solution are not always the same. Also, X-ray diffraction does not always provide a complete and definitive answer. For example, H atoms are hard to locate especially near heavy metals. Since H atom locations are important indicators of the nature of the M-HE interaction, DFT calculations have often been used to confirm or support positioning hydrogens. Various types of electronic structure analysis can also be helpful in interpretation of bonding. For example, bond distances and the corresponding Wiberg bond indexes[37] (WBI) are used to indicate the degree of oxidative addition which could be between the extremes of simple σ-complex coordination and full oxidative addition.

1.4.2 Synthesis and manipulation of sensitive compounds

Figure 1- 6. Glovebox in Budzelaar Laboratory.

For carrying out experiments, the two techniques which are of significance

and commonly used among organometallic chemists are glovebox (Figure 1-6) and Schlenk Technique (Figure 1-7). The purpose is to work under an inert gas atmosphere. Gloveboxes or dryboxes used today were pioneered by Brown et al. as an evolution from the plywood and Plexiglas home-made version from the 1960's.[38] In addition, reactions can also be carried out outside the glovebox by attaching to a Schlenk line.[39] Schlenk techniques were developed by Wilhelm Schlenk. The apparatus consists of an inert gas delivery system attached to a dual manifold with several ports and a high vacuum pump. The reaction tubes are sealed with the greased cap and connected to each port by a rubber tube which allows for air to be purged and replaced by dry-inert gas. In our case, Schlenk line is flowed with Argon and the glovebox is filled with nitrogen in which oxygen and water levels are below 0.1 ppm, but these are just possible choices. A glovebox is extremely convenient for keeping air-sensitive chemicals and weighing organometallic complexes. The reactions described in this thesis were mostly carried out using Schlenk technique under argon, but there were cases in which nitrogen atmosphere is vital.

Figure 1- 7. Schlenk Technique in Budzelaar Laboratory.

Chapter 2

Low-coordinate diamagnetic Rh and Ir complexes

2.1 Introduction

The group of Gal reported the synthesis of (^{Me}BDI)Rh(COE) in 1998[16] and the synthesis of (^{Me}BDI)Ir(COE) in 2000[15] (Scheme 1-1). Both have been found to activate strong bonds, such as C-H, C-O[4] and Si-H[5] bonds and this makes them interesting as potential catalysts for reactions involving such strong bonds. Notably, they also reversibly bind N_2 to form dinitrogen complexes. However, when the reactions were carried out under argon, the iridium complex decomposed fast while the rhodium complex stayed reasonably stable. Stephan's group reported the activation of P-P bond by (^{Me}BDI)Rh(COE)(N_2).[40, 41] In addition, Si-H bond activation was achieved by the reaction of (F-BDI)Rh(CO)(NCMe) with excess $HSiMe_3$ which was reported by the group of Meier (Figure 2-1).[42]

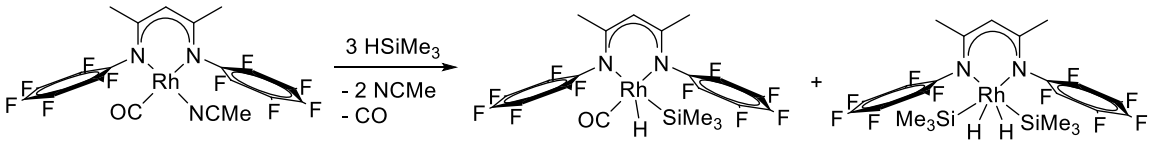

Figure 2- 1. H-Si activation by the reaction of (F-BDI)Rh(CO)(NCMe) with excess $HSiMe_3$.

($^{i\text{Pr}}$BDI)Rh(phdi) (phdi=9,10-phenanthrenediimine) was synthesized by Shaffer et al.[43] This complex shows interesting redox behavior.[44, 45] The treatment of ($^{i\text{Pr}}$BDI)Rh(phdi) with bromine and chlorine result in two octahedral *trans*- Rh(III) complexes.[46] In contrast, the reaction with iodine produced a square pyramidal I_2 complex with an intact I-I bond (Figure 2-2).

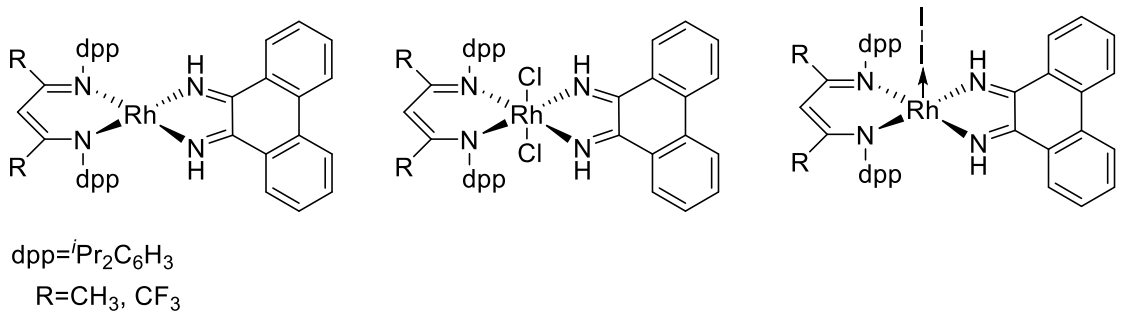

Figure 2- 2. Structures of ($^{i\text{Pr}}$BDI)Rh(phdi), ($^{i\text{Pr}}$BDI)Rh(phdi)(Cl)$_2$ and ($^{i\text{Pr}}$BDI)Rh(phdi)(I)$_2$.

It is worthwhile to mention here the general differences between 4d (Rh) and 5d (Ir) transition metals. Although they have a similar atomic radius and their chemistries are roughly similar, the 5d elements tend to prefer higher oxidation states and form stronger bonds to ligands. For example, the treatment of ($^{\text{Me}}$BDI)Rh(COE)(N_2) with H_2 in benzene results in Rh(I) complex [($^{\text{Me}}$BDI)Rh]$_2$(C_6H_6) while Ir(V) complex ($^{i\text{Pr}}$BDI)IrH_4 was successfully synthesized by the reaction of ($^{i\text{Pr}}$BDI)Ir(COE)(N_2) with H_2.[47] (Scheme 2-1). This complex is able to activate the relatively inert C-H bonds of benzene (Scheme 2-2).[48] This is the first example of the successful

synthesis of the tetrahydride iridium compound of β-diiminate. No examples of the analogous tetrahydride rhodium complexes of β-diiminate have been reported yet.

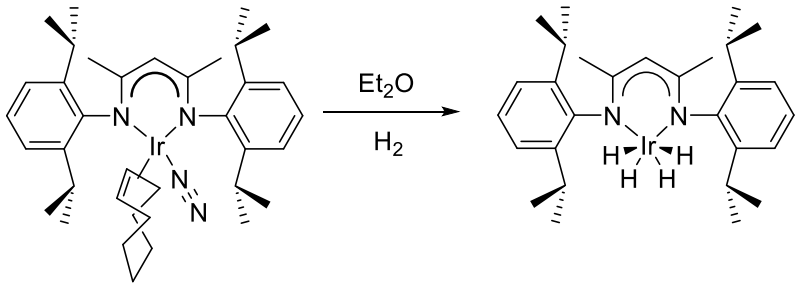

Scheme 2- 1. Synthesis of (^{iPr}BDI)IrH$_4$.

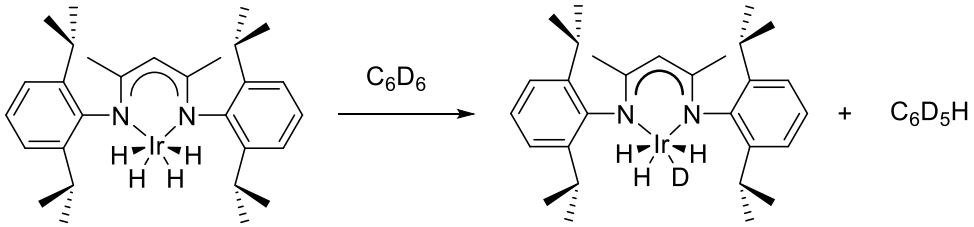

Scheme 2- 2. Activation of C-H bond in benzene.

In 2012, the synthesis of (^{Me}BDI)Rh(HSiEt$_3$)$_2$ was reported by the group of Budzelaar.[5] Interestingly, ligand functionalization happened in this complex which involves the cleavage of an Si-C bond (Scheme 2-3). This rearrangement was only observed in solution. An intermolecular variation would be more useful (silylation of C-H bonds of an added substrate) but entropy strongly favours intramolecular reactions.[26]

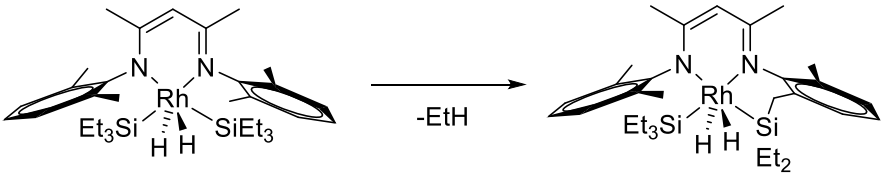

Scheme 2- 3. Rearrangement of (^{Me}BDI)Rh(HSiEt$_3$)$_2$.

The proposed pathway of the ligand functionalization requires the dissociation of a HSiEt$_3$ group first and followed by a Si-C activation. Then a benzylic C-H bond is activated followed by the leaving of EtH group and a Si-C bond formation. In the end, the HSiEt$_3$ group associates to the rhodium again to form the final product (Scheme 2-4).

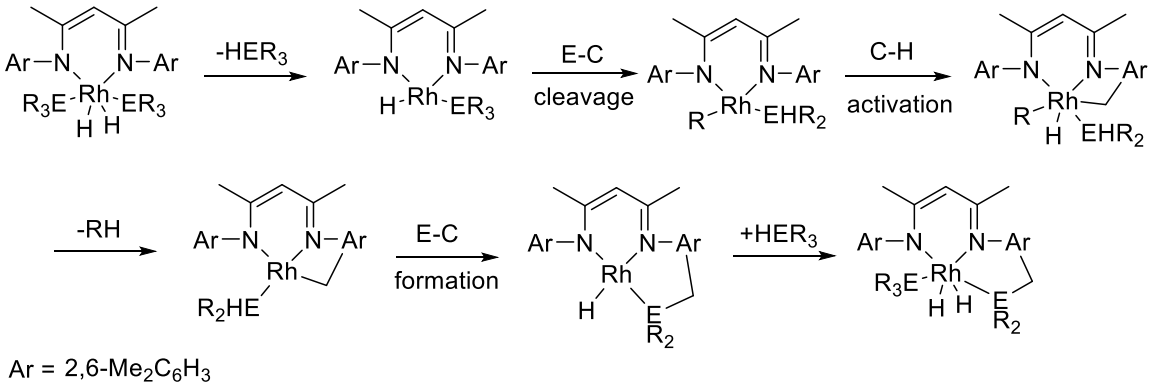

Scheme 2- 4. Proposed mechanism for ligand functionalization.

The choice of solvent can be important carrying out these reactions especially when dealing with Rh(I) complexes. Aromatic solvents such as benzene and toluene can coordinate to Rh(I) and result in formation of binuclear complexes [(^{R}BDI)Rh]$_2$(C_6H_6) and [(^{R}BDI)Rh]$_2$(C_7H_8).[49] [(^{Me}BDI)Rh]$_2$(C_6H_6) was accidentally crystallized twice in my experimental

works. Red crystals were obtained over a weekend in hexane (Figure 2-3).

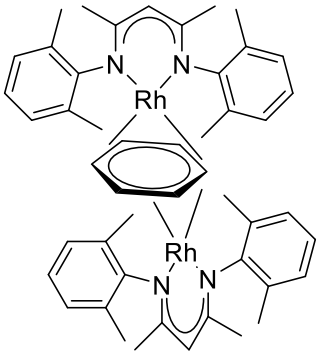

Figure 2- 3. Structure of $[(^{Me}BDI)Rh]_2C_6H_6$.

In the present work, we explore the scope of formation of HE adducts, as well as potential for the above-mentioned rearrangement, as a function of metal (Rh/Ir), ligand (Me/Et/MeO BDI variations) and substrate H-E (silanes, germanes, stannanes, boranes). This should provide us with increased insight in possibilities for using C-E and E-H activation as steps in some form of homogeneous catalysis.[14]

2.2 Synthesis of β-diiminate Rh and Ir complexes of boranes, silanes and stannanes

2.2.1 New complexes

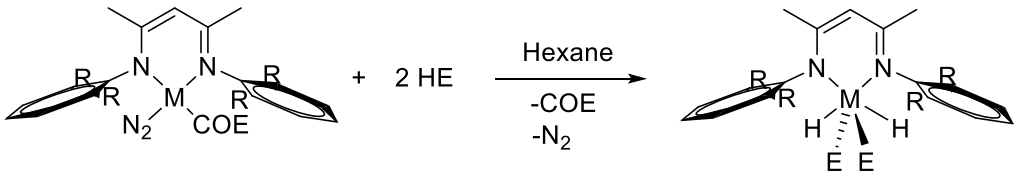

2.1 M= Rh E= $SiEt_3$ R= Et
2.2 M= Rh E= BPin R= Me
2.3 M= Rh E= Sn^nBu_3 R= MeO
2.4 M= Rh E= $SiEt_3$/Sn^nBu_3 R= Me
2.5 M= Ir E=$SiEt_3$ R= Et
2.6 M= Ir E=$SiEt_3$ R= Me

HBPin = 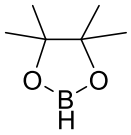

Scheme 2- 5. Synthesis of (^{R}BDI)M(HE)$_2$.

Reactions of (^{R}BDI)Rh(COE)(N_2) with different HE substrates were carried out in Schlenk line (Scheme 2-5). When (^{Et}BDI)Rh(COE)(N_2) was treated with $HSiEt_3$ in hexane, the solution color turned from brown-red to yellow within 5 min. Single crystals of **2.1** were obtained from hexane at -35 ℃ overnight. Similar to the Si-H activation at Rh, the reaction of (^{Me}BDI)Ir(COE)(N_2) and (^{Et}BDI)Ir(COE)(N_2) with $HSiEt_3$ results in the oxidative addition of Si-H bonds to iridium. Bright yellow crystals of **2.6** were obtained from pentane at -35 ℃ over weeks. Similarly, orange crystals of **2.5** was obtained in $^iPr_2O$ overnight.

B-H activation was observed by the reaction of (^{Me}BDI)Rh(COE)(N_2) with HBPin(4,4,5,5-tetramethyl-1,3,2-dioxaborolane). When (^{Me}BDI)Rh(COE)(N_2)

was treated with HBPin in hexane, a yellow solid precipitated after 5 min. After centrifuging, the solution part was removed and the solid part was dissolved in THF/Hexane. Yellow crystals of **2.2** were obtained overnight at -35 °C.

As an extension of earlier work, we want to explore analogous stannanes chemistry and the reactions of (^{R}BDI)Rh(COE)(N_2) with stannanes are challenging. HSn^{n}Bu$_3$ is toxic and decomposes easily. In addition, isolation of products turned out to be more difficult due to the high solubility of HSn^{n}Bu$_3$ and its coordination complexes.

Reaction of (^{MeO}BDI)Rh(COE)(N_2) with HSn^{n}Bu$_3$ was carried out under argon, the solution color turned from brown-red into yellow after 5 min. The solid was further extracted with Et_2O and put in the fridge at -35 °C. Due to the high flexibility of the HSn^{n}Bu$_3$ groups, growing crystals is hard and big yellow crystals of **2.3** were only obtained after months. However, the reaction of (^{Me}BDI)Rh(COE) with HSn^{n}Bu$_3$ was not as clean. Under the same experimental conditions, although the new hydride peak formed, a lot of free ligand was observed in ^{1}H NMR and no crystals were obtained.

Complex **2.4** was prepared by the reaction of (^{Me}BDI)Rh(COE)(N_2) with 2 equivalents of $HSiEt_3$ followed by 1 equivalent of HSn^{n}Bu$_3$. The stannane binds more strongly to the metal center than the silane does, so the added

HSn^nBu_3 successfully replaced one $HSiEt_3$ group. Red crystals were obtained from $^iPr_2O$ overnight.

2.2.2 The rearrangement of complex 2.2

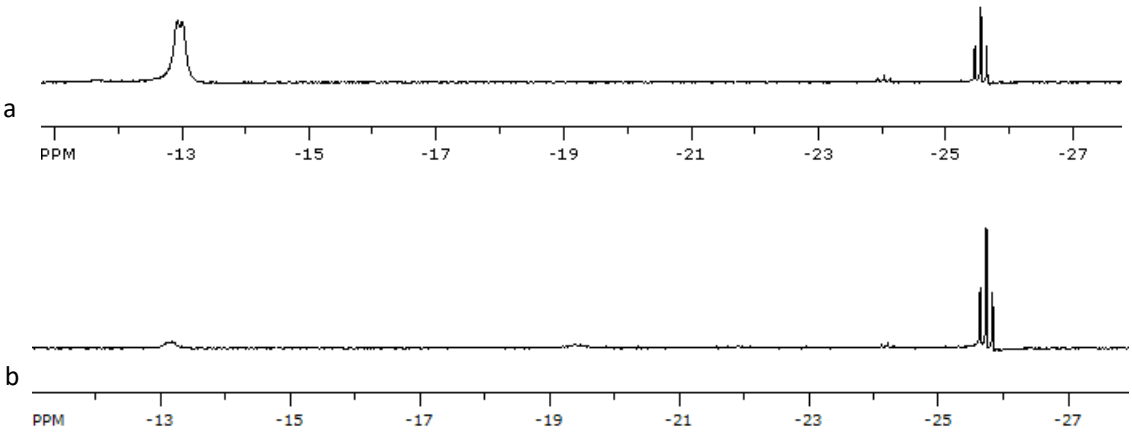

Figure 2- 4. Hydride region of (^{Me}BDI)Rh(H)$_2$(BPin)$_2$ in C_6D_{12}.

The complex **2.2** is not stable in solution. Interestingly, we found a rearrangement of (^{Me}BDI)Rh(HBPin)$_2$ in solution after around one day. From ^{1}H NMR (Figure 2-4, a), a new triplet peak grows at -25.5 ppm. The integration against the new BDI central proton peak shows one hydride and the splitting pattern is likely due to the coupling to the two equivalent Rh atoms. Therefore, it is likely to be a binuclear hydride. After one week, (^{Me}BDI)Rh(HBPin)$_2$ was nearly consumed (Figure 2-4, b). It is possible that this rearrangement involved a dimerization with the loss of two HBPin groups which results in a Rh(III) dimer with the bridge by hydrides[50] and this structure has two equivalent Rh atoms and two equivalent hydrides (Scheme

2-6). We have not yet been able to get crystals of this complex.

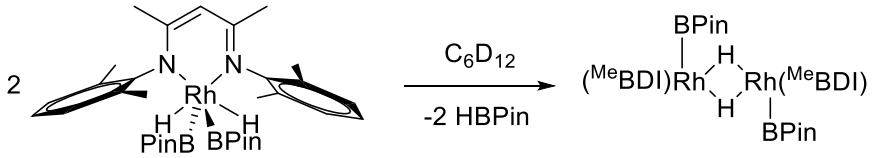

Scheme 2- 6. One possible rearrangement of 2.2.

2.2.3 NMR and X-ray characterization

Complexes **2.1**-**2.6** show effective C_{2v} symmetry in solution with two equivalent hydrides and two equivalent HE groups. ^{1}H NMR spectra of **2.1** (Figure A-1), **2.2** (Figure A-3), **2.3** (Figure A-5) and **2.6** (Figure A-11) show hydride peaks at -14.82, -13.36, -15.34 and -16.33 ppm, respectively. Compared to (^{Me}BDI)Rh(HSiEt$_3$)$_2$, iridium analogue **2.6** does not undergo ligand functionalization in solution. Complex **2.1** has a J_{SiH} 9 Hz which is determined from ^{29}Si satellites. For Ir silane complexes **2.5** and **2.6**, J_{SiH} determined by ^{29}Si satellites are both less than 3 Hz. These small values indicate complexes **2.1**, **2.5** and **2.6** are close to the extreme oxidative addition.[51] The hydride peak of **2.2** shows broadness and as mentioned before, the broadening indicates incomplete activation and/or dynamic behaviour of this complex in solution. Even though HBPin does not dissociate fast from the complex and there are clearly localized B-H bonds, the short and long B-H contacts exchange is fast. ^{117}Sn/^{119}Sn satellites were observed in hydride signals of **2.3** and **2.4** which have J_{SnH} 23 Hz and 24 Hz. Both values are much

smaller than direct $^{1}J_{SnH}$ values,[52] suggesting that structures are close to the extreme oxidative addition. Two hydrides of **2.4** are equivalent and the reason is the fluxionality of two hydrides, that is, one is close to Si but moves closer to Sn and the other does the opposite.

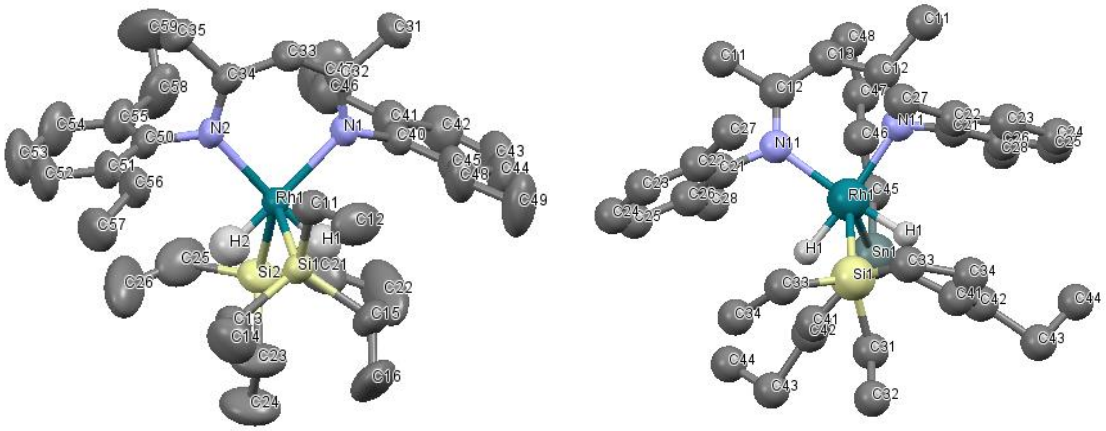

a b

Figure 2- 5. X-ray structure of 2.1 (a) and 2.4 (b), showing thermal ellipsoids at 35% probability. All hydrogen atoms except hydrides have been omitted for clarity.

Bond distances of Rh-Si, Rh-H and Si-H from X-ray structure of **2.1** (Figure 2-5, a) further proves that it is neither a full activation nor a typical Si-H side-on coordination but somewhere in between. From X-ray structure of **2.4** (Figure 2-5, b), the bond lengths of Rh(1)-Si(1) and Rh(1)-Sn(1) are 2.356(11) Å and 2.601(8) Å. In the X-ray structure of **2.6** (Figure 2-6), each hydride has one long and one short Si contact, so the two hydrides are equivalent. In addition, there is only one resonance of two methyl groups of BDI backbone,

thus the Si and H atoms are in a highly dynamic situation and the exchange is fast enough that only an average can be seen in NMR at room temperature.

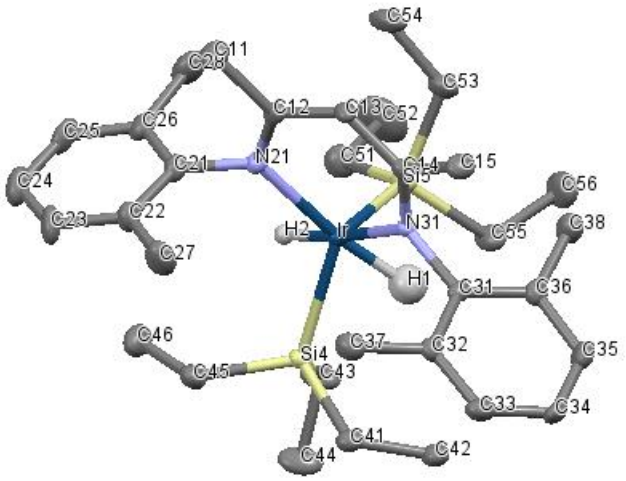

Figure 2- 6. Crystal structure of 2.6, showing thermal ellipsoids at 40% probability. All hydrogen atoms except hydrides have been omitted for clarity.

2.2.4 HE dissociation energies and degree of oxidative addition

DFT calculations were performed by Prof. Budzelaar: geometry optimization with Turbomole, def-TZVP basis, DFT-D3 dispersion corrections, and enthalpy and entropy corrections to free energies.[14]

Cp*Rh and Cp*Ir fragments are effective in activating E-H and C-H bonds[53-56] and Cp*M(HE)$_2$ and (BDI)M(HE)$_2$ show strong analogies.[25] Dissociation free energies of the first and second HE substrate to the metal were calculated by DFT. The trend shows that the first HE dissociation energy increases consistently in the order H_2<HBPin≈$HSiMe_3$≈$HGeMe_3$<$HSnMe_3$.

Cp*M fragments have higher dissociation energies than (BDI)M fragments and binding to Ir is stronger than binding to Rh.

Compared to β-diiminate ligand, Cp* ligand is good at stabilizing high oxidation states. BDI systems are best described as somewhere between σ-complex side and oxidative-addition side. The set of complexes studied in this chapter displays a variation between full oxidative addition and σ-coordination. Based on the M-E, M-H and H-E bond distances from X-ray/neutron diffraction, M-HE dissociation energies and Wiberg bond indices obtained from DFT calculations, the nature of M-HE interaction was analyzed for Cp* and BDI ligand with Rh and Ir centers. DFT results reveal that Cp* complexes are best described as M(V) with nearly full oxidative addition. For example, Cp^*IrH_4[57] and $Cp^*RhH_2(SiEt_3)_2$[58] have been successfully isolated and they both have +5 oxidation state. Compared to Cp*, BDI complexes show less oxidative addition. ($^{i\text{Pr}}$BDI)IrH_4 is best described as tetrahydride while ($^{\text{Me}}$BDI)$Rh(H_2)_2$ is predicted to be a σ-complex with the coordination of dihydrogen.

2.3 Attempted synthesis of trihydride β-diiminate Ir complexes of boranes, silanes and germanes

2.3.1 New complexes

In addition to (^{R}BDI)Ir(COE)(N_2), (^{iPr}BDI)Ir($H)_4$ also shows high reactivity towards activating HE bonds. Starting from (^{iPr}BDI)Ir($H)_4$, several trihydride and dihydride complexes were successfully synthesized. Due to the high reactivity of this tetrahydride iridium complex, the reactions with 1 equivalent of $HSiEt_3$ and 1 equivalent of $HGeEt_3$ result in the activation of Si-H bond and Ge-H bond (Scheme 2-7), respectively, and eventually produce trihydride iridium β-diiminate complexes **2.7** and **2.8**. Further addition of one more equivalent of $HSiEt_3$ failed to produce dihydride iridium complexes.

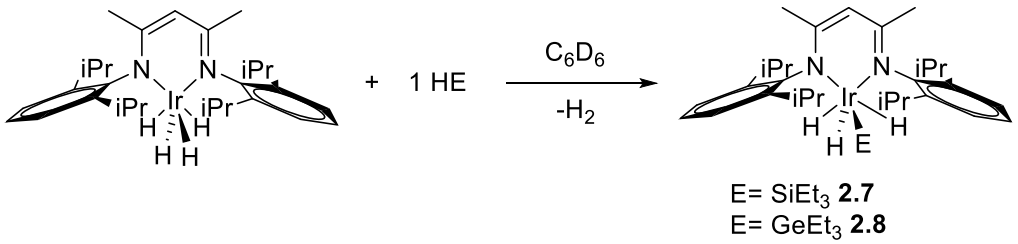

Scheme 2- 7. Synthesis of (^{iPr}BDI)Ir($H)_3$(E).

Interestingly, the reactions of (^{iPr}BDI)Ir($H)_4$ with 1 equivalent of HBPin and 2 equivalents of HBPin produced different results (Scheme 2-8).

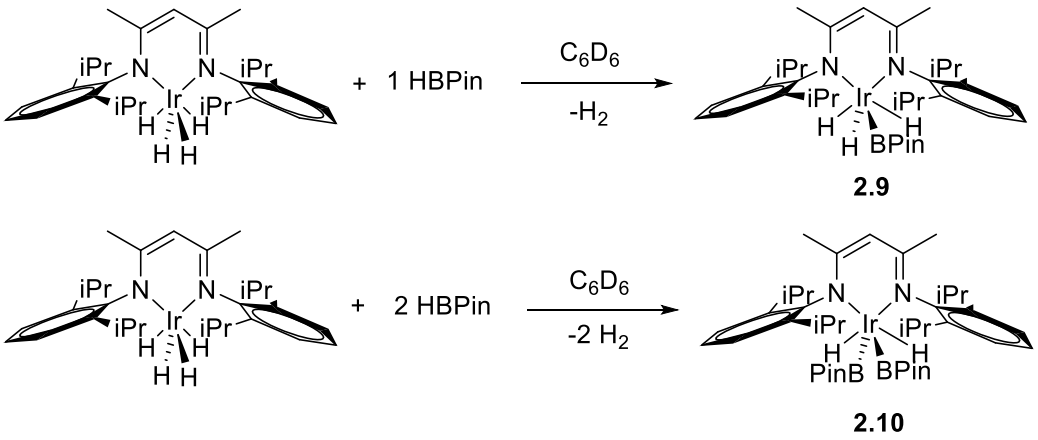

Scheme 2- 8. Reactions of ($^{i\text{Pr}}$BDI)Ir(H)$_4$ with 1 equivalent and 2 equivalents HBPin.

To further explore the reactivity of ($^{i\text{Pr}}$BDI)Ir(COE)(N_2) towards HBPin, the reaction of ($^{i\text{Pr}}$BDI)Ir(COE)(N_2) with 1 equivalent of HBPin was carried out in hexane (Scheme 2-9). Yellow crystals of **2.11** were obtained in $^{i}Pr_2O$ after weeks.

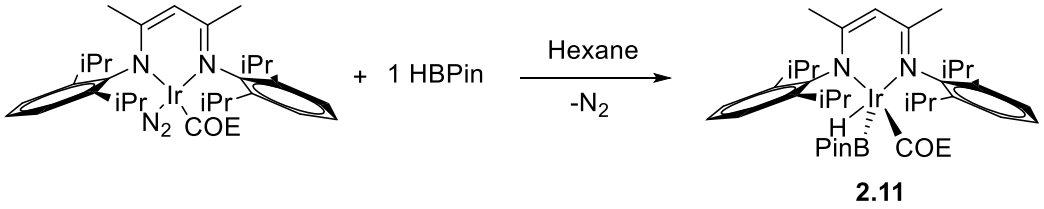

Scheme 2- 9. Synthesis of ($^{i\text{Pr}}$BDI)Ir(H)(BPin)(COE).

2.3.2 NMR spectroscopic characterization

Reactions of ($^{i\text{Pr}}$BDI)Ir(H)$_4$ with $HSiEt_3$ and $HGeEt_3$ were followed by ^{1}H NMR in C_6D_6 (Figure 2-7, b and c). The peaks of hydrides were integrated against the BDI central proton peak. After the addition of ($^{i\text{Pr}}$BDI)Ir(H)$_4$ and $HSiEt_3$ in C_6D_6 deuterated solvent, complex started to display additional

hydride peaks while the 0-10 ppm region of the spectrum hardly changed. After two hours, the starting material was totally consumed and the integration indicates that the hydride number is three. Further adding of one more equivalent $HSiEt_3$ failed to produce dihydride iridium complexes presumably due to the steric hindrance of both the bulky $^{i\text{Pr}}$BDI ligand and the $HSiEt_3$ substrate. Indeed, earlier attempts to prepare ($^{i\text{Pr}}$BDI)Rh$(HSiEt_3)_2$ failed to produce any silane complexes.[5] Similarly, the reaction with $HGeEt_3$ produced a trihydride iridium complex of β-diiminate and failed to form dihydride product.

In contrast, when ($^{i\text{Pr}}$BDI)Ir$(H)_4$ was treated with 1 equivalent of HBPin in C_6D_6, the immediate ^{1}H NMR showed the formation of a trihydride complex **2.9** indicated by an additional hydride peak. After 5 min, ($^{i\text{Pr}}$BDI)Ir$(H)_4$ is almost consumed. Further adding of one more equivalent of HBPin results in the dihydride complex **2.10** and this new hydride peak was displayed beside the trihydride peak immediately. After 5 min, trihydride complex was nearly consumed.

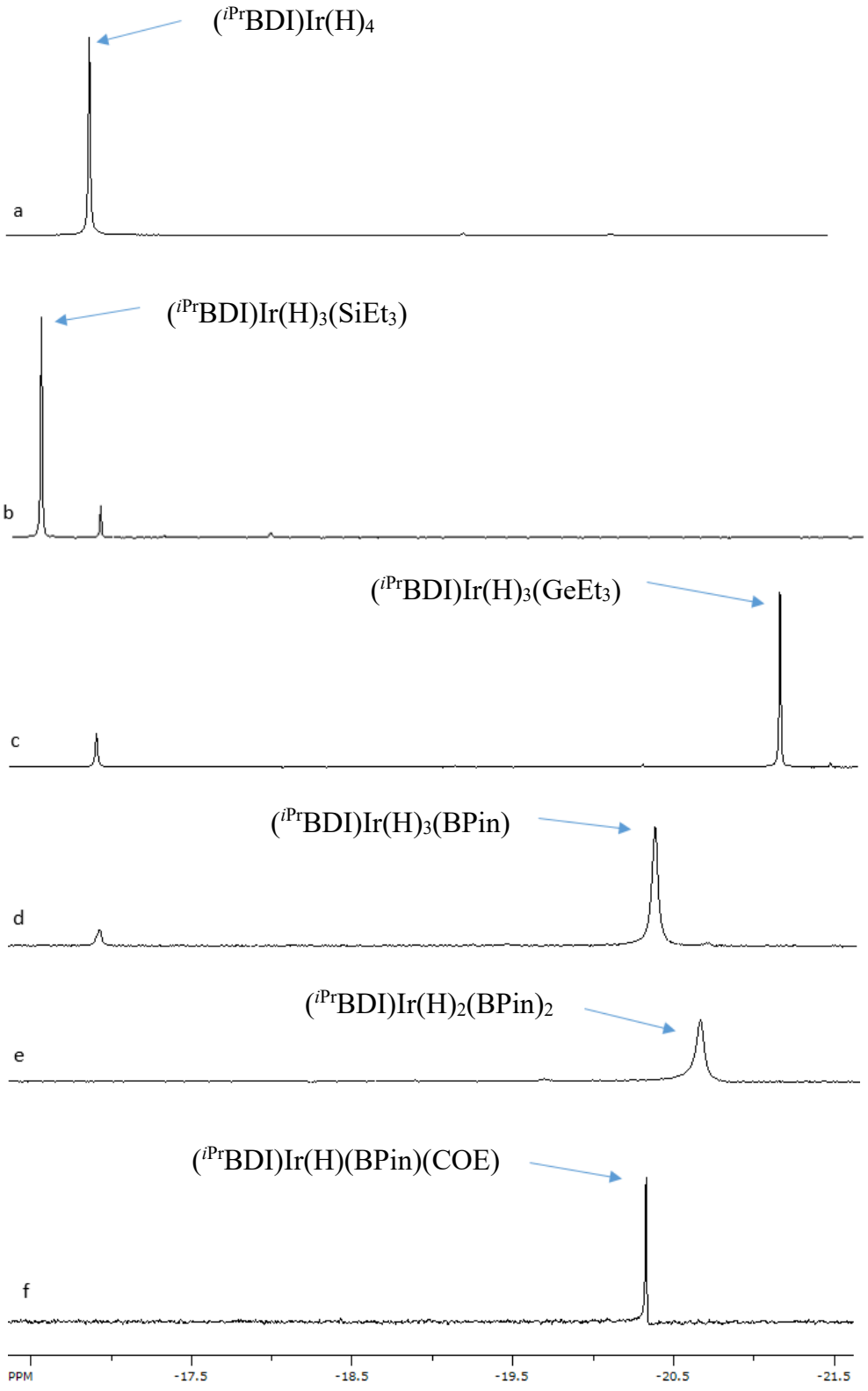

Figure 2- 7. Hydride region of (^{iPr}BDI)Ir(H)$_4$, 2.7, 2.8, 2.9, 2.10 and 2.11.

Compared to $HSiEt_3$ and $HGeEt_3$, the binding of HBPin is weaker and therefore a bis(HE) complex with Si rather than with B would normally be expected. However, B is sp^2 hybridized while Si is sp^3 hybridized in this case, thus HBPin might take up less space than $HSiEt_3$. Different from the broad hydride peaks of B-H in Rh cases, the hydride peaks of **2.9**, **2.10** and **2.11** (Figure 2-7, d, e, f) shown by ^1H NMR are much sharper, suggesting that they are close to the extreme oxidative addition side. Furthermore, ($^{i\text{Pr}}$BDI)Ir$(H)_4$ is an effective H/D exchange catalyst but the similar reactivity was never observed for bis(HE) adducts, presumably due to steric factors.

X-ray structure of **2.11** (Figure 2-8) showed that cyclooctene and BPin groups are both coordinating to the iridium center, thus it is noteworthy that the insertion of the hydride into the cyclooctene and the hydroboration of cyclooctene failed to take place. This complex is stable in both solution and solid state. The 16e electron count of iridium, the preference for +3 oxidation state and steric factors are presumably the main reasons for the stability of this complex. Crystallization of complexes **2.7**, **2.8**, **2.9** and **2.10** has not yet been tried due to the limited time.

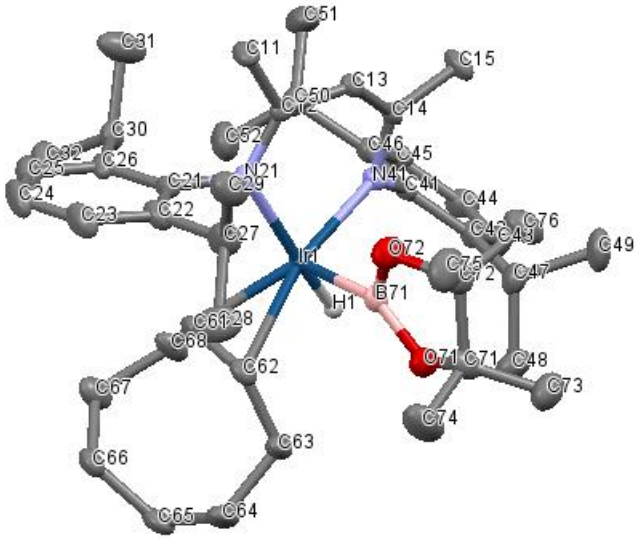

Figure 2- 8. Crystal structure of 2.11, showing thermal ellipsoids at 50% probability. All hydrogen atoms except hydride have been omitted for clarity.

Based on the synthesis of ($^{i\text{Pr}}$BDI)IrH_4, I have explored other ligands which have potential resulting in tetrahydride compounds. However, I have not yet found any β-diiminate ligands other than ($^{i\text{Pr}}$BDI) which form stable ($^{\text{R}}$BDI)IrH_4 complexes. The ligand variations have been used are ($^{\text{Me}}$BDI), ($^{\text{OMe}}$BDI), ($^{\text{Et}}$BDI), and ($^{t\text{Bu/Me}}$BDI). Activation of inert Sn-Sn bond was tried by the reaction of ($^{i\text{Pr}}$BDI)IrH_4 with $(CH_3)_3$Sn-Sn$(CH_3)_3$. No reactions were observed, unfortunately.

2.4 Ligand functionalization

Exploring the scope of BDI ligand functionalization is one of the motivations for studying HE adducts. The proposed path for the formation of the silane-functionalized ligand reveals that the reaction requires HE

dissociation, rearrangement and re-capture the HE group. We have attempted to achieve the same type of ligand functionalization using HSn^nBu_3, but the use of smaller amount of HSn^nBu_3 result in a messy mixture while the excess makes it difficult to dissociate. To circumvent this problem., we came up an idea reacting (^{Me}BDI)Rh(COE)(N_2) with $SnMe_4$ under a hydrogen atmosphere. $SnMe_4$ first adds to "(^{Me}BDI)Rh" followed by the addition of H_2 and elimination of methane through which way (^{Me}BDI)Rh(H)($SnMe_3$) was generated.

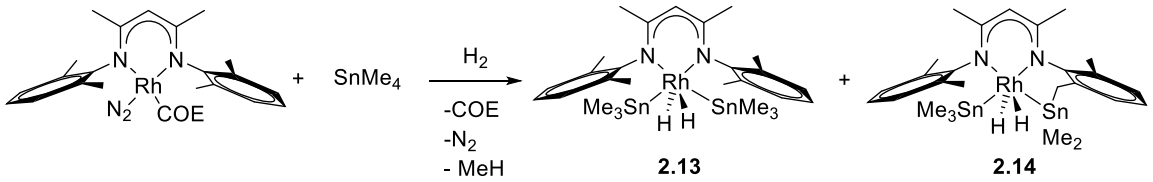

Scheme 2- 10. The reaction of (^{Me}BDI)Rh(COE)(N_2) with $SnMe_4$ and H_2.

To that end, Me_4Sn was reacted with (^{Me}BDI)Rh(COE)(N_2) in the presence of H_2 (Scheme 2-10). The hydride region of **2.14** shows broad peaks at room temperature which indicates complex **2.14** is fluxional, so it is necessary to cool down the samples to observe separate resonances and clear splitting patterns. Therefore, the products were further analyzed by VT (Variable Temperature) NMR (Figure 2-9). At all temperatures in VT NMR, complex **2.13** does not have temperature dependent NMR spectrum. It has shown equivalent hydrogens and they show equal coupling to the rhodium and two

tin atoms. Thus, we believe this complex has effective C_{2v} symmetry and the most reasonable assignment for this complex would be (^{Me}BDI)Rh($HSnMe_3$)$_2$. Complex **2.14** has two broad hydride peaks at room temperature which indicates two inequivalent hydrides. On cooling down the complex, the two signals become sharper. The splitting pattern reveals that they have coupling to Rh, to two tin atoms and to each other. From the ^{1}H NMR of 0-10 ppm region, it shows that the complex has no symmetry and one aryl methyl group is missing. Instead, a tin-bound CH_2 group has been formed. Thus, it seems reasonable that complex **2.14** is a ligand-functionalized version of **2.13**. In addition, the averaged J_{SnH} of **2.14** is 79 Hz which is significantly larger than that of **2.13** (J_{SnH}: 41 Hz) and it indicates that complex **2.14** is closer to σ-complex formation. Therefore, we have good evidence for the in situ generation of Me_3SnH complexes but the reaction is capricious and not easily reproducible, in part due to the volatility of $SnMe_4$ and difficulties in

controlling the amount of H_2 used.

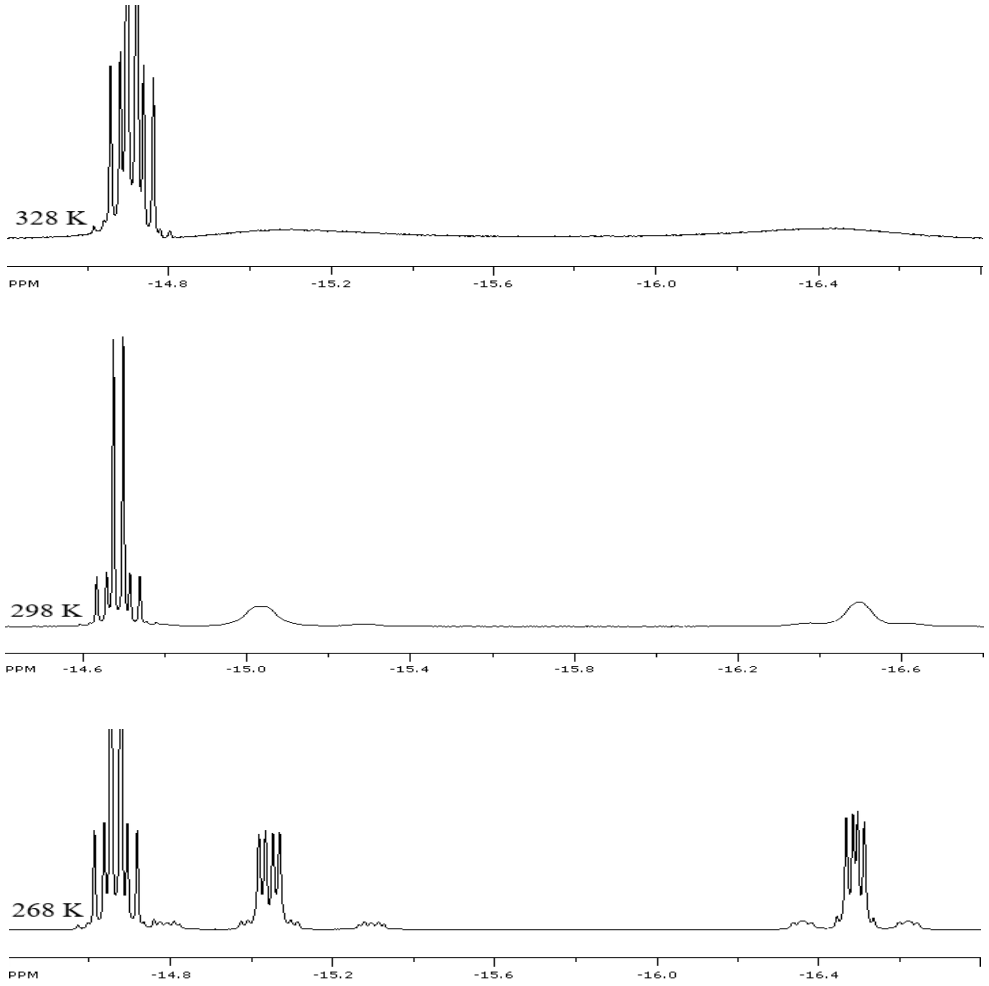

Figure 2- 9. VT NMR of the hydride region of the mixture of 2.13 and 2.14 in THF-d_8.

2.5 Steric limitation

Phosphorus compounds are good σ electron-donors as well as π acceptors.[33] Triphenylphosphine consists of phosphorus and arene rings which can both coordinate to the Rh center. However, molecular models indicate that the coordination of P to Rh might be impossible due to the

steric hindrance. Thus, we believe that it is interesting to determine which reaction would be preferred.

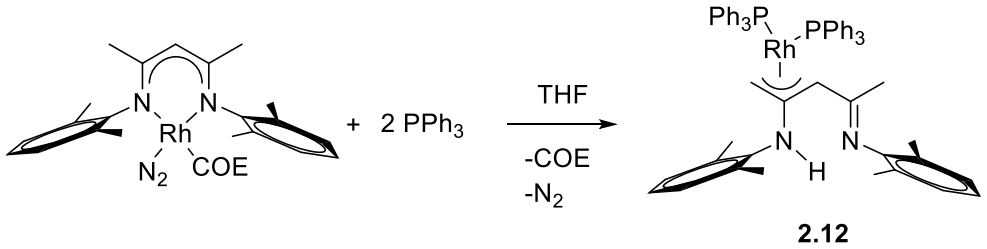

2.12

Scheme 2- 11. Reaction of (^{Me}BDI)Rh(COE) with PPh_3.

The reaction of (^{Me}BDI)Rh(COE)(N_2) with two equivalents PPh_3 was carried out in THF (Scheme 2-11). The reaction firstly produces a brownish solid and after four days at room temperature, it converts to the bright yellow solid which is the final product. Crystals of **2.12** were obtained from C_6D_6 in an NMR tube and the X-ray structure (Figure 2-10) shows the migration of the PPh_3 groups together with the metal atom. To the best of our knowledge, this is the first example that Rh center prefers to bind to the BDI carbon backbone instead of the nitrogen atom. Although we do not have concrete evidence, it seems possible that this ligand isomerization could on occasion be responsible for side reactions during the formation of HE complexes.

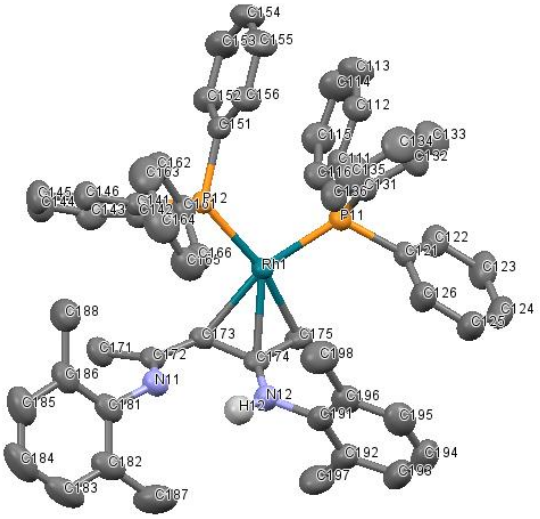

Figure 2- 10. Crystal structure of 2.12, showing thermal ellipsoids at 35% probability. All hydrogen atoms except N-H omitted for clarity.

Chapter 3

Low-coordinate paramagnetic Rh(II) complexes

3.1 Introduction

Unlike the +1 and +3 oxidation states of Rh which are widely and intensely studied, the +2 oxidation state is still uncommon. Rh(I) and Rh(III) complexes are usually diamagnetic while monomeric Rh(II) complexes are paramagnetic species. Unlike the 3d transition metals, the 4d/5d metals usually prefer closed-shell states. The unpaired electron in Rh(II) complexes makes it metalloradical and highly reactive, so they are typically unstable intermediates in reactions. Also, the unpaired electron is often partly delocalized over the ligands, which can result in ligand-centered radical type chemistry.[59-61]

Dimeric Rh(II) compounds usually have a metal-metal bond and are diamagnetic: the Rh(II) formal oxidation state is an artifact of the formal oxidation state rules, and the same compound but with the second Rh group replaced by a H atom would be assigned a Rh(III) oxidation state, despite having a very similar electronic environment. Thus, if a Rh(II) dimer has a Rh-Rh bond, it is electronically like any other diamagnetic Rh(III) complex.[62-65] However, if there is not a Rh-Rh bond, the situation is totally different and

in this case, each Rh center is like a monomeric paramagnetic Rh(II) complex. Diamagnetic rhodium(II) dimers with metal-metal bonds have been widely studied while the related paramagnetic compounds are rare.

For example, Rh(II) octaethylporphyrin (OEP) dimer was successfully synthesized.[66] This compound indeed has a Rh-Rh bond, but it easily dissociates because of steric strain. Thus, the dimer itself is not very reactive but it is in equilibrium with a highly reactive monomer and was found to be able to react with hydrosilanes resulting in an activation of the Si-H bond to give silylrhodium complexes of OEP. The reaction of this Rh(II) dimer with hydrostannanes gave a similar result (Equation 3-1).

$$2\ R^1{}_2R^2SiH + (OEP)Rh^{II}\text{-}Rh^{II}(OEP) \rightleftharpoons 2\ (OEP)Rh^{III}Si\ R^1{}_2R^2 + H_2$$
$$2\ R_3SnH + (OEP)Rh^{II}\text{-}Rh^{II}(OEP) \rightleftharpoons 2\ (OEP)Rh^{III}SnR_3 + H_2$$

Equation 3- 1.

Rh(II) porphyrin metalloradicals studied by the Wayland group have shown a variety of reactions including the selective activation of C-H, H-H and O-H bonds. For example, the monomeric tetramesitylporphyrinato (TMP) complex (TMP)-Rh(II) has a preference to react with alkane (sp^3) C-H bonds over aromatic (sp^2) C-H bonds.[67] The reaction of (TMP)-Rh with methane in benzene results in a C-H activation of the methane and the formation of equal quantities of (TMP)Rh-CH_3 and (TMP)Rh-H. Furthermore, the reverse

reaction (reductive elimination) to form methane and (TMP)Rh was also observed at 353 K. In contrast, C_6D_6 and C_6H_6 do not react with the same complex. Computational studies reveal that the formation of hydride and methyl derivatives went through a linear four-centered transition state in benzene (Figure 3-2).

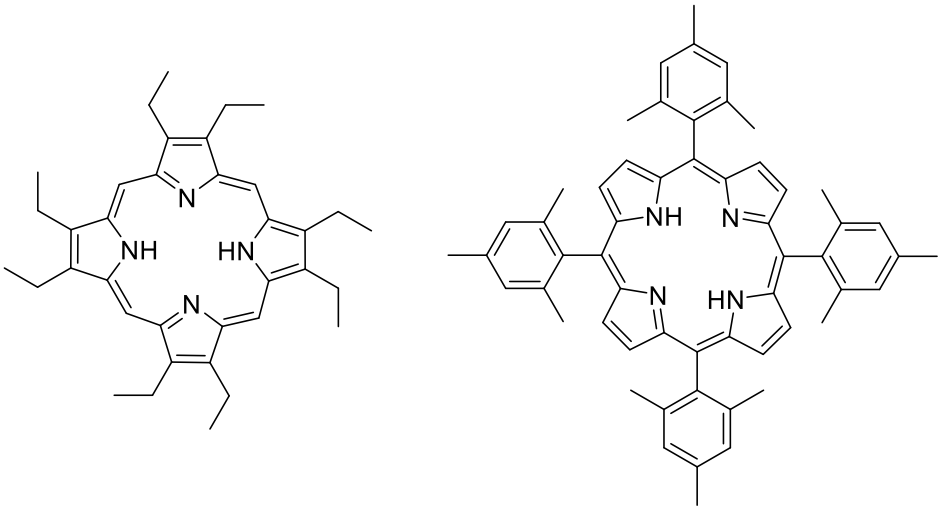

Figure 3- 1. The structure of octaethylporphyrin (OEP) (left) and tetramesitylporphyrin (TMP) (right).

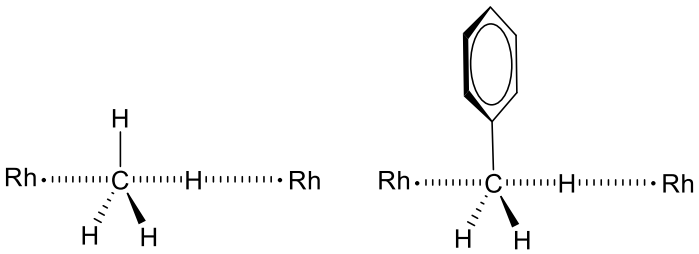

Figure 3- 2. Linear four-centered transition states for binuclear C-H activation.

Not surprisingly, the reaction with toluene (neat or in benzene) results in the formation of benzyl and hydride compounds (Equation 3-2) and there is

no evidence showing the activation of aromatic C-H bonds of toluene. It seems like the C-H bond strength is a key factor, that is, sp^2 C-H bond is stronger than sp^3 C-H bond, hence more difficult to break.

$$2(TMP)Rh + CH_4 \rightleftharpoons (TMP)Rh\text{-}H + (TMP)Rh\text{-}CH_3$$

$$2(TMP)Rh + CH_3C_6H_5 \rightleftharpoons (TMP)Rh\text{-}H + (TMP)Rh\text{-}CH_2C_6H_5$$

Equation 3- 2.

Since porphyrins (Figure 3-1) had been proved to be an excellent ligand to stabilize +2 oxidation state of rhodium, this sterically crowded ligand attracted a lot of interest.

Oxidative addition of O-H fragments to transition metal compounds is relatively rare and attracts new interest. The oxidative addition of water to a Rh(II) complex was reported by the Wayland group in 2006.[68] In 2007, the same group published an article demonstrating the oxidative addition of methanol to binuclear Rh(II) porphyrins which shows a competitive O-H and C-H bond activation.[69] Further research revealed that the different pathways depend on the concentration of the methanol (Scheme 3-1). At low methanol concentration, hydroxymethyl-hydride was turned out to be the exclusive product while H-OCH_3 bond activation was observed to form methoxide and hydride compounds at a high methanol concentration.

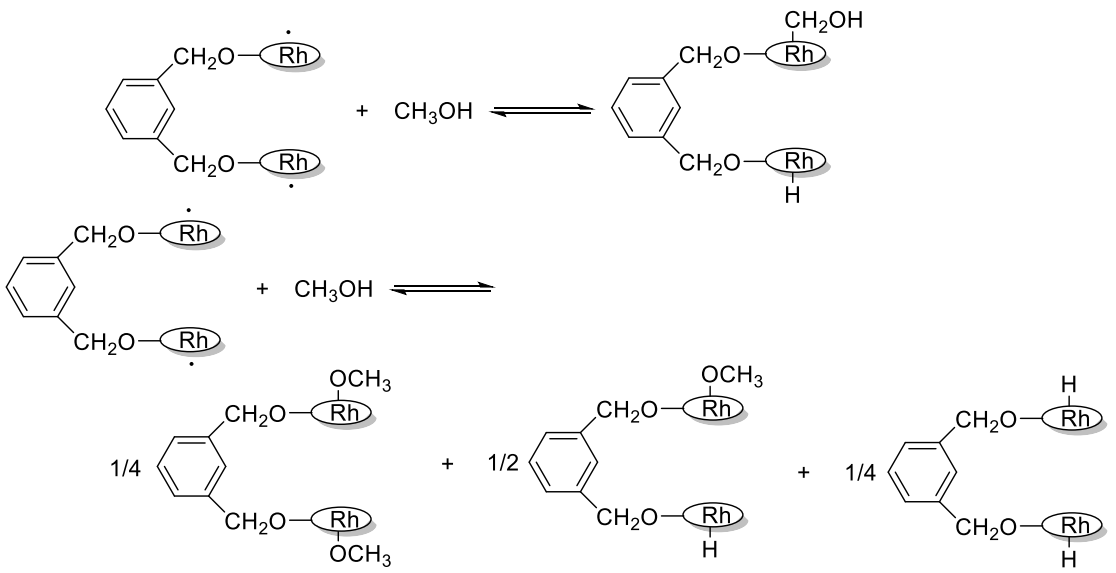

Scheme 3- 1. Different pathways depending on the concentration of the methanol. Low concentration (top) and high concentration (bottom).

From above mentioned Rh(II) monomers, we learn that bearing sterically crowded ligands is a key factor to stabilize Rh(II) oxidation state. Besides porphyrins, a few PNP type ligands also show high abilities to stabilize Rh(II) monomers (Figure 3-3).

PNP^{t}Bu (2,6-bis-(di-*tert*-butyl phosphino methyl)pyridine) has been reported to be a valuable ligand stabilizing Rh(II) monomers.[70] The complex (PNP^{t}Bu)RhCl [PNP^{t}Bu=2,6-bis-(di-*tert*-butylphosphinomethyl)pyridine] can react with silver salts AgX via anion metathesis (for coordinating anions X) and/or one-electron oxidation (for weakly coordination anions). Paramagnetic Rh(II) complex [(PNP^{t}Bu)RhCl][BF_4] was synthesized by the reaction of (PNP^{t}Bu)RhCl with $AgBF_4$ and has shown high reactivity towards

CO and phosphines. On the other hand, treatment of (PNP^{t}Bu)RhCl with one equivalent AgOC(O)CF_3 produced a diamagnetic (PNP^{t}Bu)RhOC(O)CF_3, but addition of a second equivalent of AgOC(O)CF_3 resulted in formation of the paramagnetic complex [(PNP^{t}Bu)Rh(OC(O)CF_3)][OC(O)CF_3]. Similar reactions involving the anionic PNP^{i}Pr ligand [PNP^{i}Pr=bis(2-di*iso*propylphosphino-4-methylphenyl)amido]resulted in a mixture of diamagnetic and paramagnetic compounds which illustrates the importance of sterically crowded ligands.

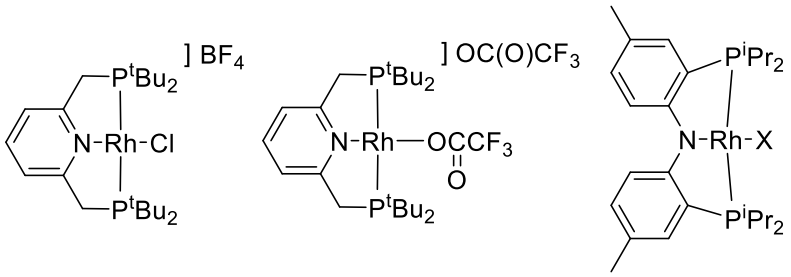

Figure 3- 3. Structures of [(PNP^{t}Bu)RhCl][BF_4] [(PNP^{t}Bu)Rh(OC(O)CF_3)][OC(O)CF_3] and [(PNP^{i}Pr)RhX].

In addition to porphyrin and PNP ligands, Rh(II) monomers bearing C_2-symmetric bisoxazoline and NCN pincer ligands have also been successfully isolated.

A C_2-symmetric bisoxazolinate Rh(II) complex was synthesized through disproportionation.[71] The group of Gal demonstrated that a rhodium(I) complex bearing anionic boxate ligand [Rh(*t*-Bu_2-boxate)(ethene)$_2$] can disproportionate spontaneously to a rhodium(II) complex and a black

precipitate of Rh(0). The reactivity of the Rh(II) complex is relatively low presumably due to the steric effect of the bulky *t*-butyl groups. A Rh(II) complex bearing the C_2- symmetric NCN pincer ligand 1,3-(S,S)-bis(oxazolyl-methyl)-4,6-dimethyl-benzene[72] was reported to have a 178.01(13)° N-Rh-N angle, resulting in close approach of the oxazolyl alkyl groups to the metal center which provides a sterically bulky environment (Figure 3-4). An analogous C_{2v} symmetric variation was also reported. These monomeric rhodium(II) complexes show unusually high stability and are stable in air at room temperature.

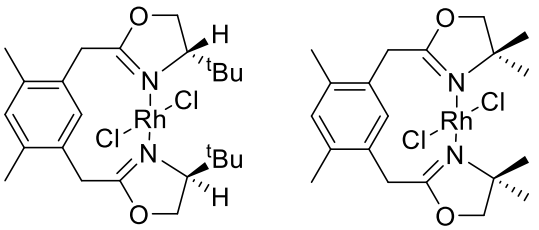

Figure 3- 4. Rh(II) complexes stabilized by C_2 (left) and C_{2v} (right) symmetry NCN pincer ligands.

Compared to Rh(II), isolation of Ir(II) monomers is even more difficult. An Ir(II) complex stabilized by a tetradentate pyridinophane ligand has been reported.[61]

β-diiminate rhodium(II) dimers without metal-metal bonds were firstly reported in 2015.[73] $[(^{Me}BDI)Rh]_2(\mu\text{-}Br)_2$ was synthesized by the reaction of $(^{Me}BDI)Rh(COE)(N_2)$ with bromine (Scheme 3-2); the iodide could be

prepared similarly. The ^{1}H NMR spectrum of $[(^{Me}BDI)Rh]_2(\mu\text{-}Br)_2$ shows broad and strongly shifted peaks (including one at 250 ppm) indicative of paramagnetism. If this complex had a metal-metal bond, one would expect it to be diamagnetic. Thus, the paramagnetic shifts suggest that one (or more) of the following applies (Figure 3-5):

1. There is a fast equilibrium between dimer and (paramagnetic) monomer
2. There is a fast equilibrium between singlet (diamagnetic) and triplet (paramagnetic) dimers
3. The dimeric compound is a pure triplet (i.e. without Rh-Rh bond)

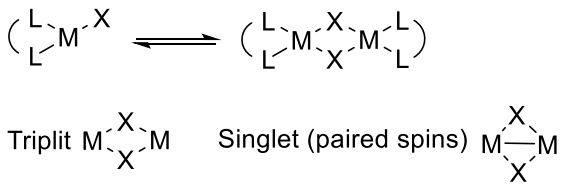

Figure 3- 5. Transformation possibilities of β-diiminate rhodium(II) dimers in solution.

Possibility 1 is particularly interesting because it implies we might have access to relatively open and presumably reactive (^{Me}BDI)RhBr monomer. Based on this, we have come up with an idea turning this dimer to monomeric complexes by replacing the bridging halides by more bulky bridging groups. Substituted anilides seemed a good choice because substituents at the 2 and 6 positions can be used to fine-tune steric bulk, and a wide variety of such substituted anilines is commercially available. Last but not the least, anilide

or amido complexes of late transition metals are key intermediates in catalysis such as hydrogenation[74] and hydroamination,[75] so there is potential for catalysis here.

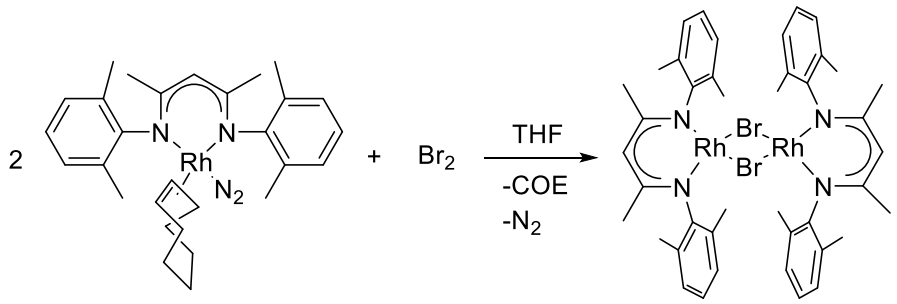

Scheme 3- 2. Synthesis of $[(^{Me}BDI)Rh]_2(\mu\text{-}Br)_2$.

Based on this idea, Zhu carried out preliminary experiments reacting $[(^{Me}BDI)Rh]_2(\mu\text{-}Br)_2$ with lithium 2,6-dimethylanilide and lithium 2,6-diisopropylanilide. The reactions seemed to lead to paramagnetic, monomeric and highly reactive compounds that were unfortunately not easy to isolate and characterize.[76] In the present work, we continue this exploration through systematic variation of the Li anilide component, eventually arriving at several structurally characterized Rh-anilide derivatives.

3.2 Synthesis of T-shape Rh(II) anilide complex

The first attempt was the reaction of $[(^{Me}BDI)Rh]_2(\mu\text{-}Br)_2$ with lithium 2,6-diisopropylanilide. It was hoped that the isopropyl groups are bulky enough to avoid Rh(II) center being attacked by other species and not too bulky to

prevent the anilide from getting bound to the Rh(II) center.

Lithium 2,6-diisopropylanilide was synthesized by the reaction of 2,6-diisopropylaniline with 1 equivalent of n-BuLi in THF (Scheme 3-3).[77, 78] After stirring under argon for 1 h at room temperature, THF was removed and the solid was washed by hexane. After filtration, the solid was dried and used for the next reaction. Other lithium anilides used in this thesis were synthesized in the same way.[79-81] For lithium 2,6-diisopropylanilides synthesized in this thesis, there is one THF molecule coordinating to the Li atom in the structure while for unsubstituted lithium anilide and lithium 2,6-dimethylanilide, there is no THF coordinating to it.

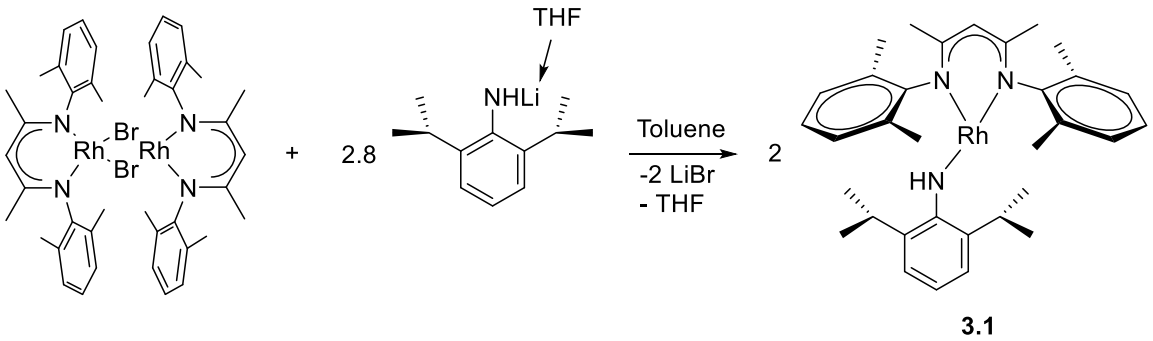

Scheme 3- 3. Synthesis of 3.1.

When [(^{Me}BDI)Rh]$_2$(μ-Br)$_2$ was treated with 2.8 equivalents of lithium 2,6-diisopropylanilide, the solution color turned from green to bright blue immediately. Solvent was removed *in vacuo* immediately and the immediate ^{1}H NMR (Figure A-19) indicates that there is a main paramagnetic complex

together with a small amount of diamagnetic compound. The blue solid was extracted with hexane and blue crystals of **3.1** were obtained over a weekend at -35 ℃. The X-ray structure (Figure 3-6) shows the three-coordinate T-shape geometry of this complex with a N(3)-Rh(1)-N(4) angle of 94.07(10)°. Compared to other β-diiminate metal amides or anilides which commonly assume to a Y-shape,[82] agostic interaction might be a factor resulting in this T-shape geometry.

The distance between the isopropyl methine H atom and the Rh(II) center is ~1.96 Å (Rh(1)-H(38)) which is much shorter than the Fe-H distance in the analogous complex ($^{i\text{Pr}}$BDI)FeNH(2,6-^{i}Pr$_2$C$_6$H$_3$) (2.6 Å).[83] This suggests the presence of a relatively strong agostic interaction in our Rh complex. The compound is stable in solid state while it rearranges to a diamagnetic compound in solution over a few hours.

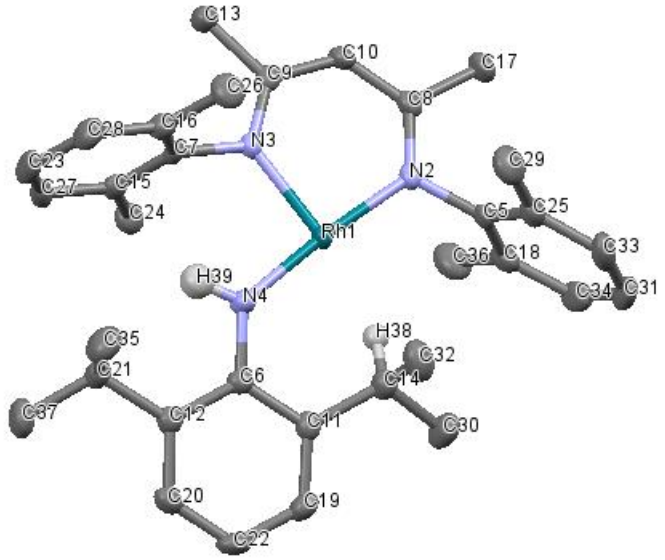

Figure 3- 6. Crystal structure of 3.1, showing thermal ellipsoids at 30% probability. All hydrogen atoms except NH have been omitted for clarity.

EPR measurements were carried out by Bas de Bruin at the University of Amsterdam (The Netherlands). Figure 3-7 shows both the low-temperature (toluene glass) and room temperature (solution) spectra. Both spectra show the presence of one main component (broad, with clear g anisotropy) and a smaller amount of an impurity with a relatively narrower spectrum. The spread in g values of the main component implies that there is significant spin density at Rh suggesting that **3.1** has metalloradical character.

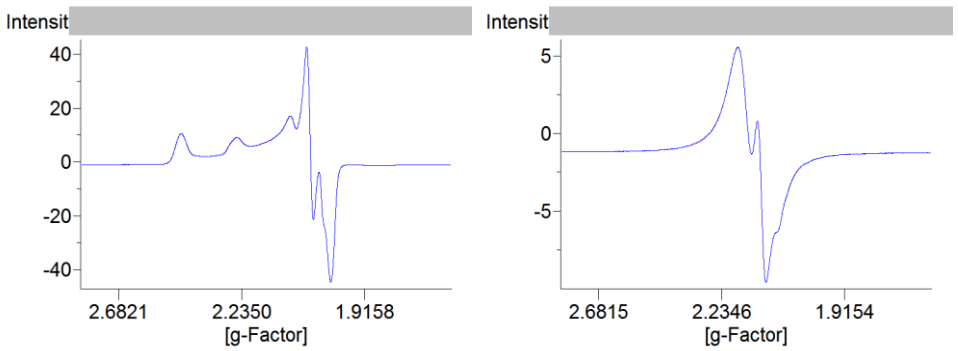

Figure 3- 7. EPR spectra of 3.1; left: toluene glass, 20 K; right: room temperature, toluene solution. Experimental X-band EPR spectra were recorded at 20 K on a Bruker EMX spectrometer equipped with a Bruker temperature control cryostat system coupled to a He-liquefier, using a frozen solution (glass) of X in toluene. The spectra were simulated by iteration of the anisotropic g-values, (super)hyperfine coupling constants, and line widths using the EPR simulation program W95EPR developed by Prof. dr. Frank Neese.

3.3 C-H activation

Proven by the result above, steric hindrance of the isopropyl groups is a key factor stabilizing the Rh(II) anilide complex of β-diiminate, despite the isolated Rh(II) monomer is not very stable in solution. To explore the effect of decreased steric hindrance, the reaction with lithium 2,6-dimethylanilide was carried out.

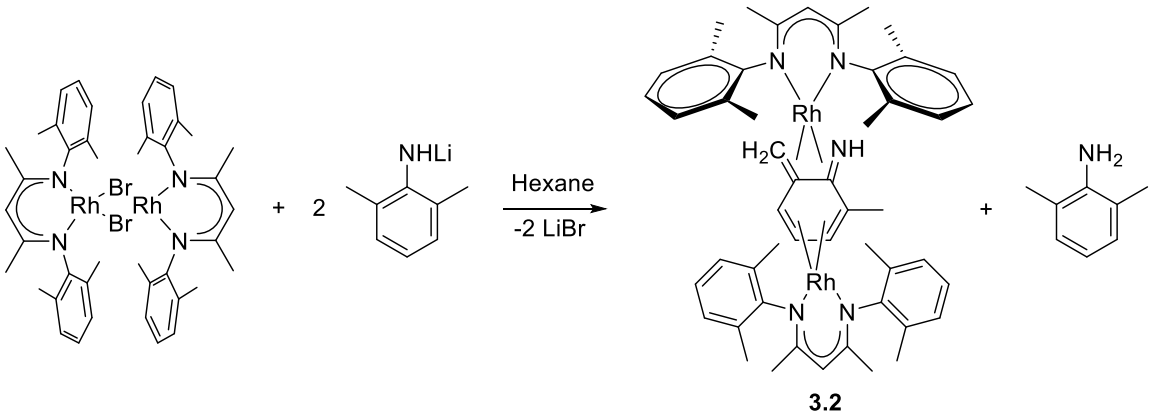

3.2

Scheme 3- 4. Formation of 3.2 through a C-H activation in hexane.

When $[(^{Me}BDI)Rh]_2(\mu\text{-}Br)_2$ was treated with lithium 2,6-dimethylanilide in hexane (Scheme 3-4), similarly, the solution color turned from green to bright blue immediately and the immediate ^1H NMR showed the presence of an Rh(II) product analogous to **3.1**. However, after a few hours at room temperature, the solution color turned from blue to red. After total 16.5 hours, solvents were removed *in vacuo* and the solid was extracted from toluene and then layered with hexane. Red crystals of **3.2** were obtained after 48 hours and the X-ray structure (Figure 3-8, a) shows a diamagnetic Rh compound which is the result of the benzylic C-H activation of the anilide. It is notable that one (BDI)Rh fragment is η^4-coordinated to the arene of the anilide and the oxidation state of the up Rh is +1 with the coordination of the N=C-C=C fragment. The bond lengths of N(5)-C(51), C(51)-C(56) and C(56)-C(58) are 1.327(7), 1.453(7) and 1.388(7) Å, respectively, suggesting that there are comparable contributions from two resonances structures

(Scheme 3-5).

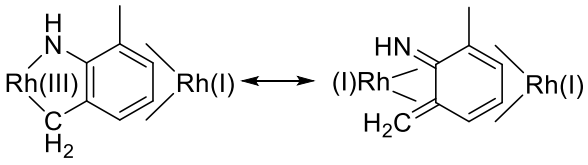

Scheme 3- 5. Resonance structures.

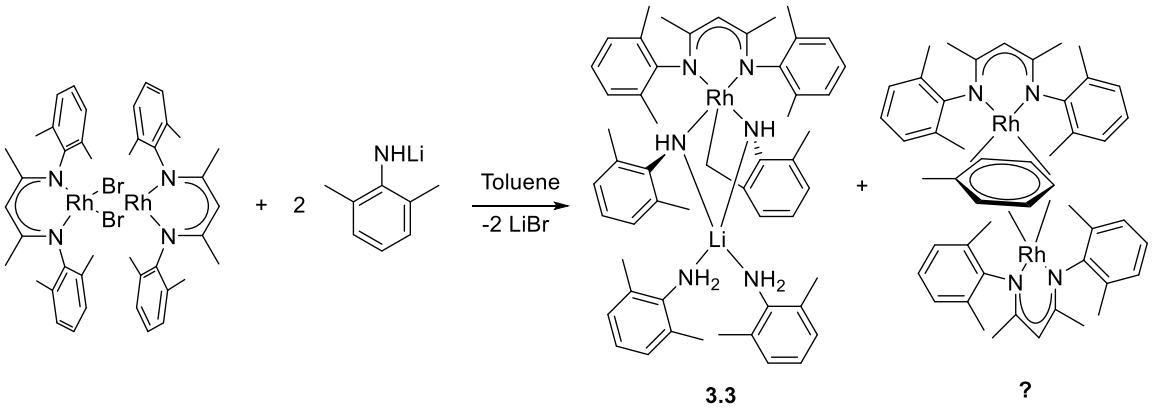

Scheme 3- 6. Formation of 3.3 through a C-H activation in toluene.

Interestingly, when the reaction was carried out in toluene instead of hexane, the result is different (Scheme 3-6). After 1 hour stirring in toluene, the solution color turned into red. Solvent was removed *in vacuo* and the immediate ^{1}H NMR shows there is another new diamagnetic complex. Yellow crystals of **3.3** were obtained from pentane with two drops toluene at -35 °C. X-ray structure (Figure 3-8, b) shows a similar CH activation as complex **3.2** and the formation of the new Rh-C bond. Each N atom of the anilide is bound by a proton and the N(3)-Rh(1) is a dative bond while N(4)-Rh(1) is a covalent bond, suggesting the oxidation state of the Rh is +3. Different from the reaction in hexane which resulted in a Rh(I) dimer, the product from the

reaction in toluene is a Rh(III) monomer. As mentioned earlier in the thesis, (^{R}BDI)Rh(I) is very likely to be coordinated by aromatic solvents which was toluene in this case. Therefore, the reaction shown in Scheme 3-5 is likely to have happened.

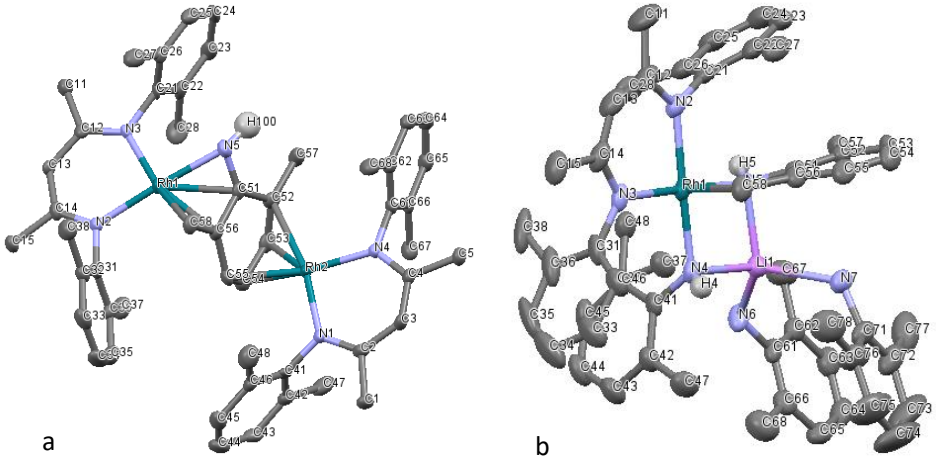

Figure 3- 8. Crystal structure of 3.2 (a) and 3.3 (b), showing thermal ellipsoids at 30% probability. All hydrogen atoms except NH have been omitted for clarity.

A possible mechanism was studied using DFT by Dr. Budzelaar. Presumably, a hydrogen atom was abstracted by one molecule of the Rh(II) monomer from a second one, generating intermediate **A** which contains an aza-xylylene unit. In hexane, **3.2** was generated by the migration of the (^{Me}BDI)Rh fragment now bound to the N atom of dimethylaniline to the arene ring of the aza-xylylene unit (Scheme 3-7).

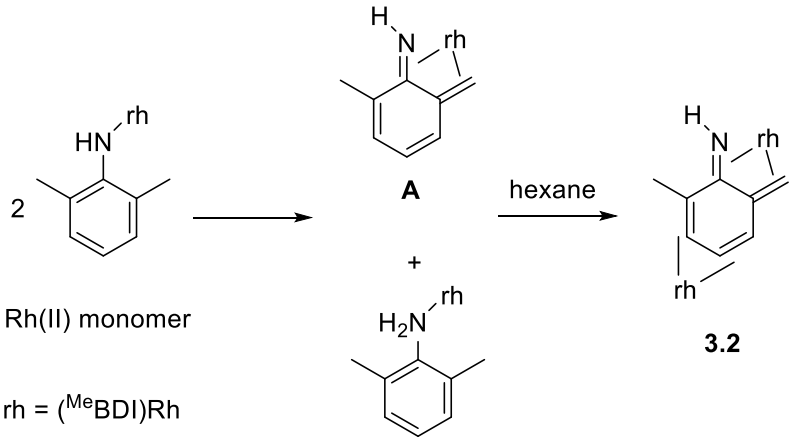

Scheme 3- 7. Possible pathway leading to 3.2 in hexane.

3.4 C-N bond formation

Encouraged by the interesting result obtained with lithium 2,6-dimethylanilide, we decided to reduce steric hindrance even further, using the Li salt of unsubstituted aniline (Scheme 3-8).

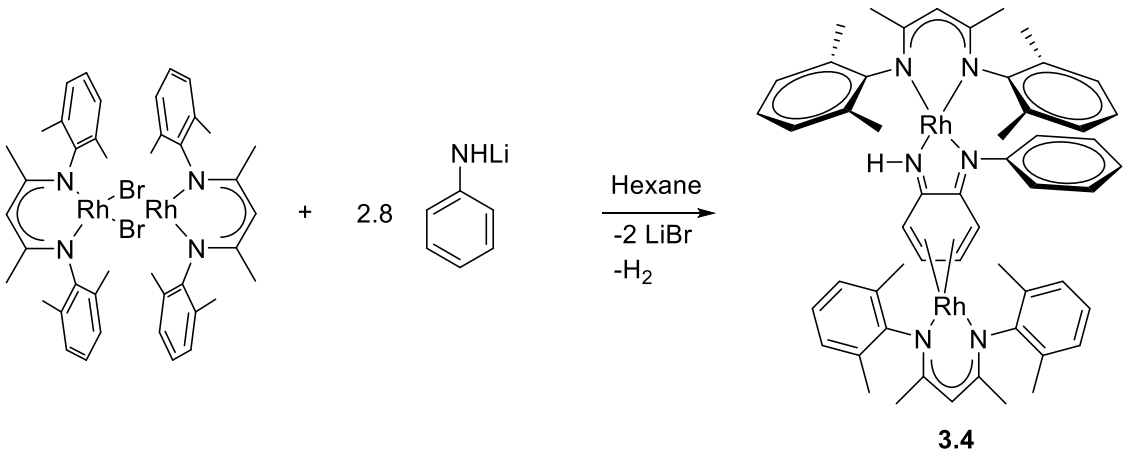

Scheme 3- 8. Formation of 3.4 through a C-N bond formation.

Different from the color change of the above two reactions, the solution color turns from green to dark blue after 50 min. Solvent was removed *in*

vacuo and an immediately recorded ^{1}H NMR (Figure 3-9, a) spectrum shows a main paramagnetic complex together with a diamagnetic asymmetric complex. After 2 h, the broad paramagnetic peaks were gone and the asymmetric compound remained. After standing overnight, ^{1}H NMR indicated that a new symmetric complex had formed and the asymmetric compound could not be observed any more (Figure 3-9, b).

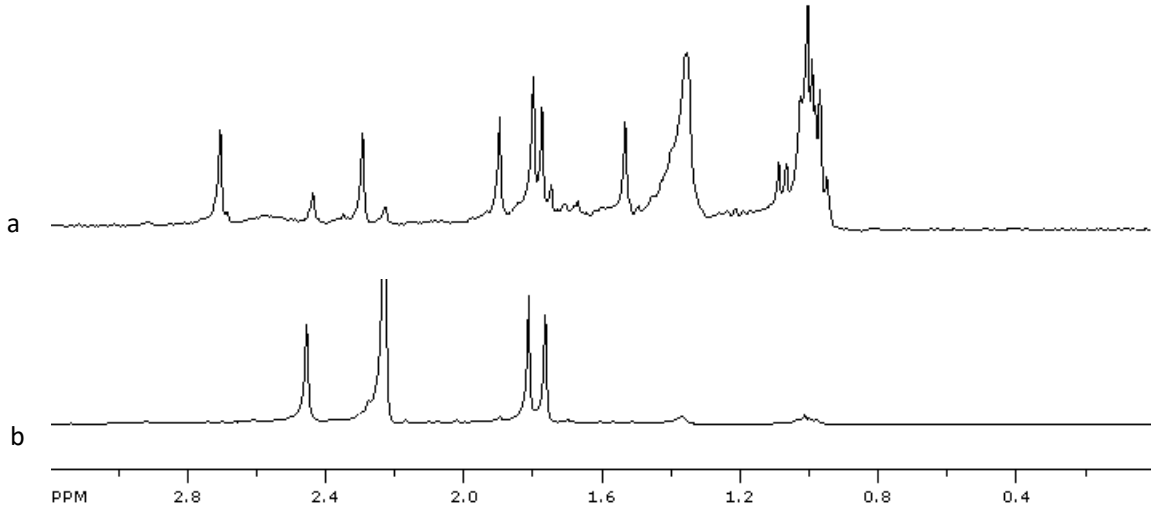

Figure 3- 9. Aliphatic region of the asymmetric complex and the symmetric complex.

The dark blue solid was extracted with pentane. Black crystals of **3.4** were obtained after weeks and the X-ray structure (Figure 3-11) shows a binuclear complex. A sp^2 C-H bond of the arene ring has been activated and a new C-N bond has been formed.

The presence of a hydrogen atom at N(3) was inferred from:

a) The diamagnetic nature of the complex, which gives clean and sharp

NMR spectra

b) DFT calculations which produce closer agreement with the X-ray structure with than without that hydrogen

c) Successful refinement of a hydrogen atom at this position

In the X-ray structure, one (BDI)Rh fragment is η^4-coordinated to the newly formed phenylenediamine ligand, while the second fragment is κ^2: N,N bound to the same ligand. The bond lengths of N(3)-C(2) and N(4)-C(1) are 1.314(5) Å and 1.334(5) Å which are between the lengths of N-C single and double bonds and indicate that there are comparable contributions from two resonances structures (Figure 3-10).

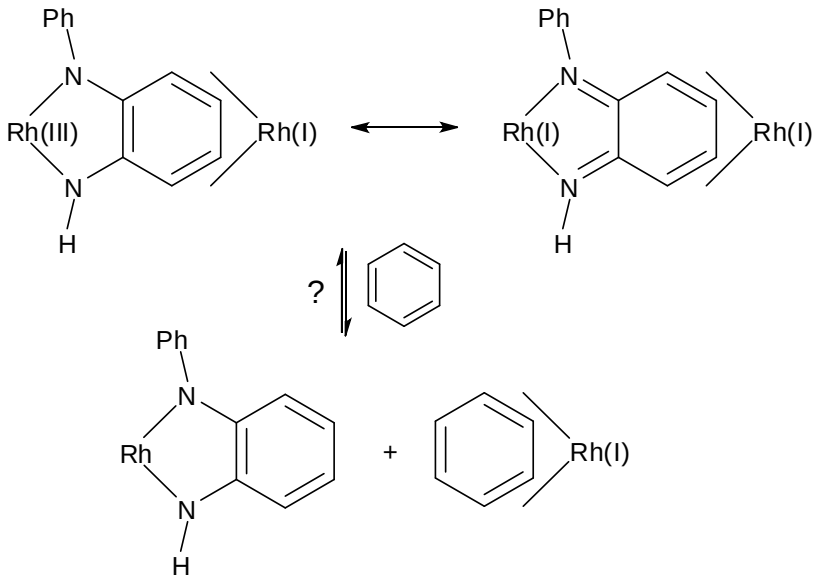

Figure 3- 10. Resonances structures and the possible exchange with benzene.

When dissolved in hexane or pentane, the whole structure stays stable and the solution color remains dark blue, while in toluene and benzene, the

solution turns in red immediately. We suspect that the arene-bound (BDI)Rh fragment easily exchanges with the arene solvent.

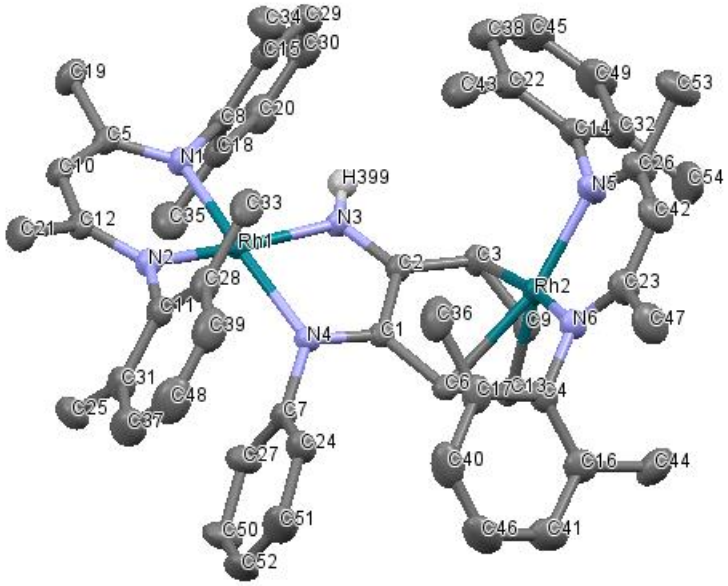

Figure 3- 11. Crystal structures of 3.4, showing thermal ellipsoids at 30% probability. All hydrogen atoms except NH have been omitted for clarity.

Mechanism was studied by DFT. Both ^{1}H NMR and DFT suggest that the immediate reaction results in a Rh(II) metalloradical and then the N atom of another anilide binds to both Rh and the *ortho*- carbon of the first anilide. Transfer of protons to the Rh followed by the loss of one equivalent hydrogen eventually produce the final product (Scheme 3-9).

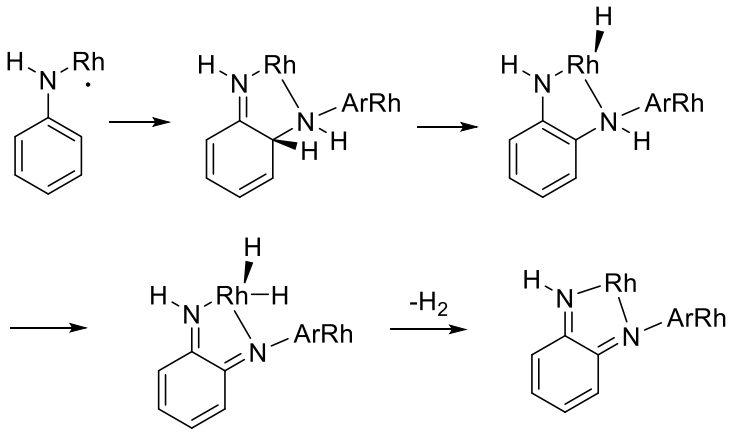

Scheme 3- 9. Proposed mechanism for C-N bond formation.

The C-N formation of aniline achieved by this reaction is remarkable because carbon-nitrogen formation reaction in aniline is an important reaction in synthesizing aromatic compounds which has a variety of functions in medicines and materials.[84-86]. Similar C-N coupling of aniline using Ru as the metal center was achieved by Goswami's group.[87] The coordination form of C=C-C=C by a 1,3-diene to β-diiminate Rh center was reported in 2016.[88] Interestingly, in this work, complex **3.4** gives us the clear evidence of N=C-C=N coordination and the complex **3.2** mentioned in C-H activation part shows C=C-C=N coordination form. Similar to the products of the reaction with lithium 2,6-dimethylanilide, products of this reaction depend on solvents and reaction time.

3.5 Further reactions of amides

Similar Rh(II) intermediates were observed by ^{1}H NMR from the reactions

of $[(^{Me}BDI)Rh]_2(\mu\text{-}Br)_2$ with lithium 2,4,6-trimethylanilide, lithium 2-*tert*-butylanilide and lithium 2,6-diethylanilide. However, due to the highly reactive nature of the Rh(II) species formed, these paramagnetic intermediates were too reactive to isolate and converted to diamagnetic complexes within hours. Attempts at isolating well-defined complexes failed. In addition, the reactions of $[(^{Me}BDI)Rh]_2(\mu\text{-}Br)_2$ with aliphatic amides were tried. The reactions with lithium diisopropylamide (LDA) and potassium bis(trimethylsilyl)amide both went through a paramagnetic compound before rearranging to a diamagnetic compound. Research is still underway.

3.6 β-diiminate Rh bipyridine complexes

3.6.1 Synthesis of (^{Et}BDI)Rh(2,2'-bipyridine) and (^{Me}BDI)Rh(2,2'-bipyridine)

Rh(III) complexes Cp^*RhX_2 have shown high reactivity towards C-H activation and C-C bond formation reactions.[3, 89, 90] Halide-bridged dimer $[(Cp^*)Rh]_2(\mu\text{-}I)$ was reported in 1979[91] and it also has high reactivity activating strong C-H bonds. To explore the scope of related BDI ligand chemistry, Zhu carried out the reaction of $[(^{Me}BDI)Rh]_2(\mu\text{-}Br)_2$ with 2,2'-bipyridine (bipy) aiming to synthesize (^{Me}BDI)RhBr(bipy) which would presumably be a Rh(II) monomer. It should be noted here that bipy is electronically similar to the α-diimine ligand formed through C-N coupling of

two anilides as described in section 3.3 above.

When $[(^{Me}BDI)Rh]_2(\mu\text{-}Br)_2$ was treated with 2 equivalents of bipy, the solution color changed from green to brown-yellow immediately. After removing all the solvent, ^1H NMR showed no paramagnetic shifted/broadened peaks (Figure A-22). Crystals of Rh(I) complex $(^{Me}BDI)Rh(bipy)$ were grown from THF at -35 °C overnight.

It is likely that a disproportionation is involved in this reaction (Equation 3-3).

$$[(^{Me}BDI)Rh]_2(\mu\text{-}Br)_2 + 2\ bipy \rightarrow (^{Me}BDI)Rh(bipy) + (^{Me}BDI)Rh(bipy)(Br)_2$$

Equation 3- 3.

Since one of the products is a diamagnetic Rh(I) complex, we checked whether the same compound could be synthesized from $(^{Me}BDI)Rh(COE)(N_2)$ which is a cheaper and more easily accessible starting material (Scheme 3-10). When $(^{Me}BDI)Rh(COE)(N_2)$ was treated with bipy, the solution color changed to the same brown-yellow color mentioned above and ^1H NMR (Figure A-22) showed clean formation of the expected product.

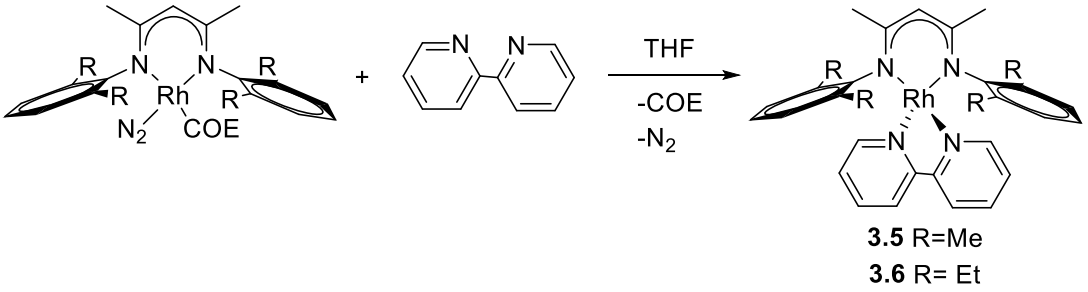

Scheme 3- 10. Synthesis of 3.5 and 3.6 from (^{R}BDI)Rh(COE)(N_2).

Similarly, **3.6** was successfully synthesized by the reaction of (^{Et}BDI)Rh(COE)(N_2) with 2,2'-bipyridine and black crystals were obtained from THF at -35 ℃ overnight (Scheme 3-10). The geometries of these two compounds (determined by X-ray structures) are halfway between square planar and tetrahedral, with approximate C_2 symmetry (Figure 3-12). ^{1}H NMR (Figure A-22 and Figure A-24) spectra have only shown one type of methyl group and ethyl group, respectively. Thus, both complexes are dynamic with fast flipping of the bipy group between its two tilted orientations.

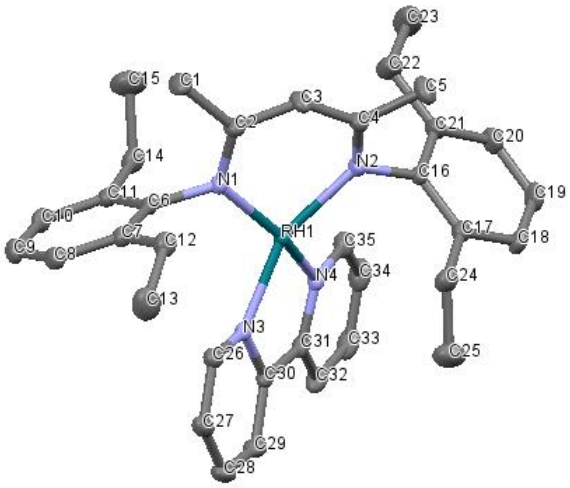

Figure 3- 12. Crystal structures of 3.6, showing thermal ellipsoids at 30% probability. All hydrogen atoms have been omitted for clarity.

3.6.2 The reaction of (^{Me}BDI)Rh(2,2'-bipyridine) with Br_2 and I_2

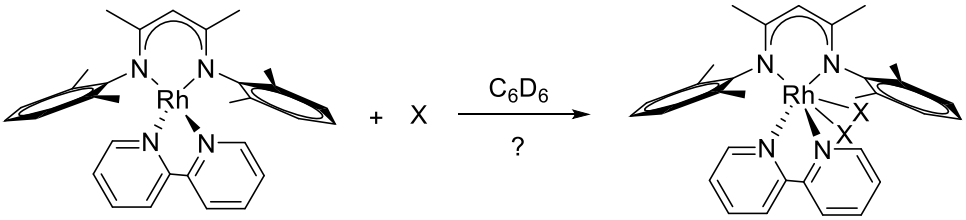

3.7 X=Br_2
3.8 X=I_2

Scheme 3- 11. Synthesis of 3.7 and 3.8.

Starting from the Rh(I) bipy adducts, Rh(III) complexes were expected to be synthesized by the reactions with Br_2 and I_2 (Scheme 3-11). Reactions were initially carried out on an NMR scale. When (^{Me}BDI)Rh(2,2'-bipyridine) was treated with Br_2 in C_6D_6 in an NMR tube, the immediately recorded ^{1}H NMR spectrum (Figure A-26) indicated a new diamagnetic rhodium complex had formed which is highly asymmetric. In a large scale, the product solid was

extracted with THF and after centrifuging, the red THF solution was layered with pentane at -35 ℃ overnight. A red crystalline solid precipitated but the quality was not good enough for a single-crystal X-ray structure determination. Unfortunately, attempts to grow larger crystals were not successful. The analogous reaction of (^{Me}BDI)Rh(bipy) with I_2 gave a similar asymmetric spectrum (Figure A-27) but attempts to grow crystals also failed here. It is likely that both structures have octahedral geometries in which iodine and bromine atoms are in *cis*- position. Similar reactions with (^{Et}BDI)Rh(bipy) resulted in messy spectra, presumably due to the steric hindrance of the ethyl groups.

Chapter 4

Experimental Methods

4.1 General Procedures

All synthesis (except for the free BDI ligands) were performed under argon with Schlenk techniques or in a nitrogen-filled glovebox. Solvents were distilled from Na/benzophenone. Related chemicals were purchased from Sigma-Aldrich and used as received. $[Rh(COE)_2Cl]_2$ was purchased from Strem Chemicals.

4.2 Instrumentation

All NMR spectra were recorded on Bruker Avance 300 MHz or Bruker Avance III 500 MHz spectrometers. Spectra were run with C_6D_6, C_6D_{12}, $C_6D_5CD_3$ or C_4D_8O as indicated and calibrated with the corresponding reference peaks.[92] All chemical shifts are in ppm and all *J* coupling in Hz. All carbon spectra were done with proton decoupled ($^{13}C\{H\}$).

4.3 Synthesis of (^{Et}BDI)Rh(HSiEt$_3$)$_2$ (2.1)

A solution of (^{Et}BDI)Li(THF) (100 mg, 0.23 mmol) in THF was added to a solution/suspension of $[Rh(COE)_2Cl]_2$ (81 mg, 0.12 mmol) in THF. All solids

dissolved, producing a dark brown solution. All solvents were evaporated *in vacuo* and the solid was extracted with hexane in a nitrogen-filled dry-box. After removal of solids by centrifugation, $HSiEt_3$ (79 mg, 0.68 mmol) was added to the hexane solution, which was stirred for 5 minutes. Solvents were removed *in vacuo*, and the residue was crystallized from $^{i}Pr_2O$ (25 / -35 °C), producing a dark green crystalline solid. The mother liquor was removed and the solid was washed with cold hexane and dried, leaving 0.066 g (42%) of **2.1**.

^{1}H NMR (THF-d_8, 300 MHz): δ 7.15-7.00 (6H, m, *m*, *p*), 5.22 (1H, s, *3*), 2.7-2.9, 2.4-2.6 (4H each, m, ArCH_2), 1.70 (6H, s, *1*), 1.24 (12H, t, *J* 7.6, $ArCH_2CH_3$), 0.70 (30H, br s, Si*Et*), -14.82 (2H, d, J_{Rh} 20.7, Rh*H*).

^{13}C NMR (THF-d_8, 75 MHz): δ 160.8, 156.0 (*2*, *i*), 136.2 (*o*), 125.7 (*m*), 125.3 (*p*), 99.3 (J_{Rh} 1.1, *3*), 25.5 ($ArCH_2$), 22.9 (*1*), 13.4 ($ArCH_2CH_3$), 13.0, 9.3 (Si*Et*).

Anal. Calcd. for $C_{37}H_{65}N_2RhSi_2$ (697.02): C, 63.76; H, 9.40; N, 4.02. Found: C, 63.53; H, 9.48; N, 3.87.

4.4 Synthesis of (^{Me}BDI)Rh(HBPin)$_2$ (2.2)

In a N_2-filled dry box, $[Rh(COE)_2Cl]_2$ (0.20 g, 0.55 mmol) was weighed into a small vial. (^{Me}BDI)Li(THF) (0.21 g, 0.55 mmol) was weighed into a 25 mL

Schlenk tube and dissolved in 10 mL dry THF. The solution was added to the $[Rh(COE)_2Cl]_2$. After all solids had dissolved, the resulting dark brown solution was transferred back into the Schlenk tube. Solvent was evaporated *in vacuo*, the dark purple solid was extracted with hexane in a N_2-filled dry-box and solids were removed by centrifugation. 0.25 ml HBPin (1.67 mmol, 3.0 eq.) was added. After 5 min stirring at room temperature, the mixture was evaporated to dryness. The residue was washed with hexane; the remaining solid was dissolved in THF/Hexane (1:3) and cooled to -35 °C, producing a yellow crystalline solid. The mother liquor was removed and the solid was washed with cold hexane, leaving 0.164 g (44%) of **2.2**. The compound decomposes in solution at room temperature in about one day.

^{1}H NMR (cyclohexane-d_{12}, 500 MHz): δ 6.94 (4H, d, *J* 7.4, *m*), 6.84 (2H, t, *J* 7.4, *p*), 5.15 (1H, s, *3*), 2.37 (12H, s, *o-Me*), 1.72 (6H, s, *1*), 1.06 (24H, s, BPin *Me*), -13.36 (2H, br d, J_{Rh} 25, Rh*H*).

^{13}C NMR (cyclohexane-d_{12}, 125 MHz): δ 160.9, 158.8 (*2* and *i*), 133.4 (*o*), 129.3 (*m*), 125.7 (*p*), 99.5 (J_{Rh} 2.5, *3*), 84.5 (O*C*), 26.0 (BPin *Me*), 23.9 (*1*), 21.3 (*o-Me*).

^{11}B NMR (Cyclohexane-d_{12},): δ 33.8

Anal. Calcd for $C_{33}H_{51}B_2N_2O_4Rh$ (664.30): C, 59.67; H, 7.74; N, 4.22. Found: C, 59.52; H, 7.77; N, 3.94.

4.5 Synthesis of (^{MeO}BDI)Rh(HSn^{n}Bu$_3$)$_2$ (2.3)

A solution of (^{MeO}BDI)Li(THF) (75 mg, 0.199 mmol) in 0.4 mL THF was added to stirred suspension of [Rh(COE)$_2$Cl]$_2$ (62 mg, 0.099 mmol) in THF. After 10 minutes, HSn^{n}Bu$_3$ (121.6 mg, 0.398 mmol) was added. After 5 more minutes, the solution was evaporated to dryness. Crystallization from Et$_2$O at -35 °C took a long time but eventually gave large orange crystals.

^{1}H NMR (THF-d_8, 500 MHz): δ 6.98 (2H, t, *J* 8.4, *p*), 6.59 (4H, d, *J* 8.4, *m*), 5.11 (1H, s, *3*), 3.78 (12H, s, O*Me*), 1.67 (6H, s, *1*), 1.15-1.35 (24H, m, C-C*H*$_2$-C), 0.86-0.92 (30H, m, SnC*H*$_2$ and CH$_2$C*H*$_3$), -15.34 (2H, d, J_{Rh} 12, J_{Sn} 23, Rh*H*).

^{13}C NMR (THF-d_8, 125 MHz): δ 160.4 (*2*), 153.1 (*o*), 140.0 (*i*), 124.5 (*p*), 104.6 (*m*), 99.2 (br, *3*), 55.6 (O*Me*), 30.3 (J_{Sn} 18, *C*H$_2$CH$_3$), 28.4 (J_{Sn} 70, SnCH$_2$*C*H$_2$), 22.7 (*1*), 17.1 (J_{Rh} 2, Sn*C*H$_2$), 14.0 (CH$_2$*C*H$_3$).

Anal. Calcd. for C$_{45}$H$_{81}$N$_2$O$_4$Sn$_2$Rh (1054.46): C, 51.26; H, 7.74; N, 2.66%. Found: C, 51.48; H, 7.88; N, 2.71%.

4.6 Attempted preparation of (^{Me}BDI)Rh(HSn^{n}Bu$_3$)$_2$

A solution of (^{Me}BDI)Li(THF) (50 mg, 0.16 mmol) in 0.4 mL THF was added to a stirred suspension of [Rh(COE)$_2$Cl]$_2$ (49.2 mg, 0.08 mmol) in THF. After 10 minutes, HSn^{n}Bu$_3$ (140 mg, 0.48 mmol) was added and the mixture was

stirred for another 5 minutes. After evaporation of the solvent, ^{1}H NMR showed the presence of product and free ligand in an approximately 4:1 ratio as well as some remaining COE. Purification attempts failed due to the high and similar solubility of the various Sn^{n}Bu$_3$ compounds.

4.7 Synthesis of (^{Me}BDI)Rh(HSn^{n}Bu$_3$)(HSiEt$_3$) (2.4)

A mixture of (^{Me}BDI)Rh(COE)(N$_2$) (79 mg, 0.145 mmol) and HSiEt$_3$ (37 mg, 0.32 mmol) in hexane was stirred for 10 minutes at room temperature. HSnBu$_3$ (46 mg, 0.16 mmol) was added and the mixture was stirred for another 30 minutes. All solvent was removed *in vacuo* and the residue was extracted with Et$_2$O at -35 °C, yielding a red crystalline solid. The mother liquor was removed and the solid was washed with cold hexane and dried, leaving 0.036 g (31%) of **2.4**.

^{1}H NMR (THF-d_8, 300 MHz): δ 7.06, 6.99 (2H each, d, *J* 7.2, *m*), 6.90 (2H, t, *J* 7.4, *p*), 5.26 (1H, s, *3*), 2.41, 2.00 (6H each, s, *o-Me*), 1.67 (6H, s, *1*), 1.10-1.55 (18H, m, C*H*$_2$C*H*$_2$C*H*$_2$), 0.89 (9H, t, *J* 7.2, *Me*(Bu)), 0.3-0.5 (15H, m, *Et*(Si)), -15.17 (2H, d, J_{Rh} 18, J_{Sn} 24, Rh*H*).

^{13}C NMR (THF-d_8, 75 MHz): δ 160.3, 157.8 (*2*, *i*), 132.0, 129.4 (*o*, *o′*), 129.1, 128.9 (*m*, *m′*), 124.9 (*p*), 99.3 (J_{Rh} 1.8, *3*), 30.5, 28.0 (*C*H$_2$(Bu)), 22.4 (*1*), 20.4 (*o-Me*), 19.7 (J_{Rh} 2, *C*H$_2$Sn), 19.5 (*o-Me*), 13.7 (*Me*(Bu)), 12.3 (*C*H$_2$Si), 8.3

(CH_3(Et)).

Anal. Calcd for $C_{39}H_{69}N_2RhSiSn$ (816.33): C, 57.43; H, 8.53; N, 3.43. Found: C, 56.63; H, 8.45; N, 3.16.

4.8 Synthesis of (^{Et}BDI)Ir(HSiEt$_3$)$_2$ (2.5)

A solution of (^{Et}BDI)Li(THF) (75 mg, 0.170 mmol) in 2 mL THF was added to a stirred solution of $[Ir(COE)_2Cl]_2$ (60 mg, 0.085 mmol) and excess $HSiEt_3$ (60 mg, 0.51 mmol) in 0.4 mL benzene. All solvent was evaporated *in vacuo* and the solid was extracted with $^{i}Pr_2O$ in a nitrogen-filled dry-box. After centrifuging, the $^{i}Pr_2O$ solution was cooled to -35 °C, forming a yellow crystalline solid. The mother liquor was removed and the solid was washed with cold hexane and dried, leaving 0.044 g (33%) of **2.5**.

^{1}H NMR (THF-d_8, 300 MHz): δ 7.0-7.2 (6H, m, *m*, *p*), 5.48 (1H, s, *3*), 2.7-2.9, 2.4-2.6 (4H each, m, ArCH_2), 1.76 (6H, s, *1*), 1.24 (12H, t, *J* 7.5, $ArCH_2CH_3$), 0.6-0.7 (30H, m, Si*Et*), -16.48 (2H, s, Ir*H*).

^{13}C NMR (THF-d_8, 75 MHz): δ 160.4, 156.5 (*2*, *i*), 135.9 (*o*), 126.0 (*p*), 125.6 (*m*), 102.7 (*3*), 25.2 ($ArCH_2$), 22.9 (*1*), 13.2 ($ArCH_2CH_3$), 13.0, 9.5 (Si*Et*).

Anal. Calcd. for $C_{37}H_{65}N_2Si_2Ir$ (786.32): C, 56.52; H, 8.33; N, 3.56%. Found: C, 56.23; H, 8.09; N, 3.69%.

4.9 Synthesis of (^{Me}BDI)Ir(HSiEt$_3$)$_2$ (2.6)

A solution of (^{Me}BDI)Li(THF) (75 mg, 0.24 mmol) in 2 mL THF was added to a stirred solution of $[Ir(COE)_2Cl]_2$ (84 mg, 0.120 mmol) and excess $HSiEt_3$ (167 mg, 1.44 mmol) in 0.5 mL diethyl ether. All solvent was evaporated *in vacuo* and the solid was extracted by pentane in a nitrogen-filled dry-box. Solids were removed by centrifuging, and the pentane solution was cooled to -35 °C. After a week, a single big yellow crystal had formed. The mother liquor was removed and the solid was washed with cold hexane and dried, leaving 0.031 g (22%) of **2.6.**

^{1}H NMR (THF-d_8, 300 MHz): δ 7.06 (4H, d, J 7.3, *m*), 6.91 (2H, t, J 7.4, *p*), 5.54 (1H, s, *3*), 2.21 (12H, s, *o-Me*), 1.74 (6H, s, *1*), 0.5-0.8 (30H, m, Si*Et*), -16.33 (2H, s, Ir*H*).

^{13}C NMR (THF-d_8, 75 MHz): δ 160.2, 157.7 (*2*, *i*), 131.0 (*o*), 129.0 (*m*), 125.6 (*p*), 102.6 (*3*), 22.7 (*1*), 19.9 (*o-Me*), 13.1, 9.5 (Si*Et*).

Anal. Calcd. for $C_{33}H_{57}N_2Si_2Ir$ (730.21): C, 54.28; H, 7.87; N, 3.84%. Found: C, 54.05; H, 7.64; N, 3.96%.

4.10 Synthesis of (^{iPr}BDI)Ir(H)$_3$(SiEt$_3$) (2.7)

(^{iPr}BDI)Ir(H)$_4$ (5 mg, 0.0081 mmol) in C_6D_6 was added into $HSiEt_3$ (0.94 mg, 0.0081 mmol, 1 eqv) in an NMR tube. After 2 hours, ^{1}H NMR spectra indicates that the starting material is totally consumed and a new compound

formed which has a new hydride peak at -16.63 ppm.

4.11 Synthesis of (^{iPr}BDI)Ir(H)$_3$(GeEt$_3$) (2.8)

(^{iPr}BDI)Ir(H)$_4$ (5 mg, 0.0081 mmol) in C_6D_6 was added into HGeEt$_3$ (1.3 mg, 0.0081 mmol, 1 eqv) in an NMR tube. After 2 hours, ^{1}H NMR spectra indicates that the starting material is totally consumed and a new compound formed which has a new hydride peak at -21.14 ppm.

4.12 Synthesis of (^{iPr}BDI)Ir(H)$_3$(BPin) (2.9)

(^{iPr}BDI)Ir(H)$_4$ (5 mg, 0.0081 mmol) in C_6D_6 was added into HBPin (1.17 µL, 0.0081 mmol, 1 eqv) in an NMR tube. After 2 hours, ^{1}H NMR spectra indicates that the starting material is totally consumed and a new dihydride compound formed which has a new hydride peak at -20.24 ppm.

4.13 Synthesis of (^{iPr}BDI)Ir(HBPin)$_2$ (2.10)

(^{iPr}BDI)Ir(H)$_4$ (5 mg, 0.0081 mmol) in C_6D_6 was added into HBPin (2.34 µL, 0.0162 mmol, 2 eqv.) in an NMR tube. After 2 hours, ^{1}H NMR spectra indicates that the starting material is totally consumed and a new dihydride compound formed which has a new hydride peak at -20.56 ppm.

4.14 Synthesis of (^{iPr}BDI)Ir(H)(BPin)(COE) (2.11)

A solution of (^{Me}BDI)Li(THF) (75 mg, 0.24 mmol) in 2 mL THF was added

to a stirred solution of $[Ir(COE)_2Cl]_2$ (84 mg, 0.120 mmol) and excess $HSiEt_3$ (167 mg, 1.44 mmol) in 0.5 mL diethyl ether. All solvent was evaporated *in vacuo* and the solid was extracted by pentane in a nitrogen-filled dry-box. Solids were removed by centrifuging, and the pentane solution was cooled to -35 °C. After 3 days, a big yellow crystal had formed. The mother liquor was removed and the solid was washed with cold hexane and dried, leaving 0.031 g (22%) of **2.11.**

4.15 Attempted synthesis of (^{Me}BDI)Rh(PPh_3)$_2$ (2.12)

A solution of (^{Me}BDI)Li(THF) (75mg, 0.194 mmol) in THF was added to a solution/suspension of $[Rh(COE)_2Cl]_2$ (69 mg, 0.097 mmol) in THF. After all solids had dissolved to give a dark brown solution, the solvent was evaporated *in vacuo* and the solid was extracted by hexane in a nitrogen-filled dry-box. After centrifuging, the hexane solution was added to a solution of PPh_3 (102 mg, 0.39 mmol) in hexane. After stirring for 6 days at room temperature the mother liquor was removed and the solid was washed with cold hexane and dried, leaving 0.08 g (44%) of (*iso*-^{Me}BDI)Rh(PPh_3)$_2$ (containing the isomerized BDI ligand) (**2.12**).

^{1}H NMR (benzene-d_6, 500 MHz): δ 10.23 (1H, s, N*H*), 7.7 (6H, m, PPh_3 *o*), 7.5 (6H, m, PPh_3 *o*), 6.8-7.0 (m, PPh_3 and Ar *m*,*p*), 3.33 (1H, d, *J* 5.5, *3*), 2.78 (3H, s, *o-Me*), 2.57 (1H, dd, *J* 7.0, 4.0, *1*), 2.42, 2.15 (3H each, s, *o-Me*), 1.67

(1H, ~q, *J* 3.8), 1.49 (3H, s, *o-Me*), 0.81 (3H, s, *5*).

^{13}C NMR (benzene-d_6, 125 MHz; assignments tentative): δ 176.4 (*4*), 150.6 (Ar *i*), 139.5 (d, J_P 24, PPh_3 *i*), 139.2 (d, J_P 20, PPh_3 *i*), 139.1 (Ar *i*), 137.7 (unresolved couplings, *2*), 136.2, 135.9 (Ar *o*), 135.3 (d, J_P 14, PPh_3 *o*), 134.3 (d, J_P 13, PPh_3 *o*), 128.8 (Ar *o*?), 128.7 (PPh_3 *o*), 127.7 (d, J_P 9, PPh_3 *m*), 127.4 (d, J_P 10, PPh_3 *m*), 125.6, 122.5 (Ar *p*), 56.8 (dd, *J* 27, 7, *3*), 44.6 (ddd, *J* 29, 9, 3, *1*), 22.2 (*5*), 20.5, 19.4, 19.4, 19.0 (*o-Me*). Remaining resonances obscured by C_6D_6 signal.

^{31}P NMR (benzene-d_6, 121 MHz): δ 51.2 (dd, J_{Rh} 214, J_P 31), 41.3 (dd, J_{Rh} 184, J_P 31).

Anal. Calcd for $C_{57}H_{56}N_2P_2Rh$ (933.94): C, 73.31; H, 6.04; N, 3.00. Found: C, 72.99; H, 5.65; N, 2.70.

4.16 Reaction of (^{Me}BDI)Rh(COE) with $SnMe_4$ and H_2

In a nitrogen-filled dry box, a solution of (^{Me}BDI)Li(THF) (50 mg, 0.160 mmol) in THF was added to a solution/suspension of $[Rh(COE)_2Cl]_2$ (49 mg, 0.08 mmol) in THF. After stirring for 5 minutes, all solvent was removed in vacuo and the solid was extracted with 5 mL of hexane. Solids were removed by centrifugation.

The hexane solution of (^{Me}BDI)Rh(COE)(N_2) was transferred into a 100 mL

Schlenk flask. Me_4Sn (115 mg, 0.64 mmol) was added. The reaction flask was transferred to a hydrogen-filled Schlenk line and stirred. The flask was opened and kept open for 1 minute, letting hydrogen flow through it to replace much of the nitrogen. The flask was closed again but left connected to the hydrogen Schlenk line for 4 more minutes; then the connection to the Schlenk line was closed and the solution was stirred for 20 hours at room temperature. Solvents were removed *in vacuo*, leaving a dark brown residue that according to NMR consisted of a mixture of **2.13** and **2.14**, and free ligand (^{Me}BDI)H in the ratio 1:1.20:0.76 based on ^{1}H NMR integration. Attempts to separate these compounds were unsuccessful.

4.17 Synthesis of (^{Me}BDI)RhNH(2,6-^{i}Pr$_2$C$_6$H$_3$) (3.1)

A solution/suspension of lithium 2,6-diisopropylanilide (THF) (255.33 g/mol, 42.6 mg, 0.167 mmol) in 0.4 ml toluene was added to a solution of [(^{Me}BDI)Rh]$_2$(μ-Br)$_2$(Toluene) (1068.65 g/mol, 64 mg, 0.06 mmol) in toluene (0.5 mL). Solvents were removed in vacuo immediately, and the residue was extracted with hexane. Cooling to -35 °C produced blue crystals after weeks. The mother liquid was removed and the solid was dried and a single crystal of **3.1** was obtained. Yield: 45mg, 64%.

Tentative assignment

^{1}H NMR (300MHz, C_6D_6): δ 13.8 (3H, $\underline{\nu}_{1/2}$ 292 Hz), 10.1 (2H, $\nu_{1/2}$

56.6 Hz), 3.53 (12H, br s, $\nu_{1/2}$ ~343 Hz, CH*Me*$_2$), 1.19 (6H, $\nu_{1/2}$ 44 Hz), -10.0 (3H, br s, $\nu_{1/2}$ 1061 Hz, N=C-*Me*)

4.18 Synthesis of [(^{Me}BDI)Rh]{μ-[η^4-NH(2-CH$_2$-6-CH$_3$-C$_6$H$_3$)-η^4]}[Rh(^{Me}BDI)] (3.2)

[(^{Me}BDI)Rh]$_2$(μ-Br)$_2$ (63.3 mg, 0.059 mmol) was weighed into a small vial and dissolved in 10 ml hexane, and then the dark green solution was transferred into a Schlenk tube. Li(THF)NH(2,6-Me$_2$C$_6$H$_3$) （30.1 mg, 0.015 mmol, 2.6 eq.）was weighed and transferred by 20 ml hexane into the same Schlenk tube. After stirring under room temperature in the drybox for 16.5 hours, all solvents were evaporated to dryness *in vauo*. Then 5 ml toluene was added into the Schlenk tube, and centrifuging to remove to mother liquid to into another new Schlenk tube. All solvents were evaporated to dryness *in vacuo* again. 1 ml toluene was added into the Schlenk tube and the solution was transferred into a small vial, then the dark red solution was layered with 1 ml hexane and put in the fridge at -35 ℃. A single crystal was obtained over the weekend. Further concentrating the mother liquid and layer with more hexane. Combined Yield: 24%.

^{1}H NMR(THF-d_8, 300 MHz): δ 6.69-7.12 (12H, m, Ar), 6.36 (1H, d, *J* 4.5 Hz, CH=CH-C*H*=CMe), 5.08 (1H, s, C3-*H*), 4.82 (1H, s, C3'-H), 4.00 (1H, dd, J_1 6.0 Hz, J_2 4.5Hz, CH=C*H*-CH=CMe), 2.28 (6H, s, *Me*), 2.28 (1H, d, peak is

hidden in the 2.28 peak, C*H*=CH-CH=CMe), 2.15(3H, s, *Me*), 2.08(3H, s, *Me*), 1.95(1H, s, *Me*,), 1.90(3H, s, *Me*), 1.87(3H, s, *Me*), 1.77 (3H, s, *Me*), 1.47(3H, s, *Me*), 1.44 (6H, s, *Me*), 1.39 (3H, s, *Me*), -0.67(3H, s, CH=CH-CH=C*Me*).

CH_2 peak might be hidden under THF peaks or methyl peaks. NH peak cannot be observed possibly due to the H/D exchange with THF-d8.

^{13}C NMR (THF-d_8, 300 MHz): δ158.1, 157.5, 156.8 (d, *J* 1.0 Hz), 155.3, 155.1, 154.6, 154.5,154.1, 154.0, 153.9, 133.8, 133.6, 132.7, 132.3, 131.2, 130.8, 130.71, 130.66, 129.4, 129.0, 128.7, 128.4, 128.2, 127.92, 127.88, 127.4, 125.3, 124.7, 124.5, 123.9, 99.3(d, *J* 3.3 Hz), 97.6 (d, *J* 3.3 Hz), 90.6 (too broad to be identified well), 80.6 (d, J 10.1 Hz), 75.2 (d, *J* 7.7 Hz), 22.6, 22.5, 21.4, 19.4, 19.0, 18.9, 18.7, 18.5, 18.47, 18.1, 12.2. (CH_2 carbon cannot be observed possibly due to the broadening by rhodium center)

Anal. Calcd for $C_{50}H_{59}N_5Rh_2$ (935.85): C, 64.17; H, 6.35; N, 7.48. Found: C, 64.263; H, 6.447; N, 7.488.

4.19 Synthesis of (^{Me}BDI)Rh{NH(*o*-Me)C_6H_3(*o*-CH_2)}{μ-NH(2,6-$Me_2C_6H_3$)}Li{NH_2(2,6-$Me_2C_6H_3$)}$_2$ (3.3)

A solution/suspension of lithium 2,6-dimethylanilide (THF) (199.22 g/mol, 21.9 mg, 0.11 mmol) in 0.4 ml toluene was added to a solution of [(^{Me}BDI)Rh]$_2$(μ-Br)$_2$(Toluene) (1068.65 g/mol, 45 mg, 0.042 mmol) in

toluene (0.5 mL). Solvents were removed *in vacuo* immediately, and the residue was extracted with hexane. After staying in hexane under room temperature overnight, hexane was removed in vacuo. Pentane with 5 drops toluene were added and cooling to -35 °C produced yellow crystals overnight. The mother liquid was removed and the solid was dried.

4.20 Synthesis of (^{Me}BDI)Rh{2-(PhN)-η^4-C_6H_3NH}Rh(^{Me}BDI) (3.4)

A solution/suspension of lithium anilide (THF) (171.17 g/mol, 48 mg, 0.28 mmol) in 0.4 ml hexane was added to a solution of [(^{Me}BDI)Rh]$_2$(μ-Br)$_2$(Toluene) (1068.65 g/mol, 75 mg, 0.07 mmol) in hexane (0.5 mL). The mixture was stirred at room temperature for 50 min. Solvents were removed *in vacuo*, and the residue was extracted with pentane. After centrifuging, the dark blue solution was cooled to -35 °C. After two weeks, black crystalline solid was deposited. The mother liquid was pipetted off and further concentrated. After another one week under -35 °C, more solid was isolated by pipetting off the mother liquor. Combined yield: 11 mg, 15%. Theoretical: (1029 g/mol, 72.03 mg, 0.07 mmol)

^{1}H NMR (C_6D_{12}, 300 MHz): δ 7.52(1H, t, *J*av 4.2Hz, N-Ar *p*), 7.27 (2H, d, *J* 5.0 Hz, N-Ar *m*), 7.21 (1H, d, *J* 6.8Hz, N-Ar *m*), 6.80-7.00 (8H, m), 6.56-6.71(6H, m), 6.21 (1H, br s, N-*H*), 5.78-7.82 (1H, m, PhNCCH=C*H*), 5.35 (1H, s, C3-*H*), 4.96-4.99 (1H, m, PhNCCH=CH-C*H*), 4.12 (1H, s, C3'-*H*),

2.59 (3H, s, *Me*), 2.31 (3H, s, *Me*), 2.08 (3H, s, *Me*), 2.07 (3H, s, *Me*), 2.00 (3H, s, *Me*), 1.89 (3H, s, *Me*), 1.88 (1H, d, *J* ~3Hz, PhNCCH=CH-CH=C*H*), 1.83(3H, s, *Me*), 1.68(3H, s, *Me*), 1.55 (3H, s, *Me*), 1.51 (3H, s, *Me*), 1.42 (3H, s, *Me*), 1.17 (1H, d, *J* 6.0 Hz, PhNCC*H*=CH), 1.14 (3H, s, *Me*).

4.21 Synthesis of (^{Me}BDI)Rh(2,2'-bipyridine) (3.5)

$[Rh(COE)_2Cl]_2$ (0.0832 g, 0.1159 mmol) was weighed into a small vial and suspended in 3 mL THF. (^{Me}BDI)Li(THF) (0.0896 g, 0.2330 mmol, 2.0 eq.) was weighed into another vial and dissolved in 3 mL dry THF. This clear lithium salt solution was added into rhodium suspension. After shaking violently for 5 minutes, the clear brown solution was transferred into a schlenk tube and evaporated to dryness. The residue was further extracted with 3 mL hexane. Undissolved solid was removed by centrifugation. This brown solution was added a solution of 2,2'-bispyridine (0.0346 g, 0.2215 mmol, 1.9 eq.) in THF (3 mL). It turned yellow brown. After stirring at room temperature for 1h, all solvents were evaporated to dryness to give black solid. Then this black solid was firstly washed with 1 mL dry Hexane, then dissolved in 4 mL THF, and layer with hexane at -35 ºC overnight. There were a lot of black solids precipitating at the bottom. The top mother liquid was pipetted off and the bottom solid was washed with fresh hexane. 0.0664 g dark color solid of **3.4** was obtained (yield 51%).

^{1}H NMR(300MHz, C_6D_6): δ 8.61(2H, d, *J* = 6.4 Hz, BiPy 3-*H* & 3′ -*H*), 6.89-7.07 (8H, m, Ar *o m* & BiPy 5-*H* & 5′ -*H*), 6.60 (2H, d, *J* = 8.2 Hz, BiPy 6-*H* & 6′ -*H*), 6.46 (2H, t, *J* = 6.7 Hz, BiPy 4-*H* & 4′ -*H*), 5.05 (1H, s, C3-*H*), 2.65 (12H, s, Ar-*Me*), 1.68 (6H, s, N=C-*Me*).

^{13}CNMR (75 MHz, C_6D_6): δ 155.4, 153.8, 152.3, 149.9(BiPy 3-*C* & 3′ -*C*), 135.2, 128.1(Ar m-*C*), 126.1(BiPy 5-*C* & 5′ -*C*), 124.3 (Ar *p*-*C*), 123.0 (BiPy 4-*C* & 4′ -*C*), 121.3 (BiPy 6-*C* & 6′ -*C*), 99.9 (3-*C*), 23.9 (N=C-*C*H_3), 20.1 (Ar *o*-*C*H_3).

4.22 Synthesis of (^{Et}BDI)Rh(2,2'-bipyridine) (3.6)

$[Rh(COE)_2Cl]_2$ (0.0718 g, 0.1001 mmol) was weighed into a small vial and suspended in 2 mL THF. (^{Et}BDI)Li(THF) (0.0882 g, 0.2002 mmol, 2.0 eq.) was weighed into another vial and dissolved in 3 mL dry THF. This clear lithium salt solution was added into rhodium suspension. After shaking violently for 5 minutes, the clear orange solution was transferred into a Schlenck tube and evaporated to dryness. The residue was further extracted with 3 mL hexane. After centrifugation to remove all undissolved solids, this brown solution was added a solution of 2,2′ -bipyridine (0.0297g, 0.19 mmol, 1.9 eq.) in hexane (2 mL). After 15 minutes, many black solids precipitate out. After another 20 minutes at room temperature, the top grey color liquid was pipetted off and the black solid at the bottom was washed with fresh hexane.

0.0801g black solid product was obtained (yield 64%).

^{1}H NMR(300MHz, C_6D_6): δ 8.44(2H, d, *J* = 6.0 Hz, BiPy 3-*H* & 3′ -*H*), 7.16-7.20 (6H, m, Ar *o m*), 7.09 (2H, t, *J* = 7.6 Hz, BiPy 5-*H* & 5′ -*H*), 6.69 (2H, d, *J* = 8.1 Hz, BiPy 6-*H* & 6′ -*H*), 6.47 (2H, t, *J* = 6.9 Hz, BiPy 4-*H* & 4′ -*H*), 5.11 (1H, s, C3-*H*), 3.22-3.42 (8H, m, C*H*$_2$CH$_3$), 1.77 (6H, s, N=C-*Me*), 1.24 (12h, t, *J* = 7.7 Hz, CH$_2$C*H*$_3$).

^{13}CNMR (75MHz, C_6D_6): δ 156.1, 153.1, 152.6, 150.4(BiPy 3-*C* & 3′ -*C*), 140.4, 126.6 (BiPy 5-*C* & 5′ -*C*), 125.8 (Ar m-*C*), 124.8 (Ar *p*-*C*), 123.0 (BiPy 4-*C* & 4′ -*C*), 120.9 (BiPy 6-*C* & 6′ -*C*), 99.8 (3-*C*), 25.4 (*C*H$_2$-CH$_3$), 24.4 (N=C-*C*H$_3$), 13.8 (CH$_2$-*C*H$_3$).

Anal. Calcd. for $C_{33}H_{57}N_2Si_2Ir$ (730.21): C, 67.73; H, 6.66; N, 9.03%. Found: C, 67.70; H, 6.66; N, 8.79%.

4.23 Synthesis of (^{Me}BDI)Rh(2,2'-bipyridine)(Br)$_2$ (3.7)

(^{Me}BDI)Rh(bipyridine) (14.9 mg, 0.026 mmol) was dissolved in 100 ml dry THF to form a brown-yellow solution. After cooled to -30 °C, this solution was kept under this temperature for 30 minutes. Then 0.08 ml Br_2 in THF (0.026 mmol) was dropped into it. It turned brown after 1 minute. The mixture was allowed to warm up to room temperature over 15 minutes. All volatile compounds were evaporated *in vacuo*. The red residue was extracted with THF. After centrifuging, the red THF solution was layered with pentane at -

35°C overnight. There are a lot of light red powder with some red crystalline solids precipitating at the bottom. The red solid was analyzed by ^{1}H NMR. Attempting to grow larger crystals cannot be successfully.

4.24 Synthesis of (^{Me}BDI)Rh(2,2'-bipyridine)(I)$_2$ (3.8)

(^{Me}BDI)Rh(bipyridine) (2.0 mg, 0.0035 mmol) was dissolved in 0.4 ml dry C_6D_6, then I_2 solid (1.0 mg, 0.00394 mmol) was added. The solution color become lighter and clearer immediately. The immediate ^{1}H NMR indicated the new diamagnetic complex generated. No free ligand was detected.

4.25 X-Ray crystallography

Crystal fragments were broken from large pieces of crystalline aggregate and sealed in a thin glass capillary. Each crystal in its capillary was mounted on a Bruker D8 three-circle diffractometer equipped with a rotating anode generator (Mo*K*α X-radiation), multi-layer optics incident beam path and an APEX-II CCD detector. Data was collected at a crystal-to-detector distance of 5 cm. Semi-empirical absorption corrections (SADABS[93]) were applied and identical data merged. The unit-cell parameters were obtained by least-squares refinement on observed reflections with $I > 2\ \sigma(I)$. Structures were solved by direct methods (SHELXS[94]) and refined by full-matrix least-squares refinement (SHELXL[94]).

Chapter 5

Conclusions and future directions

As earlier work, formation and interesting rearrangement of (^{Me}BDI)Rh(HSiR$_3$)$_2$ complexes were noted. The present work explores the scope of this chemistry systematically by attempted synthesis of corresponding complexes of germanes, stannanes and boranes, as well as variation of the metal (Ir instead of Rh) and the ligand (^{Et}BDI, ^{MeO}BDI). As a general conclusion, germane complexes are similar to silane complexes but less stable, stannane complexes are even less stable and the corresponding Ir complexes could be obtained only in a few cases. Complex stability also depends on the ligand, with ^{MeO}BDI > ^{Me}BDI > ^{Et}BDI. The reasons for these trends are not entirely clear at this point. The ligand rearrangement observed with (^{Me}BDI)Rh(HSiEt$_3$)$_2$ was not observed with any of the isolated germane or stannane complexes, but partial rearrangement was observed in the reaction with HSnMe$_3$ generated within the coordination sphere of Rh; this "trick" which involves Sn-C cleavage by Rh might be of more general interest.

In addition to the research in diamagnetic Rh complexes, a highly reactive monomeric Rh(II) anilide of β-diiminate compounds was isolated by the

reaction of rhodium(II) bromide dimer of β-diiminate with lithium 2,6-diisopropylanilide which has been characterized by ^{1}H NMR, XRD and EPR. The bulky isopropyl group is the key factor allowing isolation of this complex. The reaction of rhodium(II) bromide dimer of β-diiminate with lithium 2,6-dimethylanilide instead of lithium 2,6-diisopropylanilide results in the failure of isolating the analogous Rh(II) anilide monomer due to the benzylic C-H bond activation. When there is no ortho benzylic C-H bond to be activated, such as the reaction with lithium anilide, C-N coupling was observed in the crystal structure of final product. The study on the mechanism is still underway.

Although a monomeric Rh(II) complex was successfully synthesized and isolated, it is still too reactive and hard to handle. It might be useful to have variations on both ligand and aniline to find more stable Rh(II) monomer. For example, the reaction with 2,6-diethylanilide gives a more stable Rh(II) monomer, but the crystallization part has not been finished yet.

Rh(II) monomer has extremely high reactivity and both C-H activation and C-N formation reactions have proven that. In the future, hydroamination of olefins catalyzed by these Rh(II) monomers is a potential direction. And for the C-N bond formation rearrangement, creating a catalytic cycle based on this stoichiometric chemistry could be of significant interest.

References

1. R. H. Crabtree, *The Organometallic chemistry of the transition metals*, WILEY, 2014.
2. C. Ranken, *Industrial Chemistry*, T. C. & E. C. Jack Ltd., 1919.
3. D. A. Colby, A. S. Tsai, R. G. Bergman and J. A. Ellman, *Acc. Chem. Res.*, 2012, **45**, 814-825.
4. N. N. Langer, G. S. Bindra and P. H. M. Budzelaar, *Dalton. Trans.*, 2014, **43**, 11286-11294.
5. D. Zhu, D. J. Kozera, K. D. Enns and P. H. M. Budzelaar, *Angew. Chem., Int. Ed.*, 2012, **51**, 12211-12214.
6. C. Merckle, S. Haubrich and J. Blumel, *J. Organomet. Chem.*, 2001, **627**, 44-54.
7. G. E. Dobereiner, A. Nova, N. D. Schley, N. Hazari, S. J. Miller, O. Eisenstein and R. H. Crabtree, *J. Am. Chem. Soc.*, 2011, **133**, 7547-7562.
8. M. Sparta, K. J. Borve and V. R. Jensen, *J. Am. Chem. Soc.*, 2007, **129**, 8487-8499.
9. A. Kämper, S. J. Warrelmann, K. Reiswich, R. Kuhlmann, R. Franke and A. Behr, *Chemical Engineering Science*, 2016, **144**, 364-371.
10. K. Godula and D. Sames, *Science*, 2006, **312**, 67.
11. R. J. Phipps and M. J. Gaunt, *Science*, 2009, **323**, 1593.
12. J. -Q. Yu and Z. Shi, *C-H Activation*, Springer Link, 2010.
13. R. H. Crabtree, *J. Organomet. Chem.*, 2015, **793**, 41-46.
14. N. Zhang, R. S. Sherbo, G. S. Bindra, D. Zhu and P. H. M. Budzelaar, *Organometallics*, 2017, **36**, 4123-4135.
15. P. H. M. Budzelaar, N. N. P. Moonen, R. de Gelder, J. M. M. Smits and A. W. Gal, *Eur. J. Inorg. Chem.*, 2000, 753-769.
16. P. H. M. Budzelaar, R. de Gelder and A. W. Gal, *Organometallics*, 1998, **17**, 4121-4123.
17. Y. He, P. Krishnamoorthy, H. M. Lima, Y. Chen, H. Wu, R. Sivappa, H. V. Dias and C. J. Lovely, *Org. Biomol. Chem.*, 2011, **9**, 2685-2701.
18. L. Vaccaro, *Beilstein J. Org. Chem.*, 2016, **12**, 2763-2765.
19. E. L. Miller, *Energy Environ. Sci.*, 2015, **8**, 2809-2810.
20. A. Eftekhari, *Applied Materials Today*, 2017, **8**, 1-17.
21. M. Yu, Y. Huang, C. Li, Y. Zeng, W. Wang, Y. Li, P. Fang, X. Lu and Y. Tong, *Advanced Functional Materials*, 2015, **25**, 324-330.
22. G. Zhang, X. Liu, Y. Wang, C. Liu and S. Xing, *Chem. Eur. J.*, 2017, **23**, 5557-5564.
23. J. Gurke, M. Quick, N. P. Ernsting and S. Hecht, *Chem. Commun.*, 2017, **53**, 2150-2153.
24. J. E. Parks and R. H. Holm, *Inorg. Chem.*, 1968, **7**, 1408-1416.

25. D. Zhu and P. H. M. Budzelaar, *Dalton. Trans.*, 2013, **42**, 11343-11354.
26. C. Camp and J. Arnold, *Dalton. Trans.*, 2016, **45**, 14462-14498.
27. S. Kundu, C. Greene, K. D. Williams, T. K. Salvador, J. A. Bertke, T. R. Cundari and T. H. Warren, *J. Am. Chem. Soc.*, 2017, **139**, 9112-9115.
28. S. Hong, L. M. Hill, A. K. Gupta, B. D. Naab, J. B. Gilroy, R. G. Hicks, C. J. Cramer and W. B. Tolman, *Inorg. Chem.*, 2009, **48**, 4514-4523.
29. A. Sokolohorskyj, O. Železník, I. Císařová, J. Lenz, A. Lederer and J. Merna, *Journal of Polymer Science Part A: Polymer Chemistry*, 2017, **55**, 2440-2449.
30. D. Vidovic, M. Findlater and A. H. Cowley, *J. Am. Chem. Soc.*, 2007, **129**, 8436-8437.
31. T. K. Salvador, C. H. Arnett, S. Kundu, N. G. Sapiezynski, J. A. Bertke, M. R. Boroujeni and T. H. Warren, *J. Am. Chem. Soc.*, 2016, **138**, 16580-16583.
32. P. H. M. Budzelaar, A. B. van Oort. and A. G. Orpen., *Eur. J. Inorg. Chem.*, 1998, 1485-1494.
33. D. Shriver, M. Weller, T. Overton, J. Rourke and F. Armstrong, *Inorganic Chemistry*, Jessica Fiorillo, 2014.
34. M. M. Melzer, S. Mossin, X. Dai, A. M. Bartell, P. Kapoor, K. Meyer and T. H. Warren, *Angew .Chem., Int. Ed.*, 2010, **49**, 904-907.
35. T. R. Dugan, X. Sun, E. V. Rybak-Akimova, O. Olatunji-Ojo, T. R. Cundari and P. L. Holland, *J. Am. Chem. Soc*, 2011, **133**, 12418-12421.
36. T. R. Dugan, J. M. Goldberg, W. W. Brennessel and P. L. Holland, *Organometallics*, 2012, **31**, 1349-1360.
37. L. K. Harper, A. L. Shoaf and C. A. Bayse, *Chemphyschem*, 2015, **16**, 3886-3892.
38. E. C. Ashby and R. D. Schwartz, *J. Chem. Educ.*, 1974, **51**, 65.
39. T. Chandra and J. P. Zebrowski, *Journal of Chemical Health and Safety*, 2014, **21**, 22-28.
40. S. J. Geier and D. W. Stephan, *Chem. Commun.*, 2008, 99-101.
41. S. J. Geier and D. W. Stephan, *Chem. Commun.* , 2008, 2779-2781.
42. G. Meier, V. Steck, B. Braun, A. Eißler, R. Herrmann, M. Ahrens, R. Laubenstein and T. Braun, *Eur. J. Inorg. Chem.*, 2014, **17**, 2793-2808.
43. D. W. Shaffer, S. A. Ryken, R. A. Zarkesh and A. F. Heyduk, *Inorg. Chem.*, 2011, **50**, 13-21.
44. P. J. Chirik, *Inorg. Chem.*, 2011, **50**, 9737-9740.
45. L. A. Berben, B. de Bruin and A. F. Heyduk, *Chem. Commun.*, 2015, **51**, 1553-1554.
46. D. W. Shaffer, S. A. Ryken, R. A. Zarkesh and A. F. Heyduk, *Inorg. Chem.*, 2012, **51**, 12122-12131.
47. W. H. Bernskoetter, E. Lobkovsky and P. J. Chirik, *Chem. Commun.*, 2004, 764-765.
48. W. H. Bernskoetter, E. Lobkovsky and P. J. Chirik, *Organometallics*, 2005, **24**, 4367-4373.

49. P. H. M. Budzelaar, N. N. P. Moonen, R. de Gelder, J. M. M. Smits and A. W. Gal, *Chem. Eur. J.*, 2000, **6**, 2740-2747.
50. M. C. Lipke and T. D. Tilley, *J. Am. Chem. Soc.*, 2011, **133**, 16374-16377.
51. W. Scherer, P. Meixner, K. Batke, J. E. Barquera-Lozada, K. Ruhland, A. Fischer, G. Eickerling and K. Eichele, *Angew .Chem., Int. Ed.*, 2016, **55**, 11673-11677.
52. A. Bagno and M. Bonchio, *Magn Reson Chem*, 2004, **42**, 579-587.
53. H. Y. Chen, S. Schlecht, T. C. Sample and J. F. Hartwig, *Science*, 2000, **287**, 1995-1997.
54. B. A. Arndtsen, R. G. Bergman, T. A. Mobley and T. H. Peterson, *Acc. Chem. Res.*, 1995, **28**, 154-162.
55. A. A. Bengali, R. H. Schultz, C. B. Moore and R. G. Bergman, *J. Am. Chem. Soc.*, 1994, **116**, 9589-9589.
56. K. Kawamura and J. F. Hartwig, *J. Am. Chem. Soc.*, 2001, **123**, 8422-8423.
57. T. M. Gilbert and R. G. Bergman, *Organometallics*, 1983, **2**, 1458-1460.
58. M. J. Fernandez, P. M. Bailey, P. O. Bentz, J. S. Ricci, T. F. Koetzle and P. M. Maitlis, *J. Am. Chem. Soc.*, 1984, **106**, 5458-5463.
59. A. Takaoka and J. C. Peters, *Inorg. Chem.*, 2012, **51**, 16-18.
60. D. G. Hetterscheid, M. Klop, R. J. Kicken, J. M. Smits, E. J. Reijerse and B. de Bruin, *Chem. Eur. J.*, 2007, **13**, 3386-3405.
61. K. Fuchigami, N. P. Rath and L. M. Mirica, *Inorg. Chem.*, 2017, **56**, 9404-9408.
62. J. W. Suggs, M. J. Wovkulich, P. G. Williard and K. S. Lee, *J. Organomet. Chem.*, 1986, **307**, 71-82.
63. L. P. He, C. L. Yao, M. Naris, J. C. Lee, J. D. Korp and J. L. Bear, *Inorg. Chem.*, 1992, **31**, 620-625.
64. P. R. Sharp, D. W. Hoard and C. L. Barnes, *J. Am. Chem. Soc.*, 1990, **112**, 2024-2026.
65. C. Tejel., M. Sommovigo., M. A. Ciriano., J. A. Lopez., F. J. Lahoz. and L. A. Oro, *Angew. Chem., Int. Ed.* , 2000, **39**, 2336-2339.
66. Tadashi Mizutani, Tetsuya Uesaka and H. Ogoshi, *Organometallics*, 1995, **14**, 341-346.
67. B. B. Wayland, S. Ba. and A. E. Sherry, *J. Am. Chem. Soc.*, 1990, **113**, 5305-5311.
68. X. Fu, S. Li and B. B. Wayland, *Inorg. Chem.*, 2006, **45**, 9884-9889.
69. S. Li, W. Cui and B. B. Wayland, *Chem. Commun.*, 2007, 4024-4025.
70. M. Feller, E. Ben-Ari, T. Gupta, L. J. W. Shimon, G. Leitus, Y. Diskin-Posner, L. Weiner and D. Milstein, *Inorg. Chem.*, 2007, **46**, 10479-10490.
71. S. T. H. Willems, J. C. Russcher, P. H. M. Budzelaar, B. d. Bruin, R. d. Gelder, J. M. M. Smits and A. W. Gal, *Chem. Commun.*, 2002, 148-149.
72. Michael Gerisch, Jennifer R. Krumper, Robert G. Bergman and T. D. Tilley, *J. Am. Chem. Soc.*, 2001, **123**, 5818-5819.
73. D. Zhu, A. Z. Sharma, C. R. Wiebe and P. H. M. Budzelaar, *Dalton. Trans.*, 2015, **44**, 13460-13463.

74. T. Ikariya and A. J. Blacker, *Acc. Chem. Res.*, 2007, **40**, 1300-1308.
75. L. Huang, M. Arndt, K. Goossen, H. Heydt and L. J. Goossen, *Chem. Rev.*, 2015, **115**, 2596-2697.
76. N. Zhang, D. Zhu, D. E. Herbert and P. H. M. Budzelaar, unpublished work.
77. K. T. P., P. L. Y., R. J. and S. R. R., *J. Chem. Soc., Chem. Commun.*, 1991, 121-122.
78. D. S. Glueck, J. X. Wu, F. J. Hollander and R. G. Bergman, *J. Am. Chem. Soc.*, 1991, 2041-2054.
79. B. Rhodes, J. C. W. Chien, J. S. Wood, A. Chandrasekaran and M. D. Rausch, *J. Organomet. Chem.*, 2001, 95-100.
80. R. V. Bulow, H. Gornitzka, T. Kottke and D. Stalke, *Chem. Commun.*, 1996, 1639-1640.
81. W. Clegg, L. Horsburgh, F. M. Mackenzie and R. E. Mulvey, *J. Chem. Soc., Chem. Commun.*, 1995, 2011-2012.
82. *The exploration of CSD database leads to the following conclusions: most of three coordinate β-diiminate anilide complexes take Y-shape*.
83. N. A. Eckert, J. M. Smith, R. J. Lachicotte and P. L. Holland, *Inorg. Chem.*, 2003, **43**, 3306-3321.
84. S. H. Cho, J. Y. Kim, S. Y. Lee and S. Chang, *Angew. Chem., Int. Ed.* , 2009, **48**, 9127-9130.
85. J. P. Wolfe, S. Wagaw, J. F. Marcoux and S. L. Buchwald, *Acc. Chem. Res.*, 1998, **31**, 805.
86. J. F. Hartwig, *Acc. Chem. Res.*, 2008, **41**, 1534.
87. S. Samanta and S. Goswami, *Inorg. Chem.*, 2011, **50**, 3171-3173.
88. R. S. Sherbo, G. S. Bindra and P. H. M. Budzelaar, *Organometallics*, 2016, **35**, 2039-2048.
89. G. Song, F. Wang and X. Li, *Chem. Soc. Rev.*, 2012, **41**, 3651-3678.
90. N. Kuhl, N. Schröder and F. Glorius, *Advanced Synthesis & Catalysis*, 2014, **356**, 1443-1460.
91. M. R. Churchil and S. A. Julis, *Inorg. Chem.*, 1979, **18**, 2918-2920.
92. G. R. Fulmer, A. J. M. Miller, N. H. Sherden, H. E. Gottlieb, A. Nudelman, B. M. Stoltz, J. E. Bercaw and K. I. Goldberg, *Organometallics*, 2010, **29**, 2176-2179.
93. G. M. Sheldrick, SADABS; University of Göttingen, Göttingen, Germany, 1996.
94. G. M. Sheldrick, *Acta Crystallogr., Sect. A: Found. Crystallogr.*, 2008, **64**, 112-122.

Appendix

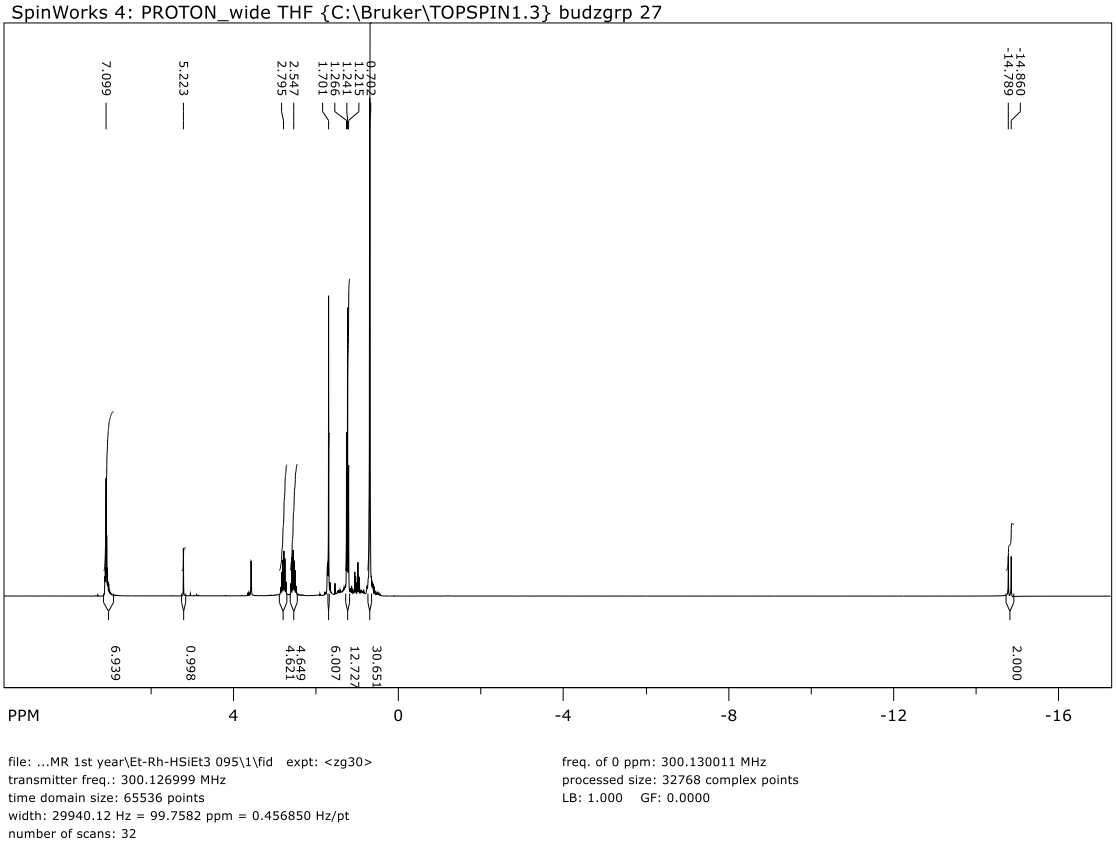

Figure A- 1. ^{1}H NMR for 2.1

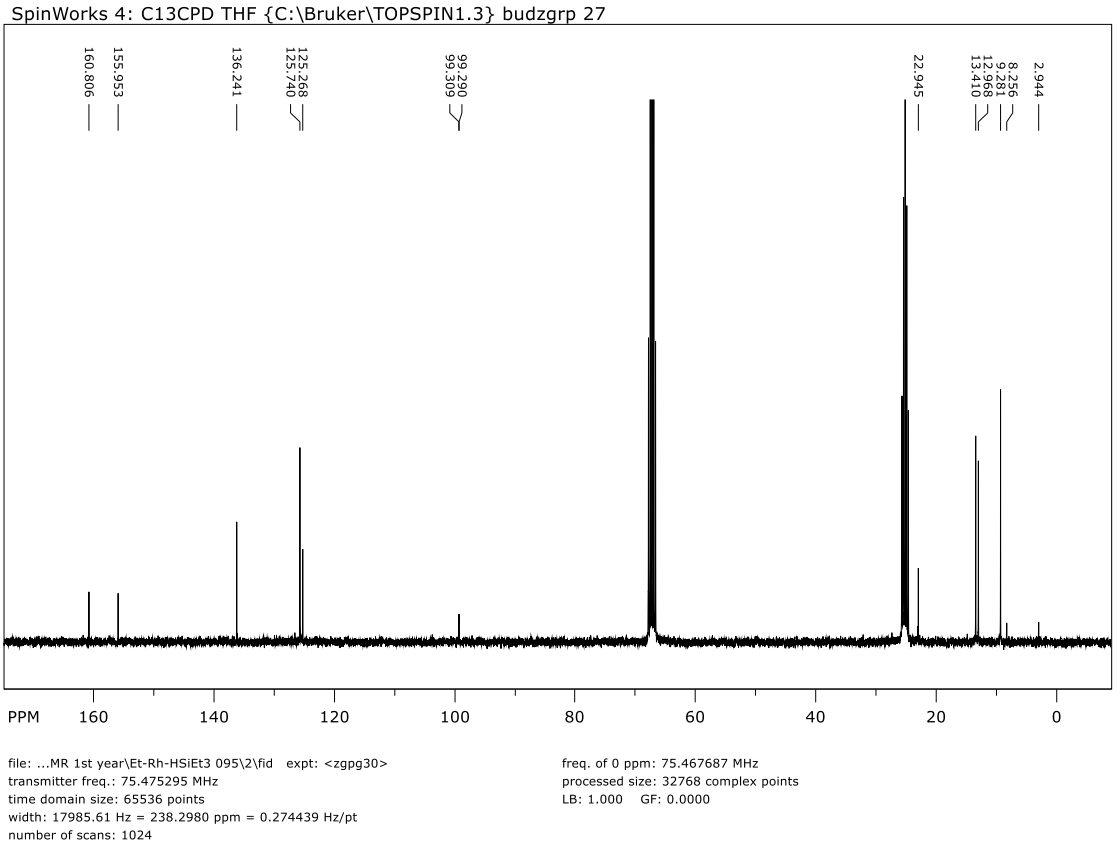

Figure A- 2. ^{13}C NMR for 2.1

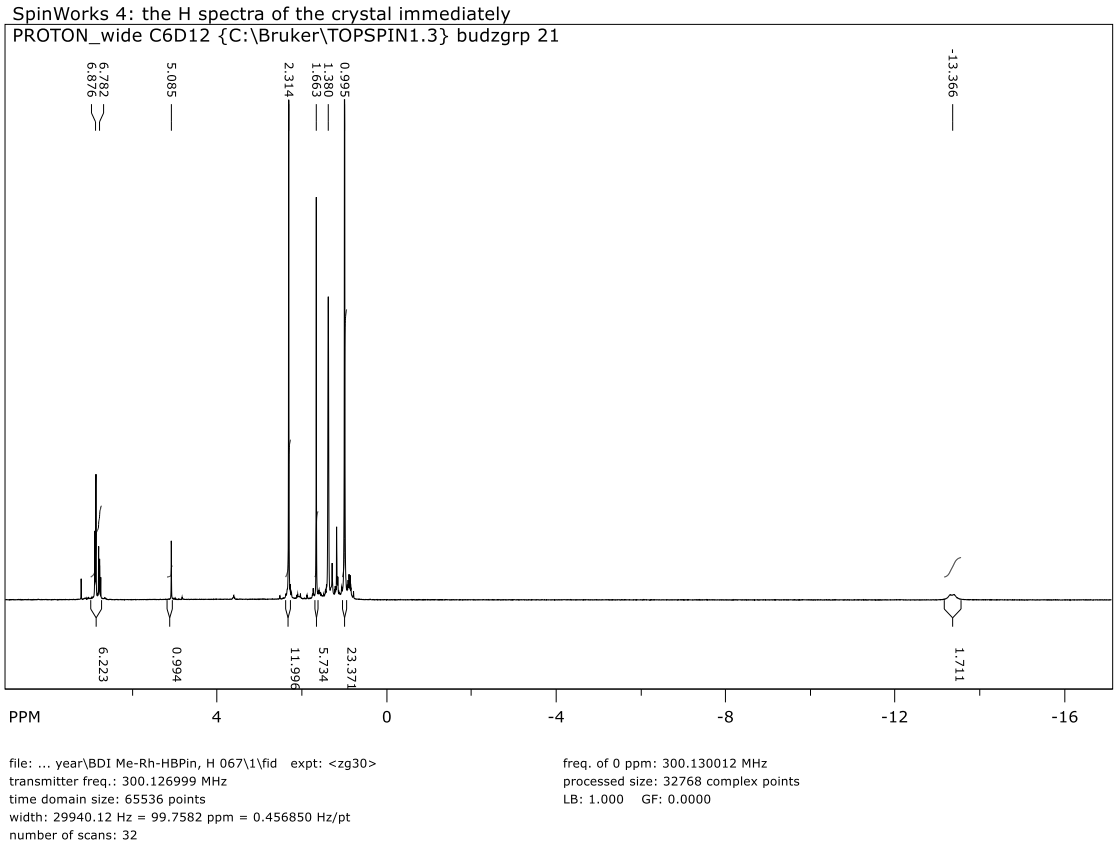

Figure A- 3. ^{1}H NMR for 2.2

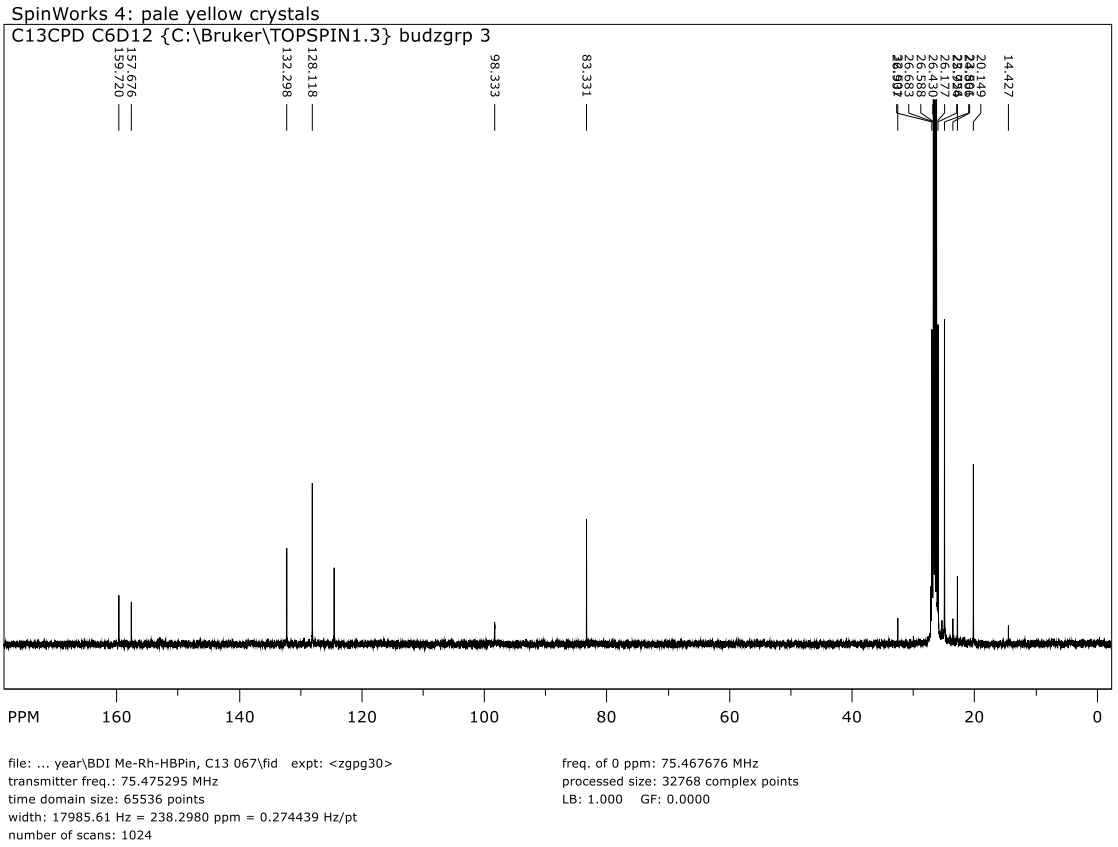

Figure A- 4. ^{13}C NMR for 2.2

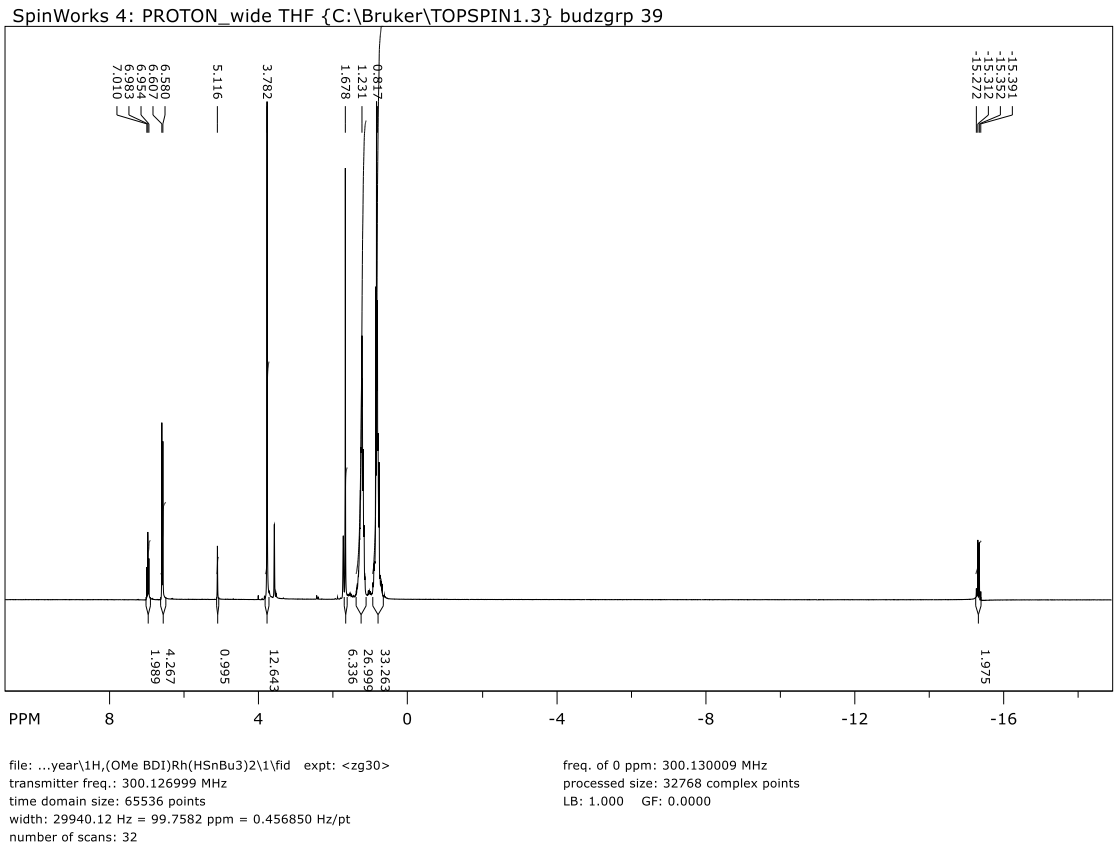

Figure A- 5. ^{1}H NMR for 2.3

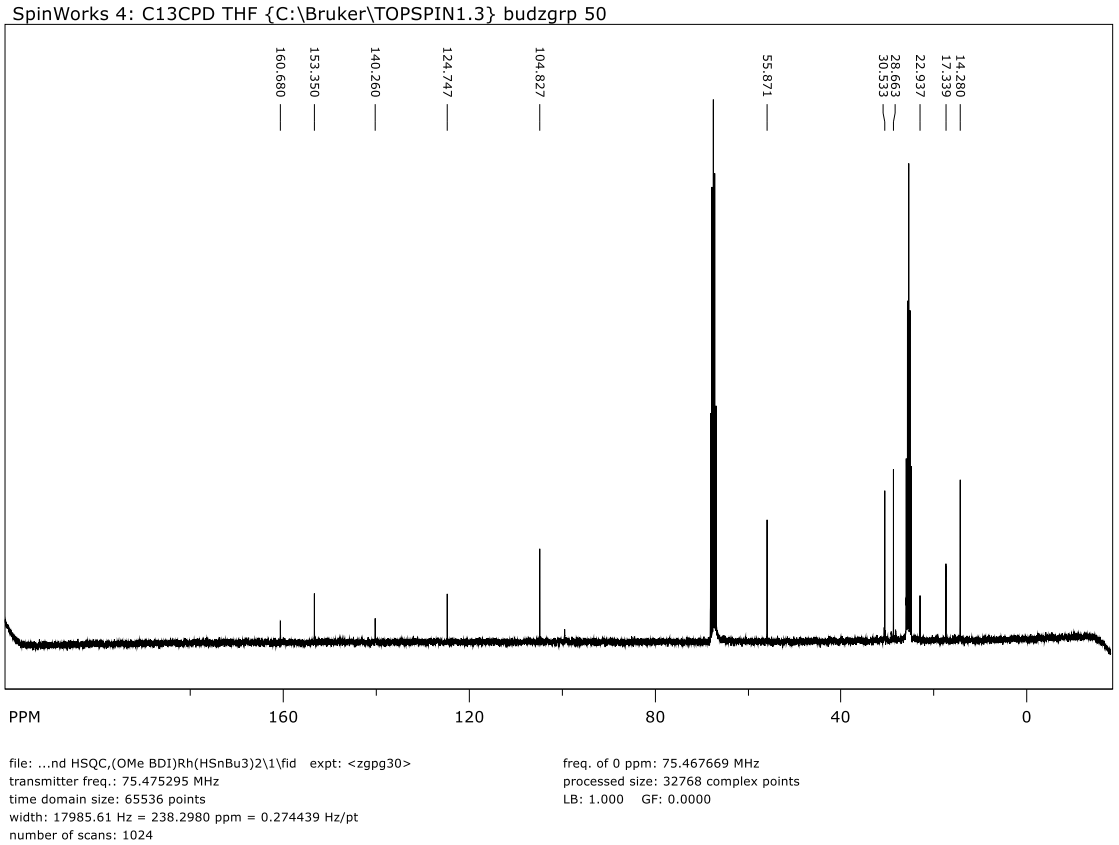

Figure A- 6. ^{13}C NMR for 2.3

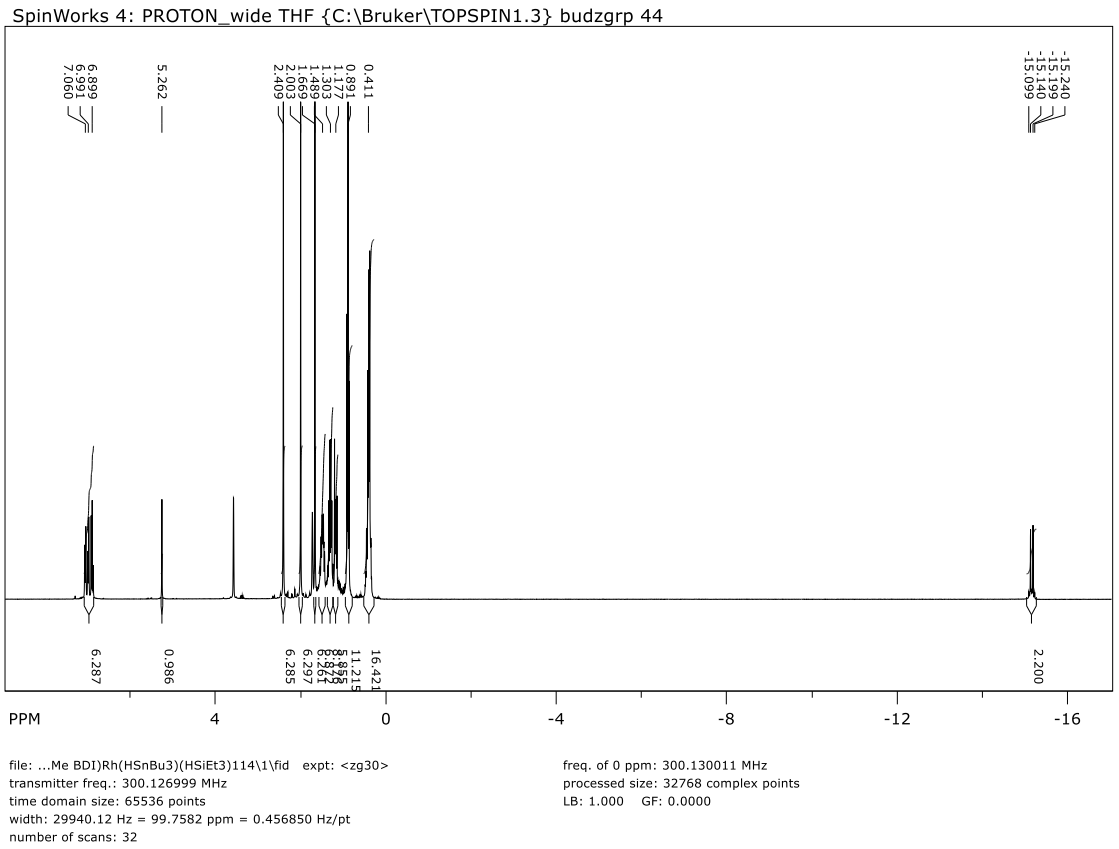

Figure A- 7. ^{1}H NMR for 2.4

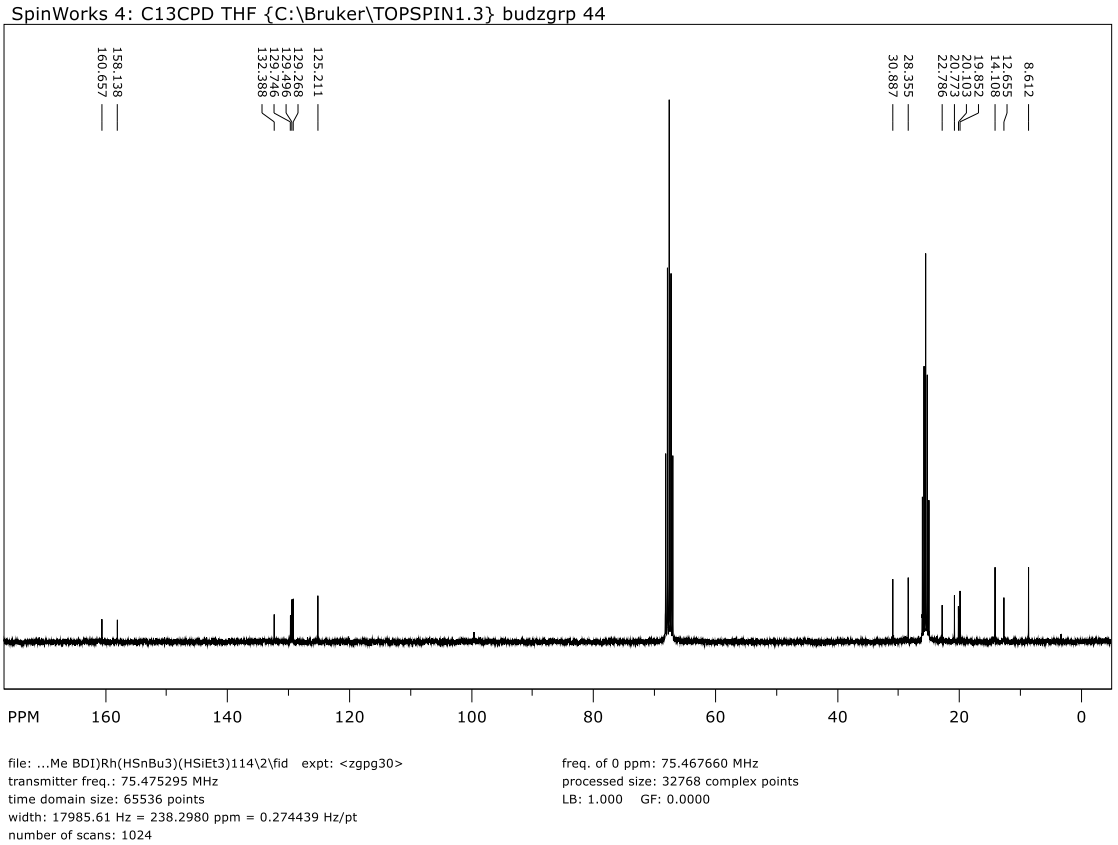

Figure A- 8. ^{13}C NMR for 2.4

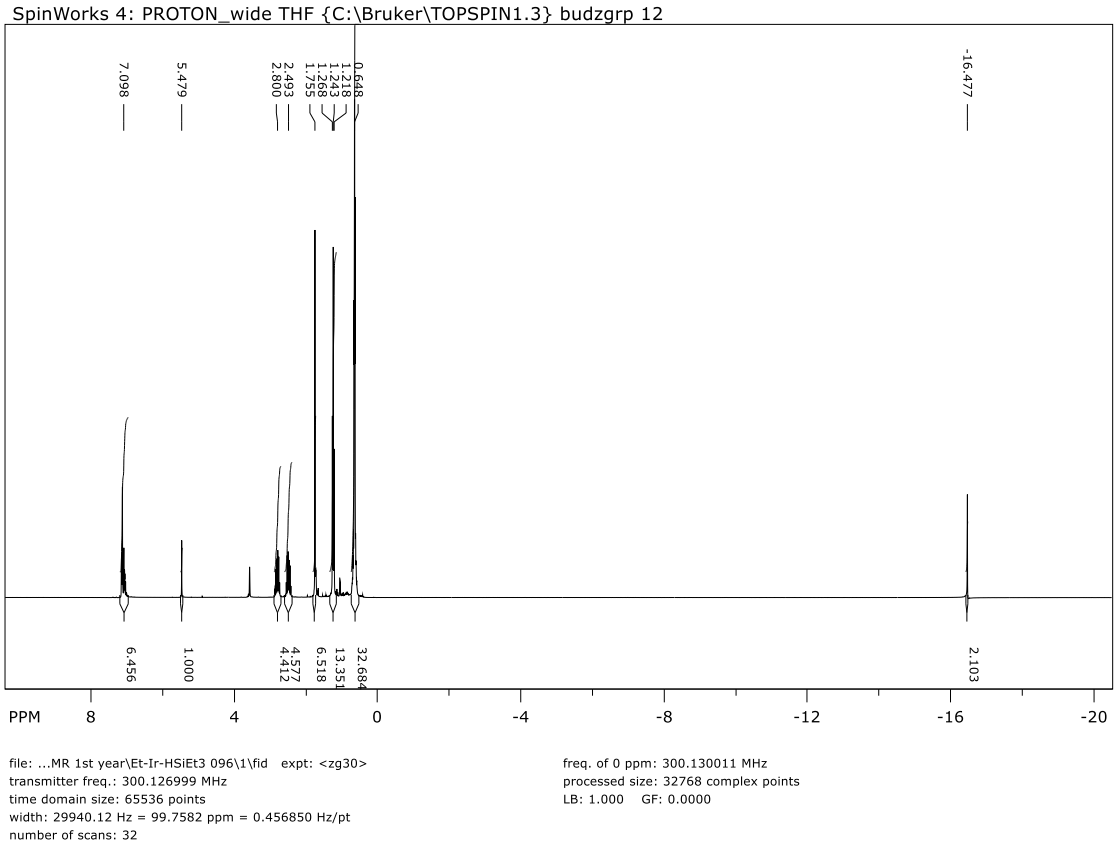

Figure A- 9. ^{1}H NMR for 2.5

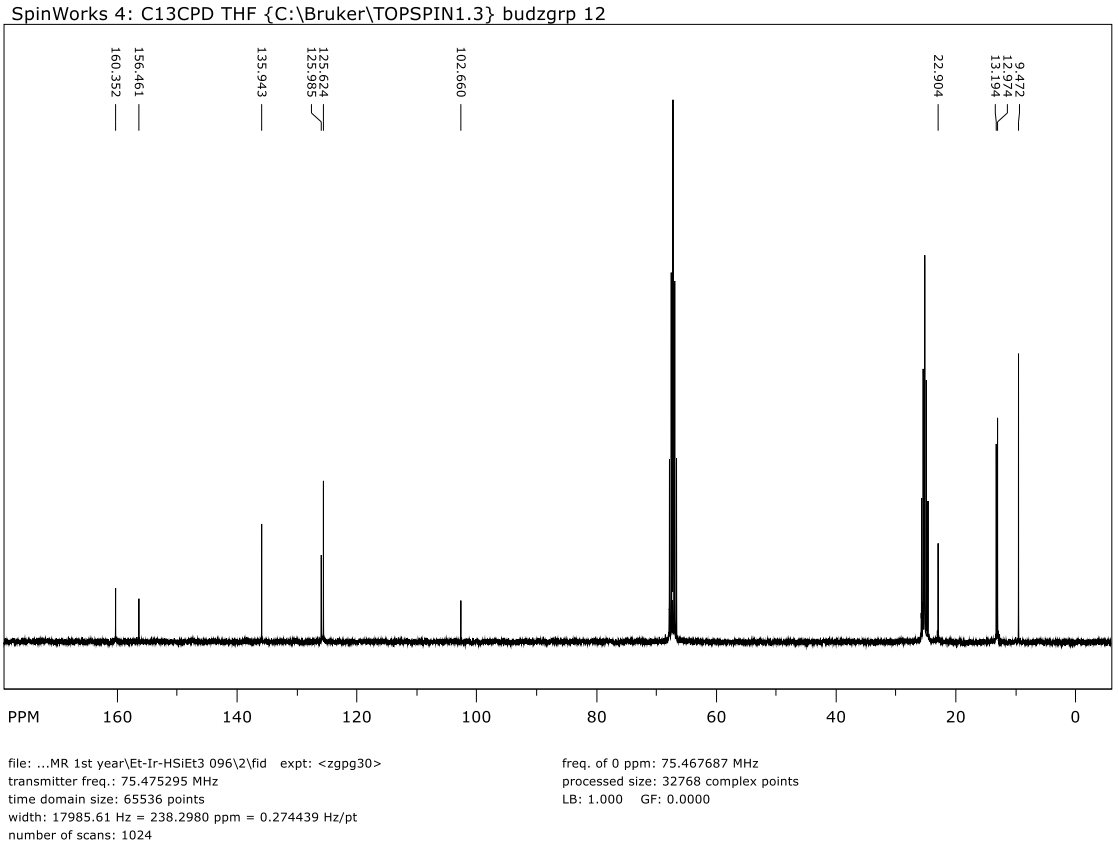

Figure A- 10. ^{13}C NMR for 2.5

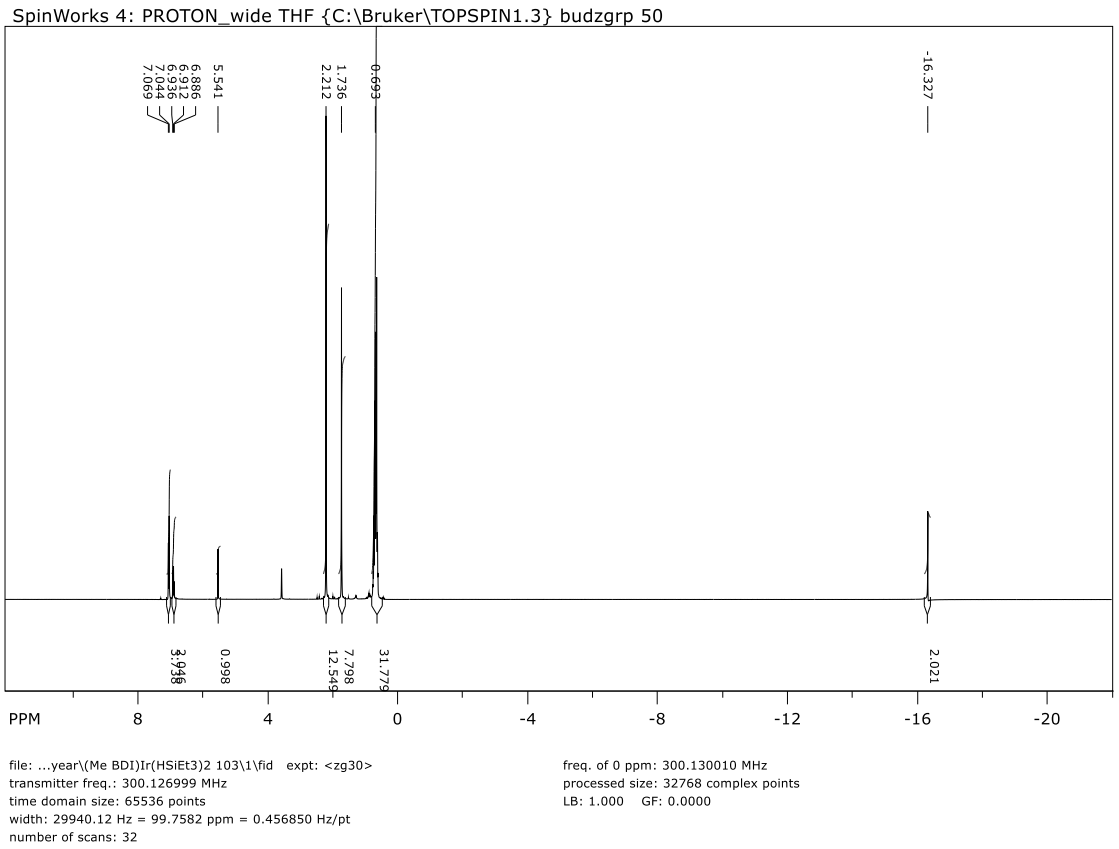

Figure A- 11. ^{1}H NMR for 2.6

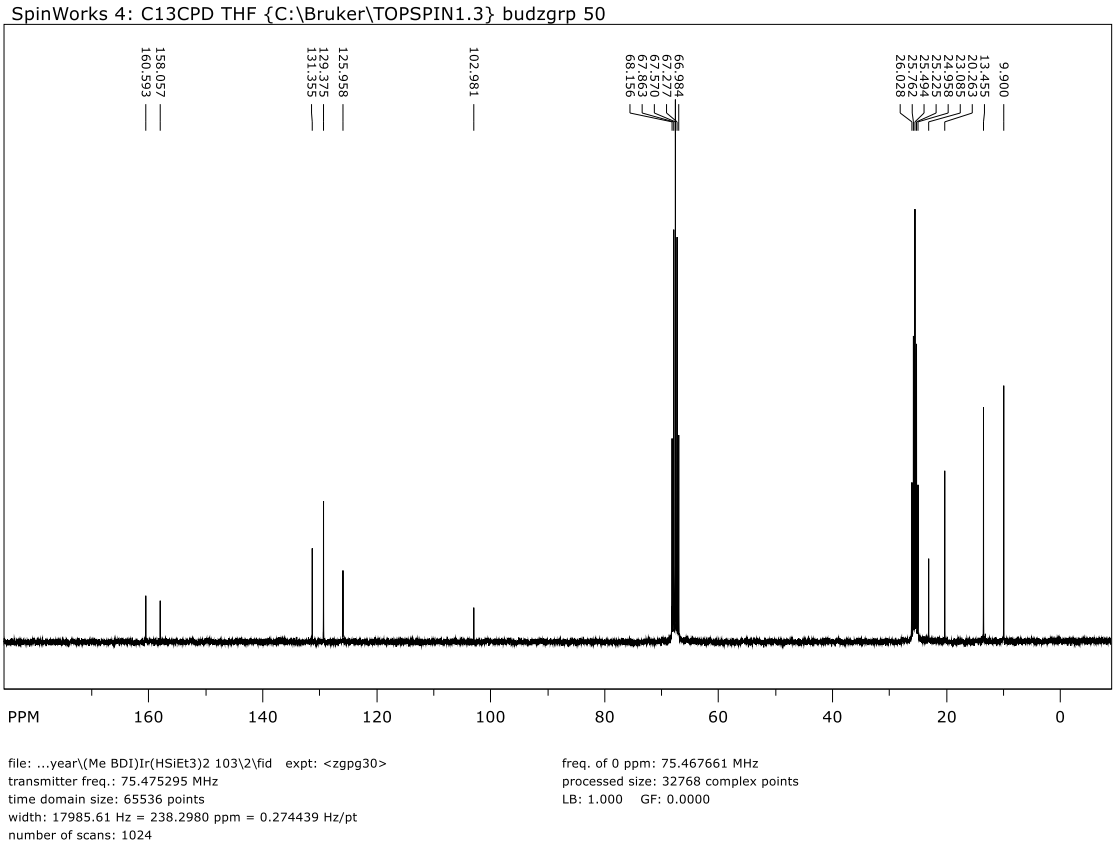

Figure A- 12. ^{13}C NMR for 2.6

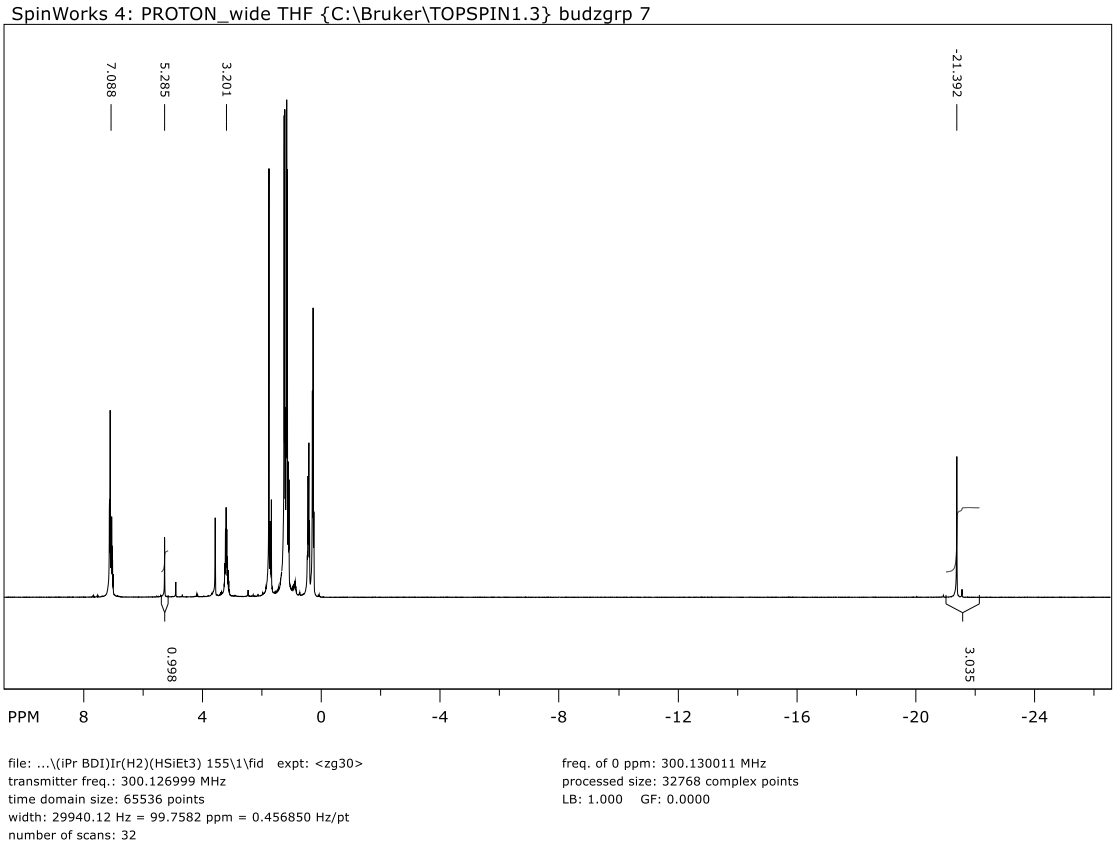

Figure A- 13. ^{1}H NMR for 2.7

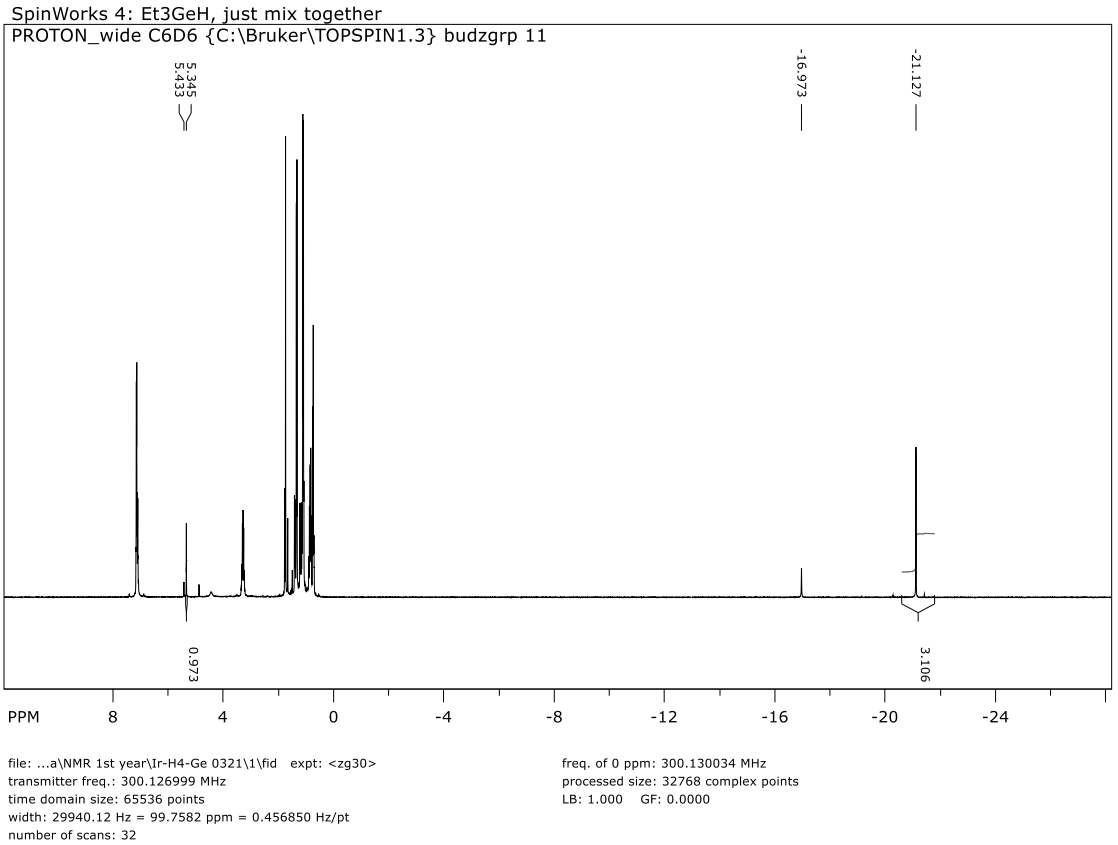

Figure A- 14. ^{1}H NMR for 2.8

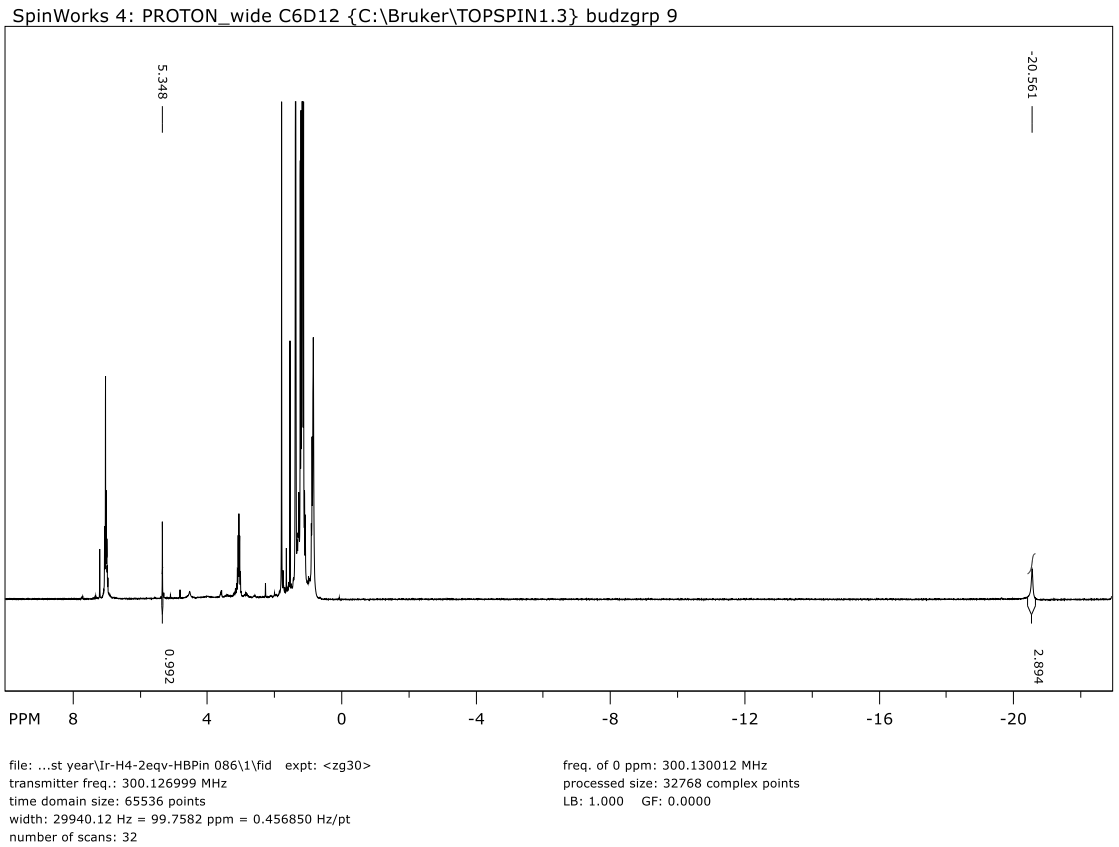

Figure A- 15. ^{1}H NMR for 2.9

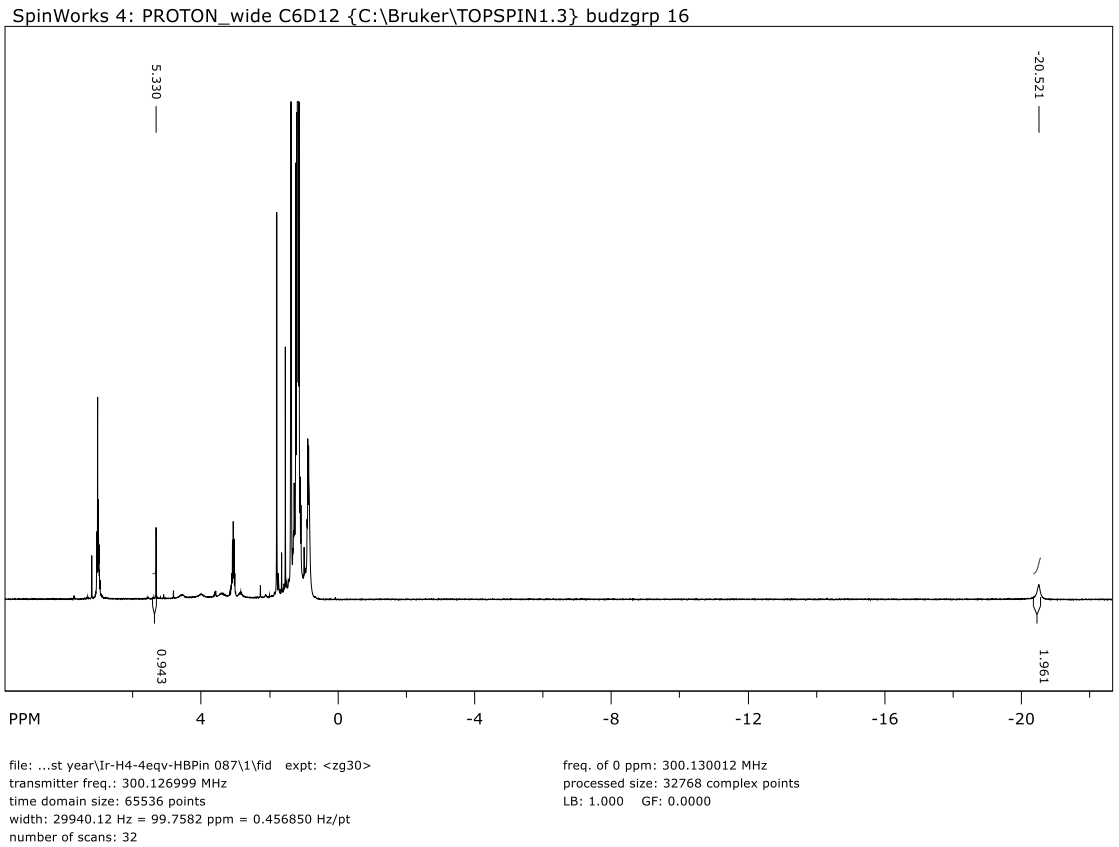

Figure A- 16. ^{1}H NMR for 2.10

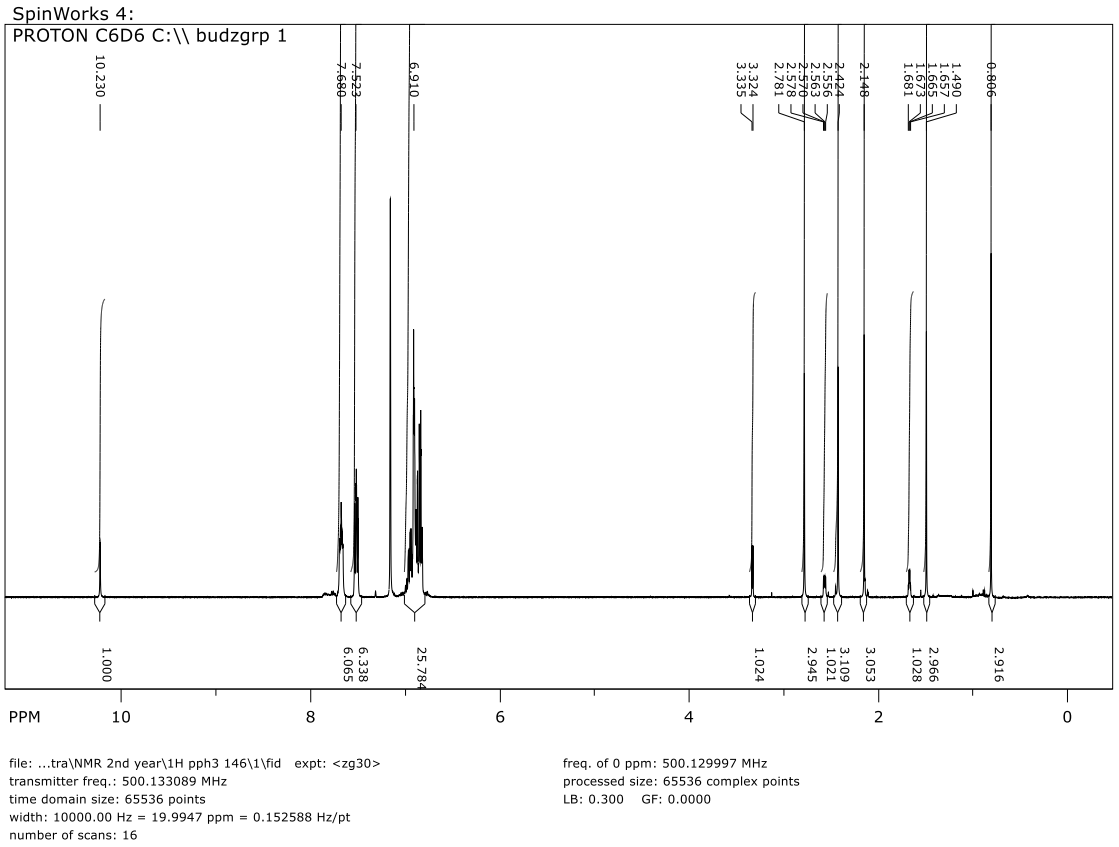

Figure A- 17. ^{1}H NMR for 2.12

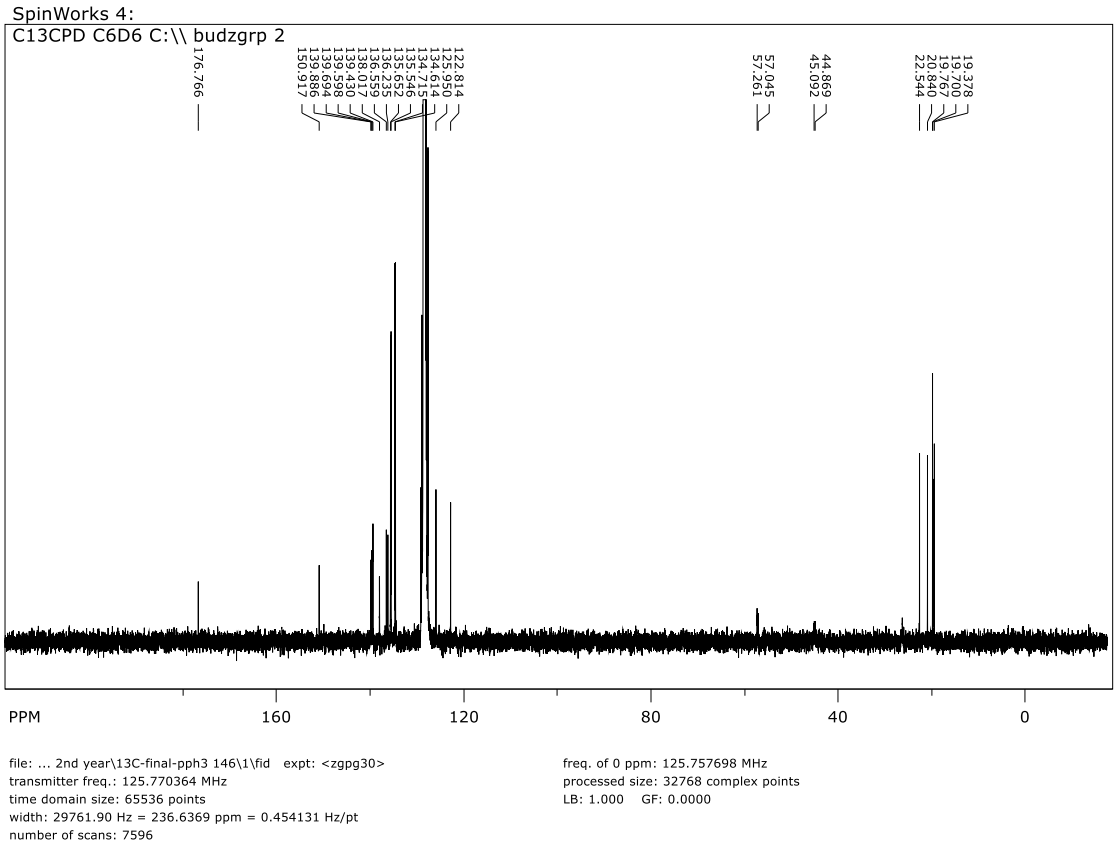

Figure A- 18. ^{13}C NMR for 2.12

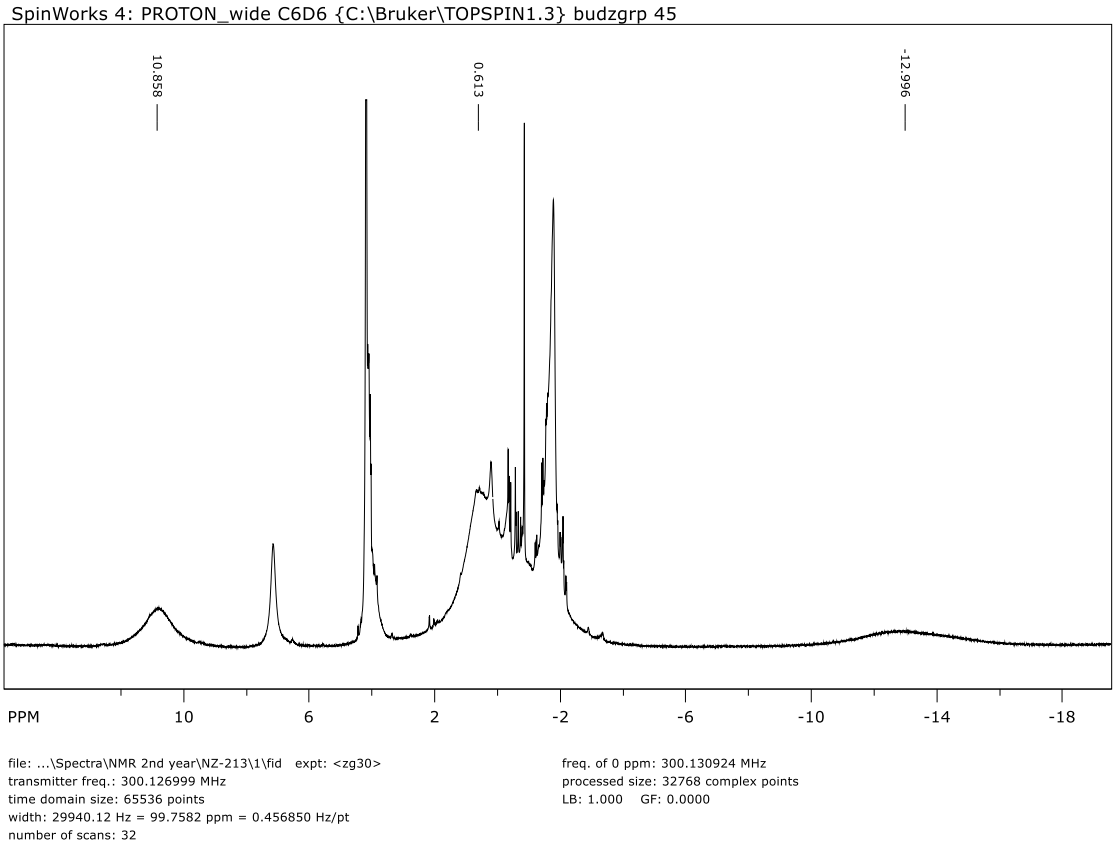

Figure A- 19. ^{1}H NMR for 3.1

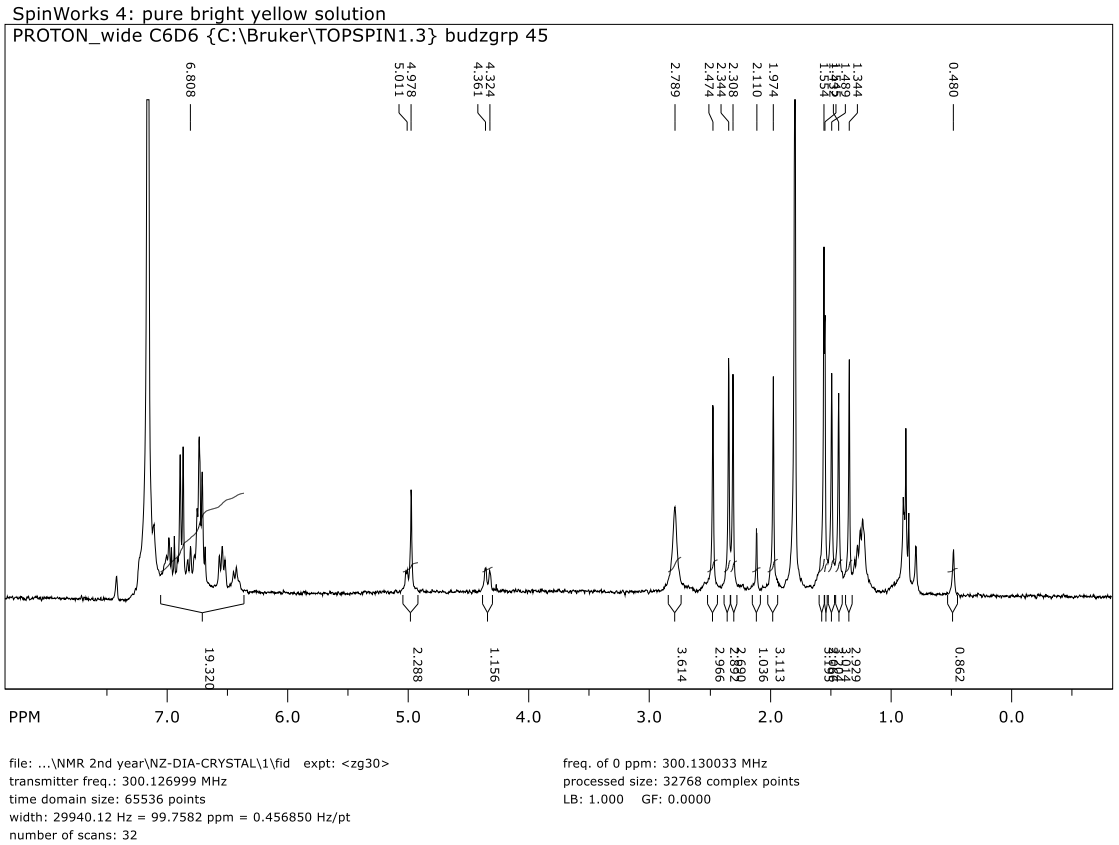

Figure A- 20. ^{1}H NMR for 3.2

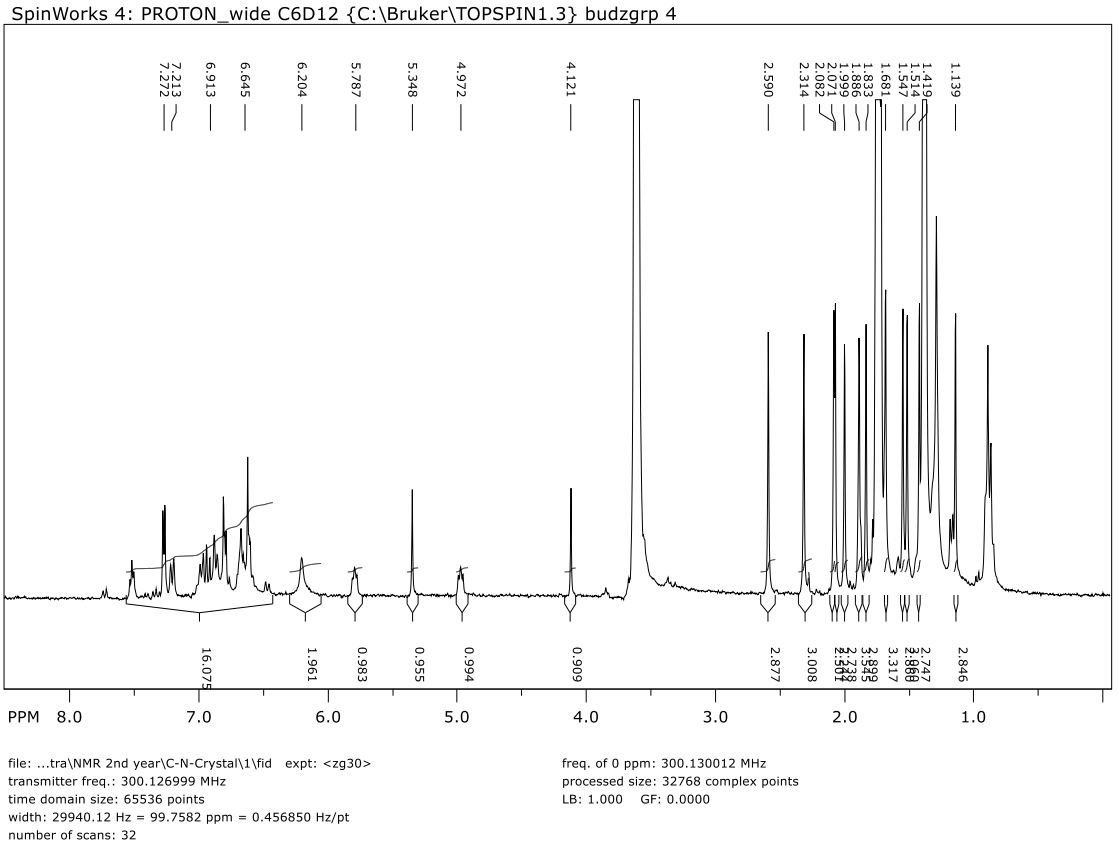

Figure A- 21. ^{1}H NMR for 3.3

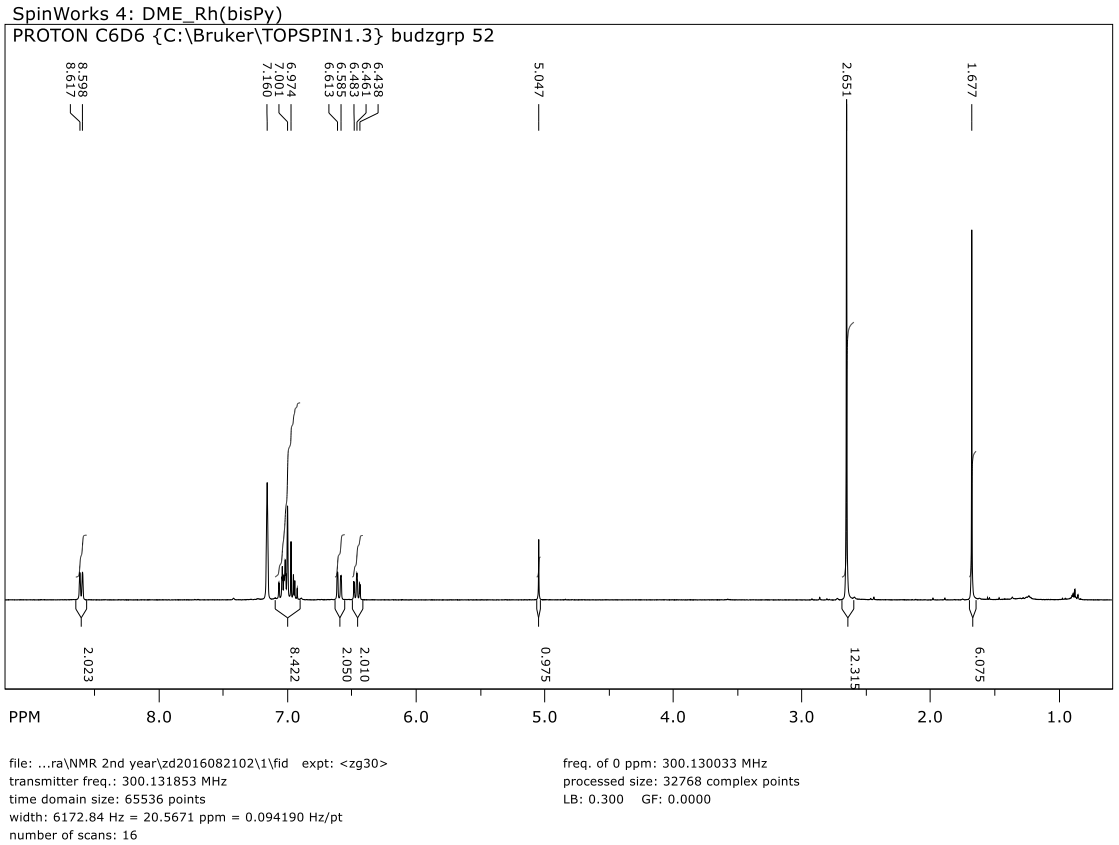

Figure A- 22. ^{1}H NMR for 3.4

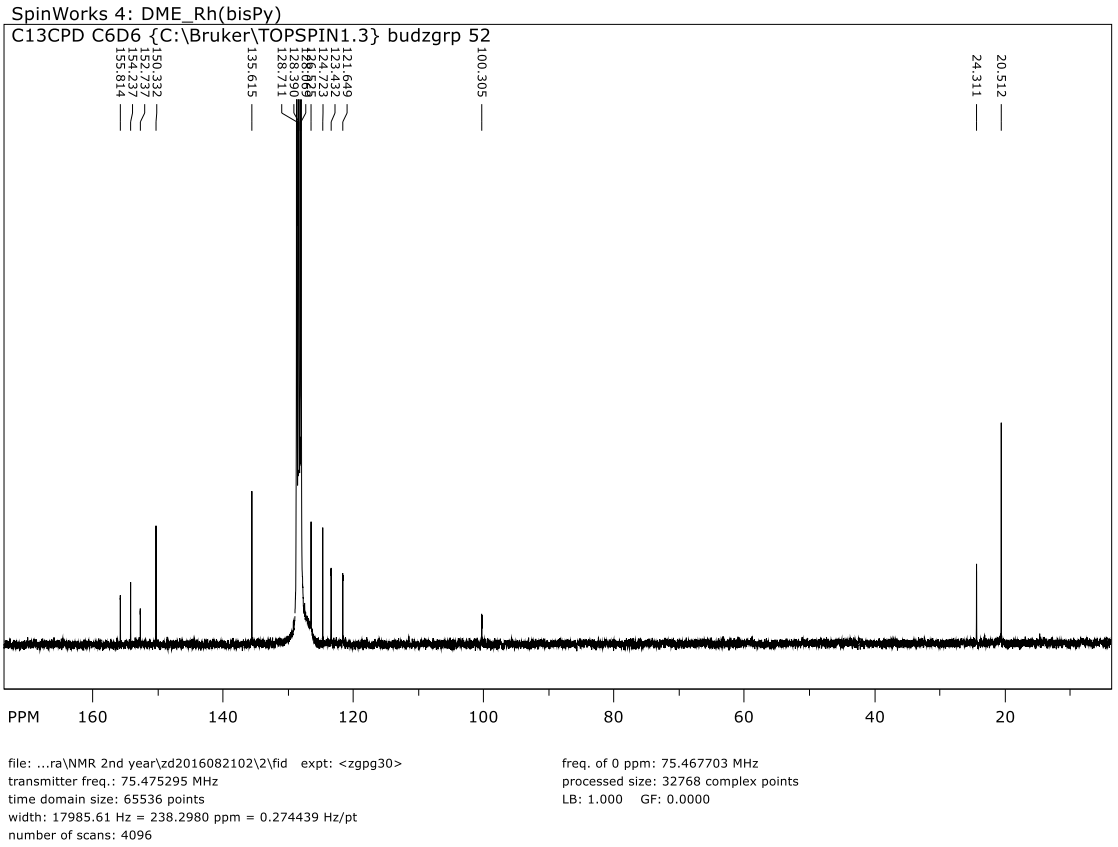

Figure A- 23. ^{13}C NMR for 3.4

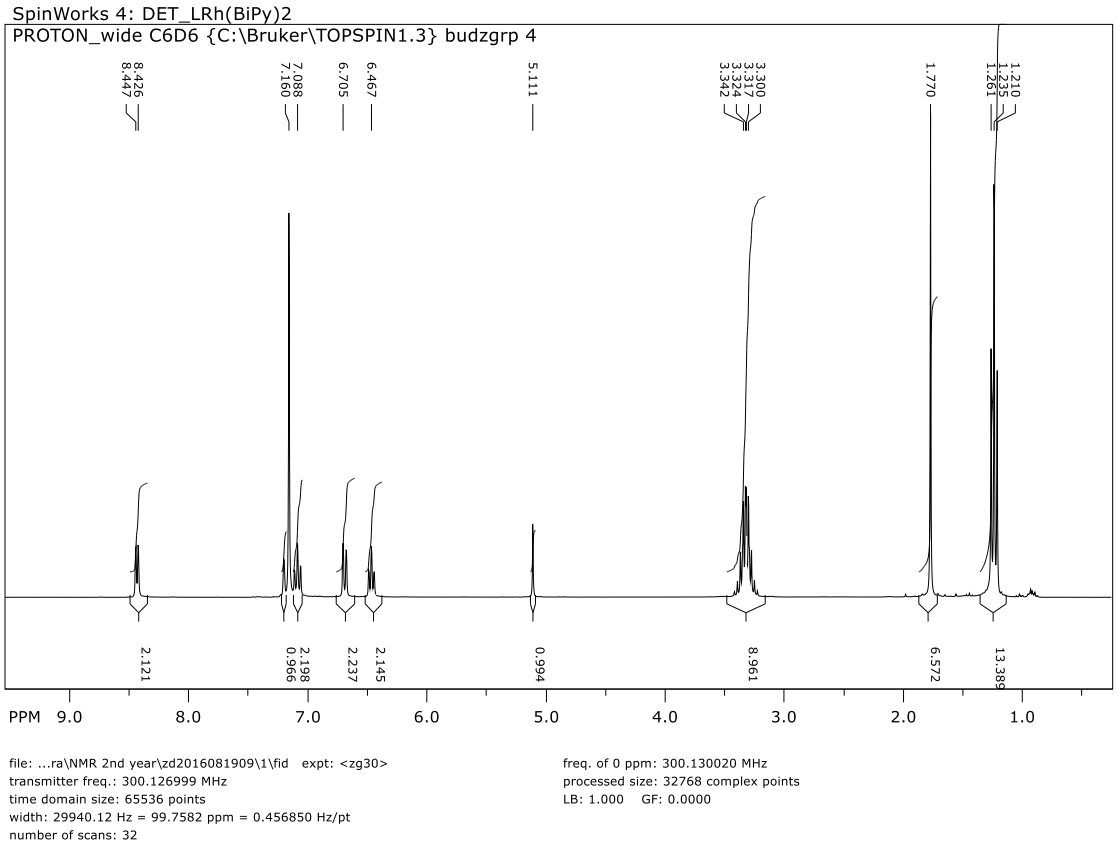

Figure A- 24. ^{1}H NMR for 3.5

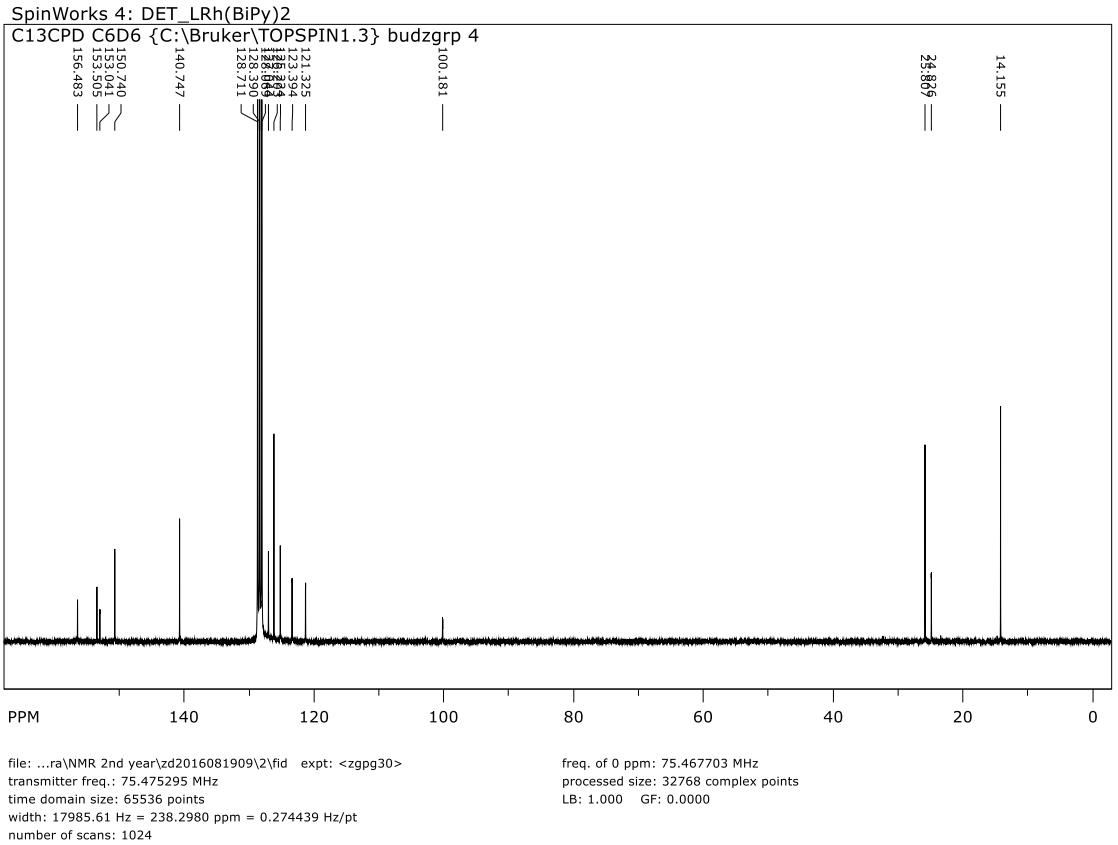

Figure A- 25. ^{13}C NMR for 3.5

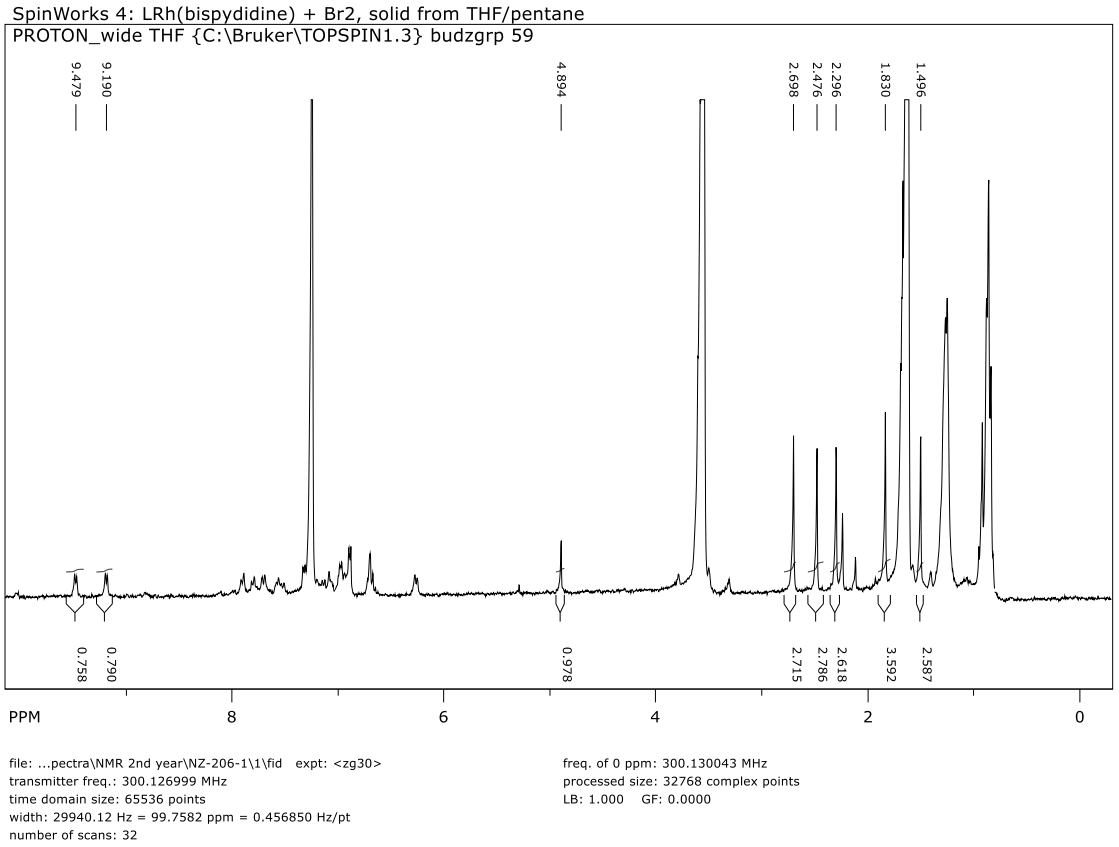

Figure A- 26. ^{1}H NMR for 3.6

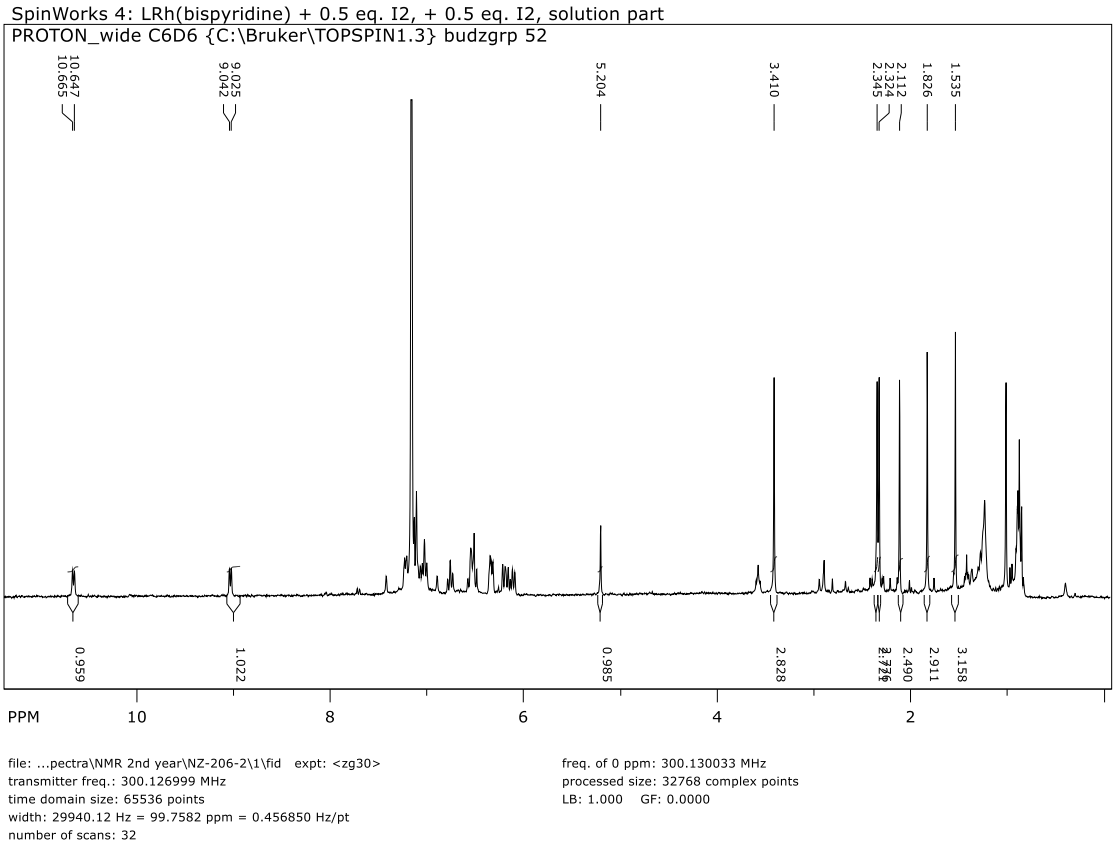

Figure A- 27. ^{1}H NMR for 3.7

Complex	**3.1**	**3.3**	**3.4**	**3.2**
Formula	$C_{33}H_{43}N_3Rh$	$C_{53}H_{66}L_iN_6Rh \cdot C_5H_{12}$	$C_{54}H_{60}N_6Rh_2 \cdot C_5H_{12}$	$C_{50}H_{59}N_5Rh_2$
Mol wt	584.61	969.11	1071.05	935.84
T (K)	150(2)	150(2)	150(2)	150(2)
Crystal system	Monoclinic	Monoclinic	Triclinic	Orthorhombic
Space group	P2(1)/c	P2(1)/n	P-1	P2(1)2(1)2(1)
a / Å	15.1673(10)	14.4157(9)	12.6337(8)	7.2577(3)
b / Å	7.9539(5)	15.7968(10)	14.9235(10)	21.6424(9)
c / Å	25.0698(16)	23.1132(14)	15.3789(10)	27.4338(10)
α/ deg	90	90.00	105.535(2)	90
β/ deg	106.011(4)	96.577(4)	95.911(3)	90
γ/ deg	90	90.00	104.176(2)	90
V / Å^3	2907.1(3)	5228.7(6)	2664.1(3)	4309.1(3)
Z	4	4	2	4
D_c / g cm^{-3}	1.592	1.159	1.335	1.443
abs coef / mm^{-1}	0.613	0.365	0.662	0.807
F_{000}	1228	2064	1116	1936
index ranges	-18 < *h* < 18 -9 < *k* < 9 -30 < *l* < 30	-17 < *h* < 17 -19 < *k* < 19 -28 < *l* < 28	-15 < *h* < 15 -18 < *k* < 18 -18 < *l* < 18	-8 < *h* < 8 -26 < *k* < 26 -33 < *l* < 33
$2\theta_{max}$ / deg	51	51	51	51
# rflctns	9067			
# unique	5408		9911	
# > 2σ	4537		8689	
GOF	1.045	1.069	1.167	1.123

Complex	**3.1**	**3.3**	**3.4**	**3.2**
# parameters	353	576	589	531
R (*F*o > 4 σ(*F*))	0.0355	0.0455	0.0408	0.0418
R (all data)	0.0486	0.0690	0.0498	0.0538
*wR*2 (all data)	0.0842	0.1352	0.1211	0.0862
largest peak, hole / *e* Å^{-3}	1.753, -0.618	1.275, -0.566	2.168, -1.032	1.083,-0.089

Table A- 1. Crystal Data for compounds